Investigation of Corrosion and Crack Morphology Behavior under Disbonded Coatings on Pipelines

by

Karina Chevil

A thesis submitted in partial fulfillment of the requirements for the degree of

Master of Science

in

Materials Engineering

Department of Chemical and Materials Engineering
University of Alberta

Abstract

Coating disbondment on pipelines is a common phenomenon that leads to exposure of the pipeline metal to the surrounding soil and ground water solutions. The exposure of pipelines to those corrosive environments is associated with development of corrosion and Stress Corrosion Cracking (SCC) on the pipeline steel. Despite the wide study of the electrochemical conditions underneath disbonded coatings, little information has been provided regarding the correlation between the coating disbondment gap size, the corrosion rate of the steel, and the SCC shallow crack morphology at the disbondment location. This research aims to understand the effect of the pipeline coating conditions on corrosion and near-neutral pH SCC of the underlying pipeline steel.

The corrosion behavior and rate of pipeline steel under coating disbondment gaps of varying sizes was investigated through field data and experimental studies. The experimental studies were performed on X-65 pipeline steel coupons in anaerobic conditions, with various CO_2 concentrations (2%, 5%, and 20% CO_2), without Cathodic Protection (CP). The steel coupons were placed into a vertical coupon holder simulating a coating disbondment on a pipeline. The findings showed that a metal ion concentration cell may develop under narrower coating disbondments.

In the analysis of the field data, dig reports provided by a Canadian gas transportation company were analyzed for cases of anaerobic corrosion under tape and asphalt coatings. The results obtained through field data analysis correlated with the experimental findings, suggesting that concentration cells under narrow coating disbondments may be responsible for enhanced corrosion on pipelines in the field.

The effect of the coating disbondment gap size on the morphology of shallow cracks was analyzed in X-60 pipeline steel, in 5% CO_2 under triangular tensile loading under coating disbondment gaps of various sizes. The results showed that the coating disbondment gap size affects the morphology of the shallow cracks under the disbondment.

ACKNOWLEDGEMENTS

I would like to express my sincere appreciation and gratefulness to Dr. Weixing Chen, for granting me an opportunity to be a part of this research, guiding me through challenges, and providing his supervision in every step of this way. I would like to warmly thank Dr. Reg Eadie for his consultation, meaningful advice, and support throughout the entire duration of my research. I also greatly acknowledge the support and contribution of Dr. Hao Zhang during our group discussions. As well, I would like to thank Dr. Jingli Luo for sharing her knowledge with me and providing valuable advice on my research.

I would like to thank Natural Science and Engineering Research Council of Canada, TransCanada Pipelines Limited, Spectra Energy, and Pipeline Research Council International for their financial support.

A special, warm thank-you goes to my colleagues: Mengshan Yu, Jiaxi Zhao, Devin Engel, Abdoulmajid Eslami, Afolabi Egbewande, Tianfei Wang, Joshua Knechtel and others. Thank you for your contribution, your help, and for making our research lab a great working place I would also like to thank Gayle Hatchard, a friend and a talented SEM-operator, for her assistance and patience during dozens of hours of SEM-imaging. As well, I would like to acknowledge the support of Shiraz Merali and Walter Boddez from the technical support group.

Words will fail to express my gratitude to my parents, Svetlana and Timur Tchevitchelov, for providing me with opportunities to fly higher than I ever imagined I would! If I wrote down every single thing I am thankful for, it would most likely exceed the length of this thesis. Thank you for your support and patience every single moment of this journey, your faith in me helped me grow! I could not stress enough my gratefulness to my partner, Connor M. Hall, for his great support: you are my rock, and we are a team! I also thank my good friends, Olya Leshcheva, Elaheh Davari, and Zeynab Shirband for their kind unconditional support and belief in me

TABLE OF CONTENTS

TABLE OF FIGURES

TABLE OF TABLES

LIST OF ABBREVIATIONS

BSE	Backscattered Electron
CCF	Combined Coating Factor
CF	Corrosion Fatigue
CP	Cathodic Protection
DA	Direct Assessment
EAC	Environmentally Assisted Cracking
EDM	Electrical Discharge Machining
FBE	Fusion Bonded Epoxy
HDPE	High Density Polyethylene
HEAC	Hydrogen-Environment-Assisted Cracking
HIC	Hydrogen-Induced Cracking
IHAC	Internal-Hydrogen-Assisted Cracking
ILI	In-Line Inspection
LDPE	Low Density Polyethylene
MAOP	Maximum Allowable Operating Pressure
MIC	Microbial-Induced Corrosion
OCP	Open Circuit Potential
OM	Open Mouth
PE	Polyethylene
PIM	Pipeline Integrity Management
PMMA	Poly Methyl Methacrylate
SCC	Stress Corrosion Cracking
SEM	Scanning Electron Microscope
SMYS	Specified Minimum Yield Strength

CHAPTER 1 :THESIS BACKGROUND

1.1 Thesis Overview

The increasing demand of energy worldwide introduces a need for a rapid supply and transport of energy products from production sites (wellheads), to processing facilities, and eventually to the customer. Pipelines are considered to be the fastest, safest, and most economically reliable means of transportation of energy products (natural gas, crude oil, and natural gas liquids (NGLs) such as ethane, butane, and propane) [1, 2].

A commercially successful operation of oil and gas transmission systems strongly relies on the integrity of the pipeline steel. The integrity of the pipeline is greatly compromised when the primary barrier between the corrosive soil environment and the pipeline, the protective coating, fails. Tape coatings were found to have a tendency to fail adhesively and create large disbondment gaps that accumulate trapped water solution. Due to the electrical insulation of the tape coatings, the secondary Cathodic Protection (CP) system,cannot provide the underlying steel full protection from environmentally-assisted cracking (EAC) processes and corrosion.

Stress corrosion cracking (SCC) is a form of environmentally-assisted cracking most commonly associated with tape-coating failure. SCC has been proven responsible for several pipeline failures through leaks and ruptures, and still remains a major integrity threat for pipeline operations worldwide. Stress corrosion cracking in a high pH environment has been studied since 1960 and its mechanism is better understood than the near-neutral pH SCC, which was discovered two decades later. Despite the extensive laboratory studies on near-neutral pH SCC conducted since its initial discovery, the synergy between environment, stress, and material, required for the near-neutral pH SCC initiation and propagation, are not yet well understood [3].

This work was performed with the goal of enhancing the knowledge of corrosion and SCC under disbonded coatings to prevent the damage to steel pipelines. The main focus of this work is to obtain an understanding of the environment developing under various scenarios of coating disbondments in the presence of CO_2 and its effect on corrosion and near-neutral pH SCC in anaerobic conditions. The obtained knowledge can contribute to a development of pipeline mitigation strategies under disbonded coatings detected during in line inspection (ILI) and field excavations. Understanding of the environment under different coating disbondments can also contribute to development of CP application strategies for better pipeline protection from EAC in the form of SCC and corrosion.

In order to understand the environment generated under various coating conditions, experimental corrosion cells were utilized in static conditions (for corrosion assessment) and under tensile loading (for SCC shallow crack assessment). In these experiments, the coating conditions were imitated with the use of Poly Methyl Methacrylate (PMMA) shieldings that isolated the environment adjacent to the steel (trapped water solution) from the bulk solution. The gap between the shieldings and the steel imitated a coating disbondment gap characteristic to tape coating; the gap between the shielding and the steel was varied to imitate various coating conditions. Additionally, corrosion and SCC data obtained from field integrity digs, provided by a Canadian pipeline company, were utilized for statistical analysis aimed to understand the effect of coating conditions on the extent of corrosion and SCC of the underlying pipeline.

The experimental findings suggested that corrosion under coating disbondments can be greatly affected by concentration gradients of metal ions and CO_2 (and carbonate) concentration of the trapped water solution under the disbonded coating. The concentration gradient appeared to be affected by the size of the coating disbondment gap. This finding was confirmed by the statistical analysis of field data, where the average corrosion rate of the metal appeared to depend on the coating condition. The findings also suggest that the crack morphology of shallow cracks under disbonded coatings is also affected by the coating disbondment size.

1.2 Thesis Structure

Commencing with a brief overview of pipeline operation and the integrity measures employed in the past and the present for safe pipeline operation, Chapter 2 contains the literature review for this thesis. It discusses the potential integrity threats that can lead to pipeline failure, focusing on near-neutral pH SCC and corrosion processes on the exposed steel as a result of coating failure.

The corrosion overview mainly focuses on CO_2-related corrosion and findings obtained in studies of corrosion inside disbondments simulating gaps in the coating, providing a basis for understanding the experimental results discussed in this thesis (with respect to corrosion).

The near-neutral pH SCC overview demonstrates the various factors (stresses, material, and environment) that affect the SCC crack growth and initiation, and emphasizes their complicated synergy. The overview leads to a review of crack growth processes in the early stages of SCC and the effect of environment on crack growth, which are the main subjects of study in this thesis with respect to SCC.

Chapter 3 discusses the experimental methods used in this thesis in the studies of the effect of the coating disbondment gap size on corrosion and crack growth on the underlying steel. Specifically, it focuses on the design of the corrosion cells and specimens that were used to simulate an environment similar to the environments generated by trapped water solutions under disbonded coatings, as well as the methods used to understand the effect of those environments on the metal.

Chapter 4 presents the experimental research performed to understand the effect of the coating disbondment gap size on steel dissolution in various CO_2 concentrations. It investigates the corrosion rate under various coating disbondment gap sizes in anaerobic condition and shows that smaller coating disbondment gaps are more detrimental to pipe, due to the fact that they can promote a stronger metal ion concentration cell effect compared to larger coatings.

Chapter 5 relates the findings of the experimental study to results of statistical analysis performed on field corrosion dig data to explain the obtained correlation between coating conditions in the field and the average estimated corrosion rate of the underlying pipe.

Chapter 6 presents the experimental research performed to understand the effect of the coating disbondment gap size on shallow cracks generated at three distinct locations under the imitated tape coating (OM, middle, and bottom of the disbondment), using findings from Chapter 4 to explain the obtained results.

Chapter 7 reviews the main findings of this dissertation, and discusses directions for future research.

1.3 References

1. Cheng, Y. F. *Stress Corrosion Cracking of Pipelines*. Hoboken, New Jersey: John Wiley & Sons, 2013.
2. Canadian Energy Pipeline Association, n.d. Web. http://www.cepa.com/about-pipelines/why-pipelines
3. National Energy Board, Stress *Corrosion Cracking on Canadian Oil and Gas Pipelines,* Report of the Inquiry, 1996.

CHAPTER 2 : LITERATURE REVIEW

2.1 Pipelines-Background

There are several million kilometers of transmission pipelines worldwide for transportation of natural gas, oil, condensates, petroleum gas (as well as other refined petroleum products), carbon dioxide, hydrogen, water, sewage, slurries, and even beer. Providing the necessary transportation function for oil and gas, which are the main forms of energy consumed worldwide, pipelines play a significant role in the energy industry and national economies [1]. In 2009, Canada’s oil and gas exports, worth $60 billion, were carried by pipelines [2].

Transporting crude oil and natural gas via pipeline is the safest, most reliable, and most economical method, compared to rail cars and tankers [1, 2]. According to the Canadian Energy Pipeline Association (CEPA), the amount of crude oil and petroleum products transported by CEPA companies every day is equivalent to 15,000 tanker truck loads or 4,200 rail cars. Pipeline transportation also has significantly lower energy requirements, compared to the alternative transportation options; oil and gas pipelines consume about 0.4% of the energy content of the transported medium per 1000 km [3]. Therefore, pipeline transportation has a lower carbon footprint, which arguably makes it a more environmentally-friendly method of transportation.

Canada has more than 550,000 km of buried oil and gas pipelines, varying from plastic gas distribution lines with a 1 inch diameter to steel oil and gas transmission lines [3]. Pipeline transportation includes integrated systems of pipelines (gathering lines, feeder lines, and distribution lines) and facilities (compressor stations or pumping stations, meter stations, and secondary storage facilities).

2.2 Integrity

The safety and integrity of pipelines are a matter of paramount importance due to the hazardous nature of the transported substances. Should a pipeline fail, the transported content can cause extensive environmental damage and affect the population living and working by the pipeline. Additionally, pipeline failure is associated with repair and excavation costs, cleaning costs, and loss of content (gas or oil). Since the integrity of a pipeline can be threatened by various phenomena, threat mitigation and verification of fitness for service are challenges that the pipeline operators must actualize.

Corrosion, identified as one of the most common causes of oil and gas pipeline failure, and Stress Corrosion Cracking (SCC), a cause of several leak and rupture events on pipelines, are important integrity threats. According to statistics provided by the National Energy Board of Canada (NEB), corrosion and metal loss (including cracking) are the primary causes of pipeline failure in approximately 63% of the cases in NEB-regulated pipelines in Canada [3]. Out of those cases, SCC is the cause of 10% to 13% of the corrosion failures. Both corrosion and SCC occur due to exposure of the pipeline to the soil environment upon coating failure.

Pipeline integrity maintenance incorporates a dual protective mechanism from the soil environment: a protective coating, and Cathodic Protection (CP). As well, pipeline operators have pipeline safety maintenance programs, called "Pipeline Integrity Management Programs" (PIM), which develop, implement, measure, and manage the integrity of a pipeline through risk assessment, mitigation, and prevention, in order to achieve the lowest, feasibly acceptable, level of risk [1]. When an anomaly is detected on a pipeline, pipeline operators evaluate integrity assessment data to detect whether the amount of deterioration is within the accepted margin of safety against failure at the operating stress level [3]. In cases where the defect condition/size is time dependent, a repeated integrity assessment is required. The integrity assessment is performed at time intervals that ensure that the defect development will not cause an unexpected failure. Common methods for integrity assessment are hydrostatic testing, in-line inspection, and direct assessment [3, 5].

a. Hydrostatic testing

Hydrostatic testing is performed on gas pipelines by pressurizing the pipeline to a stress above its MAOP (Maximum Allowable Operating Pressure) to detect defects at the onset of failure. During hydrostatic testing, the pipe is taken out of service temporarily, the natural gas is purged from the line, and the pipeline is filled with water and pressurized until it achieves the desired pressure. Defects that have failure pressures below the maximum test pressure will fail during the hydrostatic test, and will thus be detected. Such a test insures that the remaining anomalies on the pipeline (i.e. cracks) are too small to fail at the test pressure, and are therefore less likely to fail at the operating pressure. If failed sections are detected on the line, the sections are replaced prior to restoring the pipeline to service.

The interval between the tests is determined based on the operator’s knowledge of the defect growth rate; generally, a higher ratio of test pressure to operating pressure would increase the time interval length in between tests.

The drawback of hydrostatic testing is the associated costs for a removal of an entire section of pipe out of service, in addition to service disruption, land, logistics, and water disposal. As well, hydrostatic testing does not yield direct information regarding the remaining SCC features on the pipeline.

b. In Line Inspection Tools (ILI)

In line inspection (ILI) tools are instrumented devices that are equipped with sensors that can provide information (size, location) regarding the internal and external defects on the pipeline when inserted into the pipeline. Various ILI tools exist for different types of anomalies: dents, geometric irregularities, material defects, crack-like defects. ILI tools are inserted into the pipeline, and move through the pipeline using the flow of gas. As the tool moves through the pipeline, it collects location-based information of the anomalies on the pipeline. Based on the outcomes of the in line inspection, pipeline operators can locate defects with high severity, perform a dig in the location of the anomaly, and repair the anomaly if required.

It is important to mention that ILI tools can run only through pipelines that are designed to accommodate the tool (commonly referred to as “piggable”). Piggable lines would have sufficiently long radius bends and traps to launch and receive the pigs.

c. Direct Assessment (DA)

Direct assessment (DA) methods can be used for pipelines that cannot accommodate ILI tools (unpiggable), for cases of external corrosion, internal corrosion, and SCC. The assessment incorporates historical evaluation of the operation, maintenance, and environment around the assessed segment. Further analyses include indirect above-ground measurements to locate the areas affected by one of the fore-mentioned phenomena, field excavation, and examination of the pipeline segment. The findings are reviewed and evaluated, and used for a revision of the DA process or statistical analysis if necessary.

2.2.1 Coatings

Pipeline coatings for external corrosion protection were employed as early as 1930's, when coatings were applied on most of the pipelines prior to installation either at a pipeline manufacturing facility, or a construction site [5]. The coating's primary function is to serve as a barrier between the pipeline and the ground-water electrolytes and corrosive species.

The following performance characteristics describe the essential features of a pipeline coating. [6-8]

a. Adhesion/resistance to Disbondment

Adhesion/resistance to disbondment is a primary performance property that insures that the coating serves as an effective barrier to moisture and water vapor transmission, and has a decreased likelihood of being affected by mechanical soil stresses (affected by wet/dry or freeze/thaw cycles). For example, Fusion Bonded Epoxy (FBE) coatings can experience a relatively high water vapor transmission in and out of the coating. As well, coatings with good adhesion properties have a good cathodic disbondment resistance.

b. Non-shielding to CP if Disbonded

Due to the fact that CP is the secondary protection mechanism of the pipeline in case of a coating disbondment, it is important to make sure that sufficient cathodic current penetrates under the coating to ensure that the metal that is exposed to electrolytes is protected from corrosion and SCC.

c. Low Water Permeability

Water vapor can penetrate through the coating and can result in coating disbondment when the coating adhesion is not optimal, which promotes a further exposure to moisture. Additionally, electrical conductivity increases with increasing water absorption, which results in higher CP demands or a possibility of decreased cathodic current in a different location to compensate for the lack of current.

d. Effective Electrical Insulator

This property may be regarded as a two-ended sword, where good electrical properties can minimize the effect of cathodic disbondment from the pipeline; however, in an event of coating disbondment, the electrical insulation of the coating may prevent cathodic protection currents from reaching the pipeline, which may promote corrosion and SCC.

e. Abrasion and Impact Resistance

Abrasion and impact resistance are important to minimize damage from rocks or mechanical equipment.

f. Sufficient Ductility and Strength

In order to avoid cracking during pipeline handling operations, bending, installation, and operation, it is important that the coating remains sufficiently ductile. The coating strength is commonly referred to as “cohesive strength”, which refers to the force required to tear the coating.

g. Resistance to Degradation

Since coatings are made out of polymer materials, it is important that upon contact with soil and during their aging process, coatings do not deteriorate. For example, Polyethylene (PE) tapes do not show a high level of resistance to hydrocarbons or high temperature

h. Retention of Mechanical and Physical Properties

Coatings have been observed to change their mechanical properties (tensile, hardness, ductility) over time. For example, PE tapes stretche over time, while FBE coatings are known to become brittle.

i. Utilization of an Effective Surface Preparation Technique

Coatings will not bond well to poorly prepared surfaces. One of the most common and effective surface preparation methods is abrasive blasting, where the surface is cleaned with sand or slags. This method promotes surface roughness, removes millscale (iron oxide layer formed during hot-rolling), introduces compressive stresses at the surface layer, and improves adhesive strength.

2.2.1.1 Coating Types

The following is a list of the most commonly used coatings in the present and in the past [6, 9]

a. Fusion Bonded Epoxy (FBE)

Mill-applied FBE coatings were introduced in the early 1970's, and have been used on large diameter pipelines since then. FBE is considered to be a high-integrity coating, with good bonding strength; and resistance to CP degradation and disbondment, soil stresses, and soil chemicals. Osmotic blistering may promote disbondments in FBE; however, CP current can still penetrate through the coating to protect the pipeline.

b. Liquid Epoxy and Urethane

Liquid epoxy and urethanes are considered to be high integrity coatings, with good disbonding strength and resistance to deterioration. In case the coating disbonds from the pipeline, CP can still penetrate the pipeline. Another advantage provided by liquid epoxy and urethane coatings is the fact that the process of their application includes a step of millscale (oxide scale) removal through grit blasting, which affects the residual compressive stress on the pipe surface, and renders it less susceptible to SCC. No SCC accidents were associated with these coatings for over 20 years. Liquid epoxies are widely used at repair coatings, and have been proven to be the best choice for coating field joints (i.e. girth welds) on FBE-coated pipelines.

c. Extruded Three Layer Coatings

Extruded three layer coatings were introduced in 1980; they consist of an inner layer of FBE, followed by an adhesive layer, followed by a polyolefin (polyethylene or polypropylene) layer. Extruded PE can prevent the contact between the pipeline and the environment, and possess good adhesion characteristics; however, it reduces the effectiveness of CP by not being able to pass CP current. Fortunately, the polyethylene/mastic interface is more susceptible to failure compared to the mastic/pipe interface. The mastic is considered to provide the necessary corrosion protection even in cases of electrolyte penetration under the coating layers. Similarly to the liquid epoxy and urethane coatings, mill scale removal during the surface preparation for coating application improves resistance to SCC initiation. Extruded PE coatings had several SCC incident reports over the 30 years of their use in the industry.

d. Asphalt and Coal Tar

Coal tar coatings were used in the 1930’s and 1940’s, in the 1950’s and 1960’s both coal tar and asphalt coatings were widely used for field application. Asphalt and coal tar coatings are known to have low moisture permeability, and require small amounts of current to cathodically protect the pipeline due to the fact that they do not shield current. Asphalt and coal tar coatings may disbond due to poor surface preparation conditions; however, they either break in a brittle manner (due to loss of flexibility), or have moisture saturation, both of which enable CP penetration towards the pipe. Only a few instances have been documented of coal tar disbondment in a manner that shielded CP and promoted corrosion on the underlying pipeline. Asphalt and coal-tar coatings often fail due to improper surface preparation.

e. **Tape coatings**

Tape coatings were used predominantly in 1960's to 1980's, and were applied as either a single or a double wrap. They are spirally wrapped around the pipe with an overlap at the helix line. Due to the wrapping geometry, a phenomenon called "tenting" occurs between the pipe surface and the tape along the ridge created by longitudinal, spiral, and girth welds, or at the overlap between the helix of the wrap. Tape coatings are also infamous for their poor resistance to adhesive disbondment (coating delamination from the pipeline). Tape coatings are permeable to CO_2 and shield CP – a phenomena which promotes SCC formation. The wire brushing surface preparation method that was used with tape coatings is not effective, as it leaves the surface susceptible to SCC [7].

2.2.1.2 Coating Failure

The major function of a coating on a pipeline is isolation of the steel from the soil environment and groundwater electrolytes. Upon coating failure, the metal is exposed to the corrosive environment that can result in environmentally-assisted cracking, such as SCC, or corrosion on the surface of the metal, which affect the integrity of the pipeline.

Three major modes of coating failure are 1) loss of adhesion, 2) loss of cohesion (formation of breaks or gaps in the coating), and 3) general coating degradation with time [3]. Loss of adhesion refers to the coating's delamination from the pipeline which can occur due to the degradation of the organic components in the coating and permeation of water and other species under the coating. Loss of adhesion in the coating creates disbondments (loss of contact without breakage) between the coating and the pipeline, which can lead to formation of crevices. The extent of disbondment is determined by the conditions in the field (pH, CP, cyclic wetting and drying, temperature, ground water composition) and the nature of the coating itself [9,10]. Coating disbondments can also exist on the pipe prior to its placement in the field due to poor adhesion of the coating to the pipe or resulting from the geometry of the wrapped coating at the welds (such as "tenting", which is commonly observed over the longitudinal weld crown) [11].

Loss of cohesion is related to the breakage of the coating off the pipeline surface, leaving parts of the coatings attached to the pipeline and generating larger coating holidays (breaks or gaps in the coating). Field observations have shown that tape coatings are more ductile, creating longer and larger disbondment gaps, while tar coatings are more brittle, failing cohesively and creating disbondments with smaller gaps [12].

When a coating disbonding occurs, it is important that CP has access to the bare pipeline to provide the necessary protection from corrosion. Cohesive disbondment allows adequate CP to reach the pipeline behind the disbonded coating, while adhesive disbondment may shield CP, such is the case for cold applied tapes such as tape coatings. Therefore, coating delaminating and disbondment from the pipeline are considered to be the most severe form of coating failure (especially in PE tapes), since it results in CP shielding [4, 6]. This statement is supported by the fact that SCC is not commonly found in areas of large coating disbondments and holidays. It is, however, found close to longitudinal seam welds and girth welds where coating tenting generates small disbondments (less than 10 cm wide) and other areas of minor disbondment along the pipe.

2.2.2 Cathodic Protection (CP)

Since external corrosion and SCC are electrochemical processes, alteration of the electrochemical condition of the pipeline surface through alteration of the electrical field potential on the pipe can prevent those integrity threats. Providing cathodic protection to a pipeline comprises application of a negative potential on the pipeline (making it a cathode), and thus altering the environment at the surface of the pipeline [13, 14].

Upon coating failure and exposure of the pipeline to groundwater electrolytes, CP is the second protection line from corrosion. If the level of CP is inadequate, the pipeline may no longer be protected from corrosion and SCC. Two types of SCC may occur under different inadequate CP situations: high pH SCC and near-neutral pH SCC. It has been suggested that the high-pH SCC environment is generated by partial CP penetration under a disbonded pipeline, in conjunction with dissolved carbonate-bicarbonate species. A near-neutral pH SCC environment is generated by the absence of CP, when CP is either shielded by the resistivity of the soil or shielded by the coating [4, 63]. It is generally accepted that near-neutral pH SCC will not occur under standard CP criteria, the recommended level of CP is between -850 mV and -1100 mV ($Cu/CuSO_4$) [6].

Potentials more negative than -1100 mV are not recommended to avoid atomic hydrogen generation. Hydrogen atoms generated from the electrochemical process of corrosion may diffuse into the steel and can promote hydrogen embrittlement of steel. Re-combination of atomic hydrogen under disbonded coating forms hydrogen gas, which may cause coating blistering, generation of a high-resistivity environment (that can cause CP loss), and cathodic disbondment of the coating. As well, when applying CP, it is important to consider seasonal fluctuations in the CP potential to minimize its effect on pipeline cracking on a seasonal basis.

2.3 Corrosion on Underground Pipelines

Corrosion, similar to SCC, is a major integrity threat to pipeline operators. Between 1991 and 2009, metal loss (corrosion) accounted for 66% of the rupture causes on the NEB regulated pipelines [15].

Upon the protective coating failure, underground pipelines are exposed to the ground electrolytes and can be affected by a variety of external corrosion mechanisms, including general corrosion, pitting corrosion, differential cell corrosion, and microbial induced corrosion, with different corrosion morphologies [42]. The nature of the corrosion process is evaluated based on analysis of the corrosion products found under the coating during field excavations. Some of the common corrosion scenarios are: primary anaerobic corrosion, anaerobic Microbial-Induced Corrosion (MIC), anaerobic to aerobic corrosion, anaerobic MIC to aerobic corrosion, primary aerobic corrosion, and aerobic corrosion morphing into anaerobic MIC [16].

Wall loss due to corrosion and pitting corrosion are significant integrity threats on their own; however, they can also promote SCC in pipelines. Due to the fact that SCC initiates at surface discontinuities and stress-raisers, pitting-corrosion can provide SCC initiation sites. Additionally, it has been established that hydrogen plays a key role in near-neutral pH SCC crack growth, and hydrogen is often generated through corrosion reactions on the steel (e.g. carbonic acid dissociation). Moreover, corrosion can be involved in crack tip dissolution and blunting processes.

2.3.1 CO_2 Corrosion

Anaerobic corrosion in the presence of CO_2 is one of the primary corrosion scenarios found in the field, identified by the milky white siderite deposit ($FeCO_3$) found on the pipeline [16]. It has been shown by multiple researchers that the presence of CO_2 increases the corrosion rate of steel in various aqueous environments [17-19].

2.3.1.1 CO_2 Corrosion in Near-Neutral pH

Carbon dioxide corrosion of mild steel in de-aerated near-neutral pH environments proceeds through the reactions described below [20]. In these environments, a passivating oxide layer cannot form.

CO_2 is fairly soluble in water, close amounts of CO_2 can be found in both phases (in terms of volumetric molar concentrations). Dissolution of carbon dioxide in water happens via Reaction 1.

$$CO_{2\,(gas)} \rightarrow CO_{2\,(dissolved)} \quad \text{(Reaction 1)}$$

Only a small fraction of the dissolved carbon dioxide is hydrated into a weak carbonic acid, via Reaction 2.

$$CO_2 + H_2O \rightarrow H_2CO_3 \quad \text{(Reaction 2)}$$

And carbonic acid dissociates into bi-carbonate through Reaction 3. This reaction is very fast, compared to carbon dioxide dissolution in water and hydration reactions.

$$H_2CO_3 \rightarrow H^+ + HCO_3^- \quad \text{(Reaction 3)}$$

The reactions responsible for CO_2-induced corrosion are heterogeneous reduction/oxidation reactions that occur on the steel surface. The anodic reaction is iron dissolution:

$$Fe \rightarrow Fe^{2+} + 2e^- \quad \text{(Reaction 4)}$$

The corrosion rate of steel related to this reaction is dependent on the cathodic reaction. Higher pH and positive anodic potentials favor the formation of a ferrous carbonate film, which can lead to steel passivation and reduction of the corrosion rate. The cathodic reactions are presented in the following Reactions 5 and 6. The presence of CO_2 facilitates the hydrogen evolution in water, thus increasing the corrosion rate [20].

$$2H^{+} + 2e^{-} \rightarrow H_2 \qquad \text{(Reaction 5)}$$

This reaction described hydrogen evolution, which depends on the H^+ concentration, and therefore on pH. This reaction is thermodynamically more favorable than H_2CO_3 and HCO_3^- reactions; however, it is limited by the mass transport (diffusion) of hydrogen ions to the steel surface. Water reduction is a reaction which is thermodynamically equivalent to the hydrogen evolution reaction, presented in Reaction 6. However, the water reduction reaction is kinetically hindered and cannot be the main reaction that explains the high corrosion rates in CO_2-saturated aqueous solutions.

$$2H_2O + 2e^{-} \rightarrow H_2 + 2OH^{-} \qquad \text{(Reaction 6)}$$

In the near-neutral pH range, the presence of the H_2CO_3 weak acid enables hydrogen evolution, thus promoting high corrosion rates; these high corrosion rates are hindered mostly by the slow CO_2 hydration step. In neutral and alkaline conditions, the concentration of H_2CO_3 is similar to the carbonate concentration, which can make carbonate reduction reaction (Reaction 7) the dominant cathodic reaction.

$$2HCO_3^{-} + 2e^{-} \rightarrow H_2 + 2CO_3^{2-} \quad \text{(Reaction 7)}$$

Increasing the carbon dioxide partial pressure in the solution promotes a higher corrosion rate. The overall CO_2 corrosion reaction is presented in Reaction 8, where oxidization of iron in the presence of CO_2 and water generates bicarbonate and hydrogen.

$$Fe + CO_2 + H_2O \rightarrow Fe^{2+} + CO_3^{2-} + H_2 \text{ (Reaction 8)}$$

2.3.1.2 CO_2 Corrosion in High pH

One of the main differences between high pH and near-neutral pH environments is the fact that high pH environments promote the formation of an iron-carbonate film of the steel surface that can decrease the corrosion rate. When the bi-carbonate concentration is sufficiently high, a protective $FeCO_3$ film is formed to inhibit the dissolution of iron. Research on iron-carbonate film formation shows that a stable film does not form in dilute carbonate-bicarbonate solutions characteristic to the near-neutral pH range, at temperatures below 60˚C [21, 22].

In concentrated carbonate-bicarbonate solutions, the formation of the $FeCO_3$ protective film proceeds according to one or both of the following Reactions . Reaction 9 shows a direct formation of iron carbonate by reaction of iron and carbonate.

$$Fe + HCO_3^- \rightarrow FeCO_{3(s)} + H^+ + e \quad \text{(Reaction 9)}$$

Reaction 10 shows a formation of a pre-oxidation $Fe(OH)_2$ deposit layer, which in the presence of carbonate turns into iron carbonate according to Reaction 11 [21].

$$Fe + H_2O \rightarrow Fe(OH)_2 + 2e \quad \text{(Reaction 10)}$$

$$Fe(OH)_{2(s)} + HCO_3^- \rightarrow FeCO_{3(s)} + H_2O + OH^- \quad \text{(Reaction 11)}$$

2.3.2 Transport Processes

In addition to the thermodynamic and kinetic considerations of the reactions representing the electrochemical processes at the steel surface, it is important to account for the transport processes of the different species. While certain species (e.g. Fe^{2+}) are produced at the metal surface due to corrosion, other species are depleted at the surface (e.g. H^+); this concentration gradient in species results in molecular diffusion of the species towards and away from the metal surface. The concentration gradient governing the diffusion process is established based on the competition between the diffusion processes and the electrochemical processes. When the electrochemical processes are slower than the diffusion processes, the resulting concentration gradient are small, and vice versa. Simultaneously, the concentration of the different species at the surface affects the rate of the electrochemical processes. This results in the electrochemical processes both being affecting and affected by the diffusion of the boundary layer.

In a stagnant solution unaffected by convective processes, diffusion "speed" of the different species is affected by their charge. Concentration gradients promote charge separation, but short-range attraction forces between opposing charges balance this process, resulting in a potential gradient within the solution that promotes electro-migration. Electro-migration is defined as an increase in the diffusion rate of slower species and a decrease in the diffusion rate of faster species [23].

2.3.3 Differential Cells

While generalized corrosion is a uniform attack of the metal surface, and pitting corrosion is a localized attack, the most common corrosion morphology found on underground pipelines appears as a hybrid of both with an uneven metal loss in localized areas. This type of corrosion is often caused by differential cells, where the oxidation and reduction reactions occur at different locations on the metal surface. In buried pipeline, various differential cells can exist: differential concentration cells, differential soil cells, and galvanic cells with different metals.

In concentrations cells, exposure to various concentration of gas (e.g. oxygen or carbon dioxide) or a certain species (metal ion) can turn one site on the pipeline more anodic, and another one into cathodic [14, 24]. At the anode, electrical current leaves the surface as the metal corrodes, towards the cathode, which is protected from corrosion. In oxygen concentration cells, the part that is exposed to a higher oxygen concentration becomes the cathode, while the part that experiences oxygen depletion becomes the anode.

2.3.3.1 Metal Ion Concentration Cell

Metal ion concentration cells can form in the presence of a crevice, when the concentration of dissolved metal ions in the solution inside the crevice is higher than their concentration in the bulk solution (due to a higher volume of the bulk solution). This non-equilibrium condition results in an electrical potential difference between locations with different metal ion concentration, which leads to a higher dissolution rate of the metal outside the crevice, in order to restore the balance between the metal ion concentration inside the crevice and in the bulk solution. This creates a situation where the metal inside the crevice acts as a cathode, while the metal outside the crevice has an enhanced dissolution rate and serves as an anode [25].

The Nernst Equation

To determine the effect of ionic concentrations (or gas pressures) on the electrode potentials, the Nernst equation can be used as a thermodynamic basis [24, 26]. Generally, more noble and positive potentials are observed with an increased activity/concentration of a dissolved oxidizer. Nernst equation is shown in Equation 2.1.

$$E = E^0 + \frac{RT}{nF} ln \frac{activities\ of\ reactants}{activities\ of\ products} \quad \text{(Equation 2.1)}$$

Where E^o is the standard cell potential, R is the universal gas constant: $R = 8.314\ \mathrm{J\,K^{-1}\,mol^{-1}}$, T is the absolute temperature, F is the Faraday constant, and n is the number of moles of electrons transferred in the cell reaction.

When $E > 0$, the reaction is spontaneous, and oxidation occurs at the left-hand electrode. When $E < 0$, the reaction is not spontaneous, and oxidation occurs at the right-hand electrode. Based on this knowledge, it is possible to predict the cathodic and anodic sites under different concentrations.

Differential soil cells can form due to variations of moisture content in the soil, differences in pH, or differences in aggressive ion concentration in the soil (e.g. chlorides).

2.4 Environmentally Assisted Cracking (EAC)

Stress Corrosion Cracking (SCC) is a type of “environmentally-assisted cracking” (EAC), which is a general term for cracks that occur due to exposure of a material to a potent underground environment combined with other circumstances, which eventually reduces the pressure-carrying capability of the pipeline. Three similar, yet distinct, mechanisms fall under the category of EAC: Corrosion Fatigue (CF), Hydrogen-Induced Cracking (HIC), and Stress Corrosion Cracking (SCC).

Hydrogen-induced cracking describes cracking phenomena where the presence of hydrogen plays an important role in promoting cracks in components, with or without corrosion, and sometimes even in the absence of an external stress. In certain materials and environments, HIC can overlap with SCC or CF; however, HIC may have other forms and mechanisms as well.

Corrosion fatigue occurs due to propagation of chemically-reactive agents inside formed fatigue cracks due to cyclic stress; these chemical agents can accelerate crack propagation and thus decrease the number of cycles to failure and the stress required for crack initiation and propagation. Despite the possibility of metal passivation at the crack tip, the proceeding fatigue cycle can crack the brittle passive layer and re-initiate the process [17].

SCC occurs under the synergistic interaction of a corrosive environment (condensed layer of moisture, or trapped solution) at the pipe surface, tensile stress (fabrication or service stresses), and steel susceptibility to SCC (microstructure, millscale, condition). The potent environment associated with SCC results from a protective coating failure which allows groundwater solution penetration towards the bare steel [1, 4, 7].

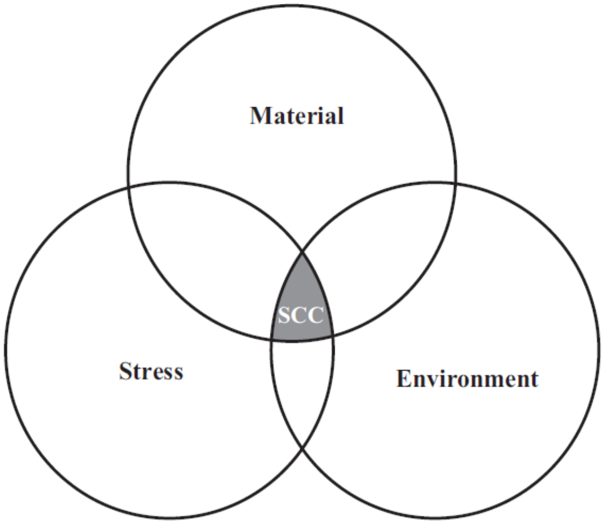

Figure 2-1 Conditions Required for SCC Initiation [1]

Several differences were observed between CF and SCC. First, CF occurs under cyclic stresses, while SCC occurs under static tensile stresses. For the case of cracking in gas pipelines, it has been proposed that crack propagation occurs under SCC with slow fluctuations of internal pressure rather than CF. Additionally, SCC crack morphology exhibits small branching, while CF cracks have little to no branching. Also, due to the ability of CF to fracture passive film at the crack tip faster than SCC, the CF stress intensity factor is often lower than SCC [1].

2.5 Stress Corrosion Cracking (SCC)

Between 1977 and 2007, Stress Corrosion Cracking (SCC) was the cause of 37 pipeline failures in Canada (17 leaks and 20 ruptures) [5]. Later, SCC mitigation methods have improved, which decreased the frequency of SCC-related failures; however, SCC still remains an issue of concern in North America and other countries, which include Australia, Russia, Saudi Arabia, and South America [1, 4, 7, 5, 11].

SCC was first discovered in a southern U.S.A pipeline in 1965, where a 24-inch pipeline rupture due to SCC resulted in 17 fatalities [7]. This form of SCC had an inter-granular crack morphology (crack grows along grain boundaries), occurred in high pH environments (8-11), and is commonly referred to as "classic SCC", "high pH SCC", or "inter-granular SCC". High pH SCC is known to develop under coatings that partially shield CP in highly concentrated carbonate-bicarbonate trapped-water solutions, and is affected by temperature.

A new form of SCC was discovered in the 1980's on Canadian pipelines, differing from the classic form of SCC both in its growth mechanism, morphology, and environmental conditions. The new form of SCC had a trans-granular morphology (crack grows across grains), was found in dilute near-neutral pH electrolytes (5.5-7.5), did not show a direct correlation to temperature, and developed under coatings that shielded the protective CP system. The new form of SCC is commonly referred to as "near-neutral pH SCC" or "trans-granular SCC" [1, 4 -7, 11].

After its discovery on Canadian pipelines, near-neutral pH SCC was detected on pipelines in Europe, Asia, Australia, and U.S.A. Near-neutral pH SCC has not been as highly studied as the high pH SCC; its mitigation has improved since it was discovered; however, its mechanism is not understood as well as the high pH SCC [4].

Both types of SCC initiate in pipelines under failed protective coatings where ground water came in contact with the exposed steel. Ground water accumulated under the failed coating in contact with the pipeline (commonly known as "trapped water") can have a different chemistry than the ground-water at the pipeline location. In locations of near-neutral pH SCC, the trapped water is a dilute carbonate-bicarbonate solution, whereas with high pH SCC the trapped water is a concentrated carbonate-bicarbonate solution.

The type of SCC that will initiate on the pipeline is dependent on the environmental conditions, the chemistry of the trapped water, and the level of CP protection. If the soil or the trapped-water have a high level of resistivity or the coating does not allow CP penetration towards the pipeline (common for tape-coatings), the chemistry of the trapped water will be unaltered and near-neutral pH SCC is likely to initiate if the appropriate stressing conditions are met. If the coating does not shield CP, and cathodic current is able to partially penetrate towards the pipeline, then the pH of the solution will increase due to generation of hydroxyl ions, forming an environment characteristic of high pH SCC [1, 5, 7]. As the chemistry of the trapped-water solution is related to the presence of CP, it was pointed out that the environmental conditions of near-neutral pH SCC and high pH SCC are related and may change from one form of SCC to another with CP fluctuations [27, 28].

SCC cracking begins with small cracks on the outside surface of a buried pipeline, which lengthen, deepen, and adjoin with time. For both types of SCC, the identical characteristic of their appearance in the field is the presence of colonies of parallel cracks on the external surface of the pipeline. The near-neutral pH SCC cracks appear more open than high pH SCC under metallographic examination, indicating corrosion occurring on the crack sides. Eventually, when the cracks become large enough, the pipeline fails by leak or rupture. A leak through the pipeline wall will occur before rupture in a case where the crack grows in the depth direction through the pipe wall prior to reaching a critical length that would cause rupture [1].

Extensive industry research has been conducted to gain a better understanding of SCC initiation and growth, and the level of contribution of various factors that affect these stages: metallurgy, environmental parameters, coatings, CP, stresses, and electrochemical reactions. As well, research has been conducted to develop detection techniques, evaluation procedures, and mitigation methods.

2.5.1 SCC Lifecycle

For a development of SCC management techniques, it is important to understand the formation and growth of SCC cracks on a pipeline. The SCC lifecycle demonstrates differences in SCC growth rate and mechanisms during its different stages, it is generally described in terms of a "bathtub model" which consists of four stages. The model was initially proposed by Parkins [29] for high pH SCC; however, it was later used to characterize near-neutral pH SCC as well [6].

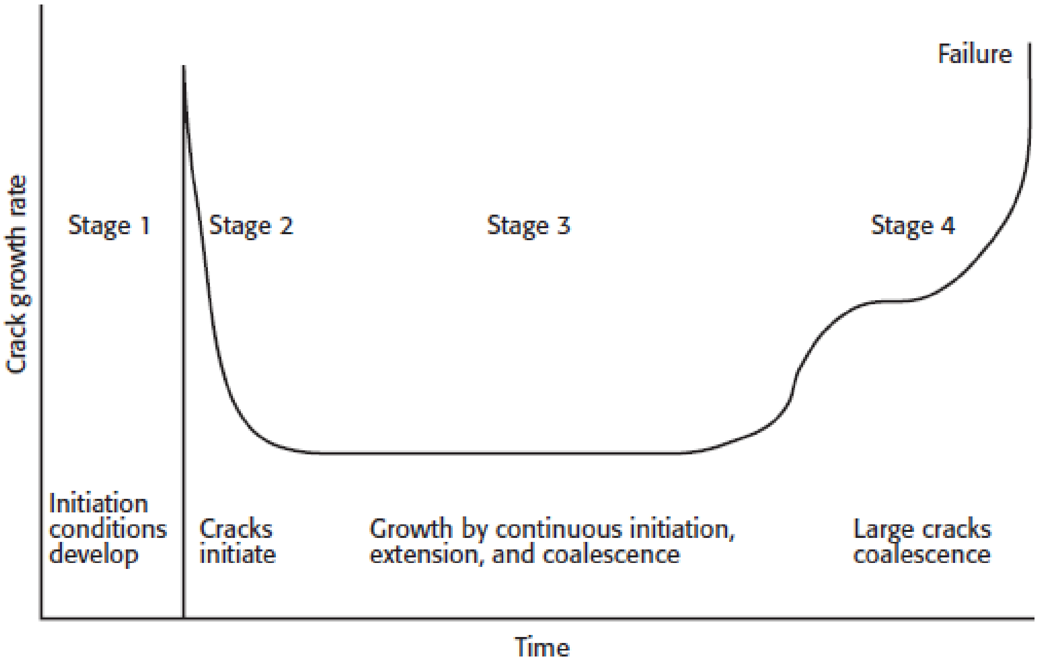

Figure 2-2: SCC Life Cycle from the Initiation Stage to Failure [4]

a. Stage 1

In Stage 1, the conditions for SCC have not yet fully developed. In this stage, the protective coating failure occurs and a potent environment under the coating forms as the electrolytes penetrate to the pipe surface. This period is commonly referred to as "incubation period". Parkins [29] identified several factors that affect the incubation period:

- Coating deterioration that results in the formation of holidays and disbondment; the incubation time is dependent on the type of coating

- Mass-transport of solution and gases under the coating
- Soil properties such as moisture content, resistivity to CP, drainage and moisture content, chemistry, and terrain
- Soil stresses that affect the coating
- Pipe surface temperature
- Coating application weather conditions, and pipeline surface conditions during coating application

It is difficult to assess the length of the incubation period, due to a possibility of coating failure soon after construction due to improper application, or later failure due to soil stresses, high temperature, CP, etc. In the industry, this stage is approximated as 12 years. This stage is also considered to be the least predictable, due to the fact that it highly varies between different pipeline segments and depends on various factors. Generally, knowledge of this stage is irrelevant for assessment of crack growth rates on pipelines that have SCC cracks; however, it is necessary for total lifetime estimation of a pipeline. In the final stages of Stage 1, a stress-corrosion crack initiates.

b. Stage 2

After the coating failure and formation of an environment that promotes SCC, SCC may initiate due to solution species that promote pitting (e.g. chloride), surface residual stresses, metallic imperfections, stress concentrations, or a combination of these. It has been observed that the crack growth rate at the start is relatively high, and tends to decrease rapidly after the initiation is complete. The length of this stage may be as short at several days for an individual crack.

c. Stage 3

In this stage, the crack grows at a relatively low rate promoted by one, or a combination of an environmental mechanism, crack coalescence, or cyclic softening [6]. During this stage, crack blunting by corrosion takes place, and the majority of the cracks become dormant. The small percentage of cracks that do not become blunt will continue to grow;

out of these cracks, some cracks will coalesce and form much larger cracks that will continue to grow through mechanical processes. Stage 3 is the key stage for prediction of the remaining life of a pipeline with small corrosion cracks.

d. **Stage 4**

This stage is the final part of the crack growth process. In this stage, large cracks coalesce and may achieve a sufficient size where the SCC growth rate will be promoted synergistically by mechanical forces and environmental growth. At the end of this stage, mechanical loading conditions start to play a larger role in the crack growth compared to the environmentally-promoted crack growth. This increase in SCC growth velocity due to mechanical growth depends on the stress cycles of the loading regime, and shape and size of the crack (length to depth ratio). High length-to-depth ratios are not uncommon, typically in the range of 20-50 to 1 [1, 4, 6, 11, 28, 29].

2.5.2 Near-Neutral pH SCC

2.5.2.1 Primary Characteristics

Near-neutral pH SCC occurs in diluted ground water carbonate-bicarbonate solutions that result from dissolution of carbon dioxide from decayed organic matter in ground water. Near-neutral pH SCC does not initiate under intact coatings. Coating defects that promote near-neutral pH SCC are coating disbondments (coating that does that not properly adhere to the surface), holidays (ruptures or gaps in the coating), or coating degradation over time, where groundwater can penetrate towards the pipe. Near-neutral SCC was mostly found under polyethylene (PE) tape, asphalt, and coal-tar coatings [4, 6, 7, 11]. Common areas of near-neutral pH SCC crack occurrence on PE-coated pipes are at or near the toe of the weld seam due to stress concentration and underground water access, and the body of the pipeline where the coating has been damaged.

Often, CP current cannot penetrate towards the surface and protect the metal due to the high electrical insulation properties of the coatings and/or soil resistivity. Near-neutral pH SCC often occurs at sites of free corrosion potential of -760 mV to -790 mV (Cu/CuSO4) where little, if any, CP reaches the pipeline, proven by long term soil box tests [6, 11].

SCC in the pipe body forms as crack colonies containing several shallow cracks, which are usually less than 10% of the pipe wall in depth. Figure 2-3 shows the common locations of SCC formation [4].

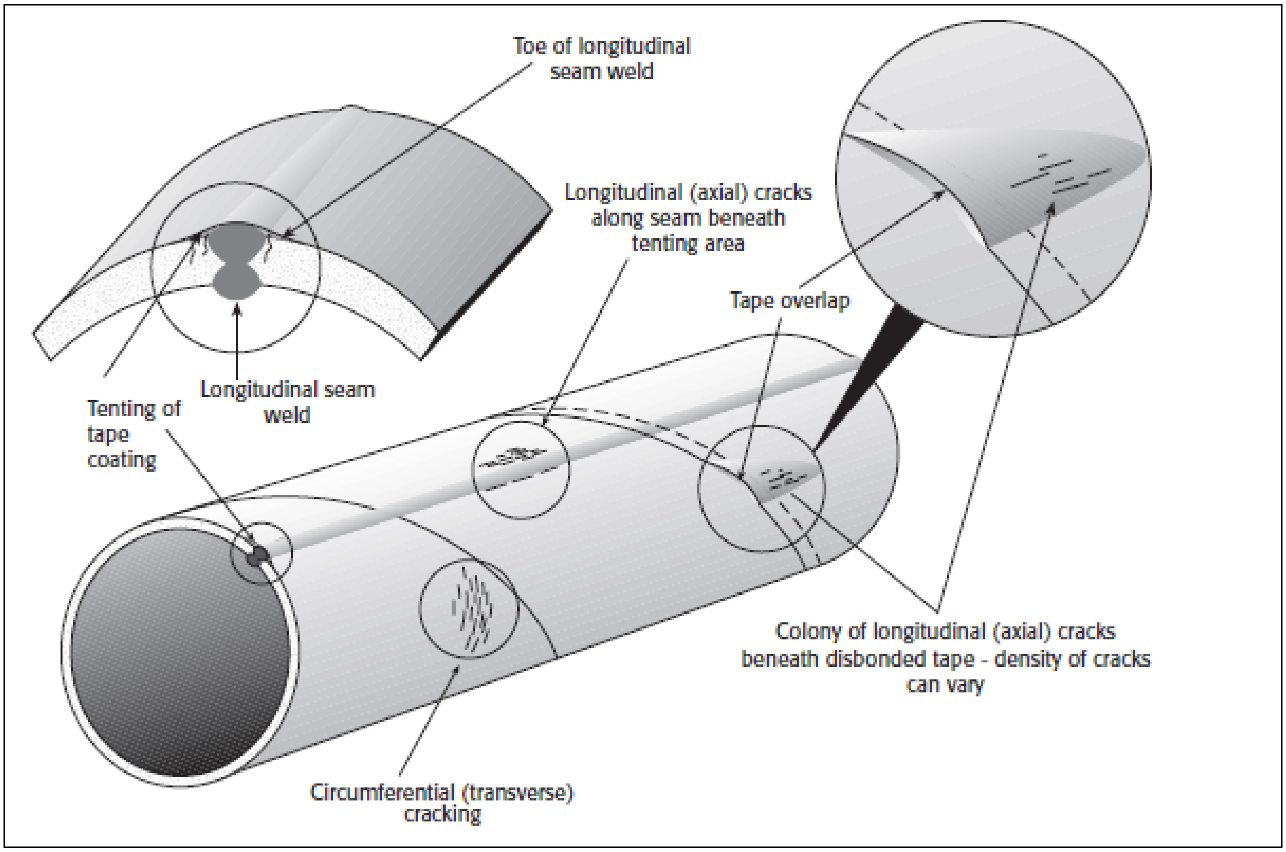

Figure 2-3: Pipeline Locations where Near-neutral pH SCC Commonly Form [4]

SCC colonies that form along the toe of a long seam weld form under coating that tents over the weld crown. As the tenting area is relatively small, “toe of the weld” SCC colonies are usually characterized by relatively linear colony dimensions. The near-neutral pH SCC crack morphology is trans-granular, and is associated with lateral corrosion of the crack sides [1, 27], as shown in Figure 2-4. Formation of a milky white iron-carbonate deposit between the coating and the pipe surface is commonly observed in near-neutral pH sites.

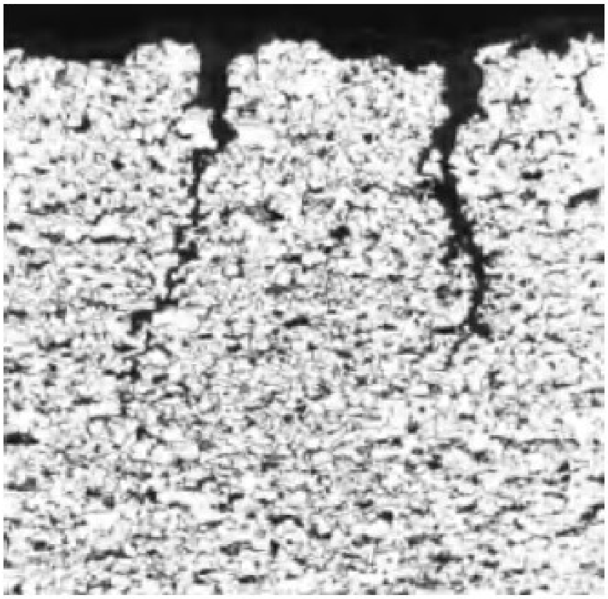

Figure 2-4: Trans-granular SCC [4]

Trans-granular SCC crack growth is characterized as brittle, cleavage-like fracture through the grain. Evidence of small amounts of plasticity commonly associated with the fracture path suggests a more complex growth mechanism. One of the most common theories is that atomic hydrogen segregated at the crack tip promotes embrittlement of the strained material ahead of the crack tip. The remaining ligament between the crack tip and the inside wall typically fails in a ductile manner (with the exception of pipelines with very low fracture toughness) [1].

2.5.2.2 Stresses Involved in SCC

The operating pressure on pipelines is defined in terms of the Specified Minimum Yield Strength (SMYS), which is identified for each steel grade, and is required by code to be lower than the yield strength. The allowable operating pressure of a pipeline is defined based on its location and the surrounding dwelling location; for a natural gas line, the maximum allowed hoop stress is between 44% and 80% SMYS. Field studies have shown that the SCC severity decreases with a decrease in the operating pressure; the critical flaw size and critical leak/rupture length of the crack increases with decreasing %SMYS, while the crack depth and the number of crack colonies decreases. The NEB report offers pressure reduction as a temporary solution for a pipeline where a threat of imminent failure was discovered. However, due to the presence of inconsistencies in the trends and the fact that a pressure threshold level for SCC initiation was not found, pressure reduction is not recommended as an effective solution for SCC prevention. Despite the decrease in SCC severity induced by stress reduction, SCC still initiated in lines operating with hoop stresses as low as 46% SMYS (to 70% SMYS) [4].

SCC initiates on the external pipeline surface beneath disbonded coatings under a tensile stresses which includes a dynamic or cyclic component, generated either in service, or as residual stresses during pipeline manufacturing (e.g. welding or bending) [1]. Below a certain value of tensile stress, known as the threshold stress, crack initiation does not occur; for near-neutral pH SCC an exact value of the threshold stress was not yet determined [4, 6]. The main challenge of determining the stresses in the pipeline and finding the threshold stress through laboratory studies is the fact that laboratory stresses are usually uniaxial tension stresses; however, the actual stress that affects SCC is a combination of internal operating pressures, residual stresses, and external stresses related to the ground movement, as shown in Figure 2-5. Therefore, the experimental comparison of the applied internal pressure with the threshold stress often generates unrealistic and unreliable results.

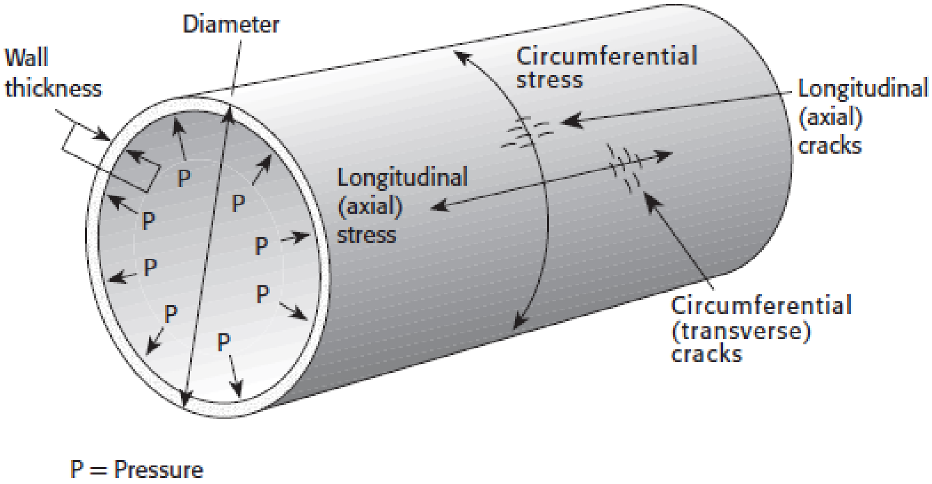

Figure 2-5: Stresses in a Pipeline [4]

2.5.2.2.1 Circumferential Stresses

Operational stresses, resulting from internal pressurization of the pipeline, exert circumferential hoop stresses on the pipeline walls, which are often the biggest source of stress. Those stresses promote crack growth along the longitudinal axis of the pipeline along the surface direction, perpendicular to the hoop stresses. More than two thirds of pipeline failures due to near-neutral pH SCC were associated with axial cracking [4].

Additionally, circumferential stresses may result from residual stresses, which remain on the pipeline after manufacturing (rolling, welding, etc.). In near-neutral pH SCC, Van Boven [31] found that areas of highest tensile residual stresses promote pitting. As well, it was shown that the residual-stresses gradient in the depth direction may have an effect on the crack dormancy; when the residual stresses near the surface change from highly tensile to lower tensile or compressive, active cracks may become dormant [32].

2.5.2.2.2 Longitudinal Stresses

Operational stresses on the pipeline can also result in longitudinal stresses, whose magnitude depends on the level of restraint from longitudinal movement imposed by the soil on the pipeline. The magnitude of the longitudinal forces varies between 28% of the hoop stress for complete restraint, and as high as 50% of the hoop stress for partial restraint [4]. Another source of longitudinal stresses on the pipeline results from movement of the surrounding soil (such as landslides and settlements), or by the physical weight of the soil above the pipeline. These stresses can promote the formation and growth of circumferential and transverse cracks. Generally, longitudinal stresses are difficult to predict or control; complex geotechnical engineering calculations are required for accurate determination of the soil-induced stresses [1]. Figure 2-6 shows the stresses on a buried pipeline [41].

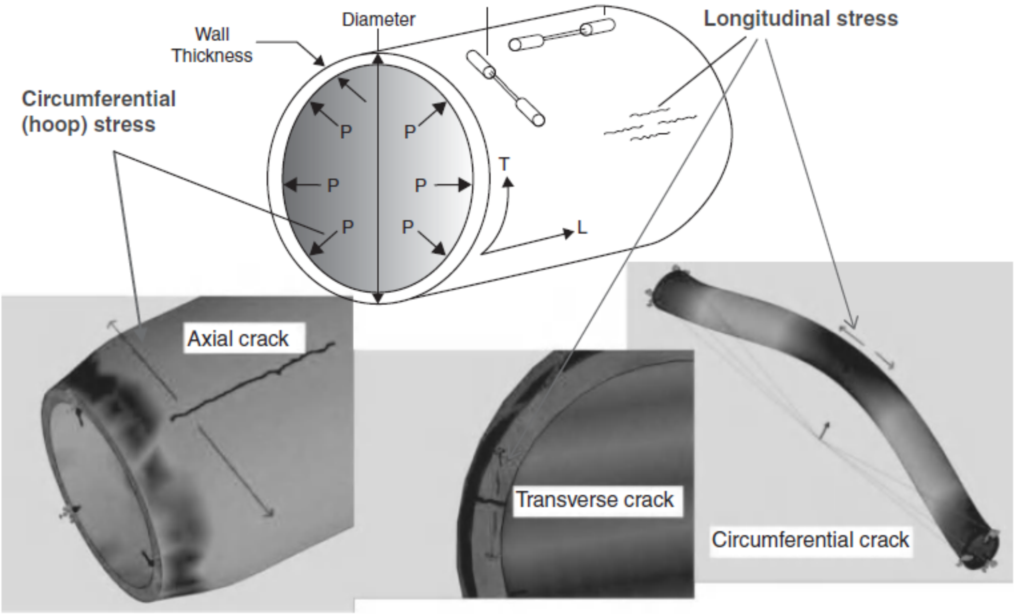

Figure 2-6: Stresses on a Buried Pipeline [1]

2.5.2.2.3 Cyclic vs. Static Stresses

Cyclic stress is known to facilitate crack propagation and reduce threshold stresses [27]. However, near-neutral pH SCC was found to initiate under constant loading conditions as well, where crack initiation was attributed to pit nucleation and growth, and the stress and strain concentration at the bottom of pits. Based on the results of several tests where crack growth was not observed under constant-load or constant-displacement conditions, it is believed that pressure fluctuations are essential for crack propagation in a pipeline [7].

The R-ratio is a parameter that describes the stress fluctuations in the pipeline in terms of their range, representing the ratio between the minimum and the maximum stress in the circumferential direction [1]. Those stress fluctuations result from pumping a certain content through the line, and are greatly affected by the operating conditions and the material that is being transported through the pipeline (gas or oil) [33].

It was shown that reducing the R pressure value affects micro-crack initiation and branching [34] and promotes the pit to crack transition [35] which is caused by stress intensity at the boundaries of the pits. Attempts have been made to correlate between the stress level and the R-ratio and the crack growth rate for pipeline; however, no strong consensus was reached [1].

Cyclic stresses can also induce cyclic softening, which occurs when application of stress cycles at maximum stress levels below the yield stress cause the metal to experience local micro-plastic deformation after a period of load cycles. Cyclic softening results in a decrease in the yield strength and threshold stress [1].

2.5.2.3 Environment

2.5.2.3.1 Temperature

No strong temperature correlation has been observed for near-neutral pH SCC, since most cracks were found further downstream from compressor stations where the operational temperatures are lower (<40°C). Therefore, it has been suggested that temperature is not a significant factor for near-neutral pH SCC [4 11, 27]. Lab experiments confirmed this observation, showing that there is no direct dependence of cracking on temperature in the range of 5°C to 45°C under near-neutral pH SCC conditions [36]. Indirectly, however, high operational temperatures have an adverse effect on near-neutral pH SCC. First, elevated temperatures can promote coating degradation, and thus provide more sites for SCC initiation. Second, elevated pipeline temperatures may cause drying of the soil around the pipeline, which increases its electrical resistance, and thus increases the CP current demand. It has been observed that trans-granular SCC is more severe at distances closer to the discharge side of a compressor and pump station, which may be related to higher discharge gas temperatures that promote coating degradation, or increased stress fluctuations and higher stress levels [6].

2.5.2.3.2 Trapped Water Chemistry

Results of hundreds of trapped water samples of near-neutral pH SCC from the field showed that the water samples were very dilute carbonate and bi-carbonate solutions with chloride and sulfate, with cations of sodium, calcium, potassium, and magnesium [37]. According to Delanty and O'Beirne, near-neutral pH SCC soil sites contain a CO_2 concentration between 4% (in the winter) to 23% (in the spring) [7, 38]. Cracking tends to occur in a cold climate where the CO_2 concentration in groundwater is high. Cheng also showed that SCC susceptibility in electrolytes extracted from under disbonded coatings was associated with high hydrogen permeation current in the solution [38].

2.5.2.3.3 Soil Conditions

No field studies detected a concrete correlation between SCC and soil chemistry [7, 38]; however, Delanty and Marr developed a severity rating model for near-neutral pH SCC from field data obtained from TransCanada's pipeline in Eastern Canada. Based on this model, the most aggressive soil types were lacustrine soil (formed by deposits in the lake), followed by organics over glaciofluvial soils (formed by deposits in streams fed by melting glaciers), and organics over lacustrine soil.

Drainage also has shown to play a role in SCC initiation; it has been identified that poorly drained environments with wet and dry seasonal fluctuations (clays) have a higher SCC susceptibility compared to well-drained environments (sandy areas, and glacial fluvial till environments). In tape coating, swelling-type clay can increase the soil stresses on the coating and promote tape disbondment. In asphalt coatings, during wet and dry fluctuations waters and salts from the soil can penetrate under delaminated or cracked coatings and promote an SCC-susceptible environment [6, 27, 39]. Industrial studies have shown that static drainage conditions (the soil being consistently wet or dry) show less SCC compared to seasonal drainage (intermittent wet-dry cycles). Near neutral pH SCC was found in asphalt-coated pipelines mostly (83% of the time) in extremely dry terrains consisting of sandy soils or a mixture of sand and bedrock. In these locations, the CP was found inadequate (pipe to soil potential) [6].

Additionally, near-neutral pH SCC is associated with local topographical depressions, for example, at the bottom of hills or streams. In these locations, water either channels along the pipeline or crosses it. Constant supply of CO_2 by the water in the environment to the trapped-water solution under a disbonded coating on a pipeline is favorable for maintaining the near-neutral pH environment [4, 6, 11].

2.5.2.4 Material

It has been shown that near-neutral pH SCC has developed on various types and grades of pipelines from a variety of pipe mills with grades ranging from 35 to 65 ksi SMYS [7].

The material properties (steel grade and microstructure) that affect its susceptibility to SCC were found to be related to microstructure. Although a full understanding of this correlation was not yet developed, observations showed that materials with a more uniform microstructure (e.g. bainite, bainitic ferrite, or polygonal ferrite) are more resistant to near-neutral pH SCC compared to steels with non- uniform microstructures (e.g. ferritic pearlite) [6].

The toughness of the material plays an important role, and dictates the fracture mode. In lower toughness materials, the crack may grow to a sufficient length without penetrating the pipeline wall, and eventually experience a fast fracture and crack propagation for long distances prior to arresting. Higher toughness materials may fail by plastic collapse.

In near-neutral pH bicarbonate solutions, it was found steels with higher strength are more susceptible to hydrogen absorption [41].

2.5.2.5 Crack Initiation

Stress corrosion cracks commonly initiate at surface discontinuities (scratches and dents), metallurgical defects (inclusions, second phase particles, grain boundaries, and voids), and primarily localized corrosion sites (pits). Pits may form due to a galvanic effect at metallurgical discontinuities such as grain boundaries [42, 43], inclusions [44, 45], or phase interfaces [46]. The galvanic effect forms between the metallurgical discontinuities and the surrounding matrix, which results in various electrochemical activities and preferential dissolution at the defect location. The presence of millscale on the surface of the metal was found to have an effect on pit initiation, due to the separation of anodic and cathodic sites promoted by the porous structure of the millscale [47].

In the field, SCC cracks were found in broad, shallow corroded areas, where pits were revealed upon microscopic examination. This leads to the belief that near-neutral pH SCC cracks initiate from stress raisers such as corrosion pits [1, 4, 6]. For crack initiation from an existing pit, several conditions must be satisfied. First, the electrochemical conditions should be more active at the base of the pit compared to its walls, to promote pit-base dissolution. Second, the pit geometry should have a high ratio of depth to width, to promote crack transition from pit to crack. Third, the material chemistry and microstructure should support the pit to crack transition by providing an active path for crack propagation (e.g. active grain boundary promotes inter-granular SCC). Finally, the local stresses and strains at the pit base are critical for the pit to crack transition by enhancing the pit base dissolution.

2.5.2.6 Crack Growth

Three main mechanisms of crack growth were identified for near-neutral pH SCC: increase in length and depth due to dissolution, hydrogen-based mechanism, and crack coalescence. While crack coalescence driven by mechanical factors may dominate in the later stages of near-neutral pH SCC crack growth, dissolution and hydrogen-based mechanisms are related to the initiation and early stage crack growth [1, 4, 6].

2.5.2.6.1 Early Stages of Crack Growth

Typically, out of all the SCC cracks initiated on the pipeline, only 5% can grow continuously or repeatedly and achieve rupture, while the rest become dormant through crack tip blunting. Crack dormancy in the field is observed at its initiation and early propagation stages. The growth of the crack is governed by two competing processes: intrinsic blunting of the crack tip, and extrinsic sharpening. The main process governing crack tip blunting is general corrosion (dissolution), the secondary process that may contribute to the blunting process is room temperature creep. Crack re-sharpening occurs through a synergistic interaction of fatigue and hydrogen [48].

2.5.2.6.2 Crack Dissolution Mechanism

The near-neutral pH crack morphology shows lateral corrosion on the crack sides, which suggest that dissolution occurs within the crack. However, laboratory experiments showed that crack growth through dissolution (calculated using Faraday's law) did not correlate well with the actual crack growth on the steel in the near-neutral pH environment [27, 36], and are lower than the minimum crack growth rate calculated based on field observations . As well, King *et al.* mention that the rate of diffusion and migration of carbonate species into the crack from the dilute trapped water solution may not be effective enough to promote rapid crack-tip dissolution. They point out, however, that transport of species into the crack through advective mixing (physical movement of the solution) promoted by cyclic loading, could cause some dissolution within the crack. They also consider the possibility of dissolution of the crack walls or tip caused by rapid Cl^- ions migration into the crack; this dissolution can explain the relatively wide morphology of near-neutral pH SCC cracks, but is insufficient to explain crack growth [49]. This leads to the belief that additional processes are involved in the crack growth mechanism in near-neutral pH environments.

2.5.2.6.3 Effect of Hydrogen on Crack Growth

Hydrogen-based crack growth in near-neutral pH environments is supported by a variety of experiments and field observations [50-56]. King *et al.* [49] showed that the rate of hydrogen evolution reaction and hydrogen permeation through steel is higher in near-neutral pH SCC environmental conditions, where the maximum hydrogen permeation was found at the near-neutral pH. Parkins showed that hydrogen promoted near-neutral pH SCC crack growth through slow-strain-rate experiments, where cracking in the steel occurred due to hydrogen entry [36].

Increase in hydrogen concentration in the steel was shown to promote crack-propagation [53] and reduce the fracture toughness of the steel [54]. Hydrogen charging and tensile stresses did not have a strong effect on active dissolution; based on this observation, it was concluded that hydrogen facilitated dissolution is not a factor in hydrogen-promoted SCC.

Gangolff [56] has categorized the hydrogen source at the crack tip into two categories: Internal-Hydrogen-Assisted Cracking (IHAC), and Hydrogen-EnvironmentAssisted Cracking (HEAC). In HEAC, atomic hydrogen that is produced at the crack surface diffuses towards the crack tip; the hydrogen source can be from hydrogen gas, water vapor, or electrolyte. IHAC, atomic hydrogen is produced at other regions and diffuses towards the crack tip through the crystal lattice. Experiments performed by Chen *et al.* show that the main source of hydrogen at the tip is IHAC [48].

Any factors that may affect hydrogen permeation and absorption will also affect the near-neutral pH SCC process. Stress-concentration is required for hydrogen accumulation, and promotes quasi-cleavage fracture. It has been shown that stressed steel and unloaded steel vary in their surface hydrogen concentration; Capelle showed that application of a gross hoop stress in the pipe wall under the operating pressure of 70 bars accelerates hydrogen absorption in X52, X70, and X100 steels [41]. King *et al.* [49] also demonstrated that mechanical factors enhance the rate of hydrogen permeation, where elastic stresses on C-steel in NS4 trapped water solution demonstrated a hydrogen permeation current 2.5 times higher compared to unloaded specimens.

2.5.2.6.4 Effect of Fatigue on Crack Growth

Several models have been developed to describe crack growth in near-neutral pH environments. One of the models estimates the crack growth rate to be affected by the combined effect of SCC and fatigue cracking; this model is commonly referred to as The Superposition Model [58], and is shown by Equations 2.2 and 2.3.

$$\left(\frac{da}{dN}\right) = \left(\frac{da}{dN}\right)_{fatigue} + \frac{1}{f}\left(\frac{da}{dt}\right)_{SCC} \quad \text{(Equation 2.2)}$$

$$\left(\frac{da}{dN}\right)_{fatigue} = \alpha(\Delta K)^{3.97} \quad \text{(Equation 2.3)}$$

Chen and Sutherby challenge the notion that cracking that occurs in near-neutral pH environments on pipeline steel is in fact SCC [59]. Since crack growth in near neutral pH environments has not been observed under constant stresses, and requires cyclic loading for crack propagation, Chen and Sutherby believe that the driving mechanism for cracking in near-neutral pH environments is CF. Analyzing the Superposition model, Chen and Sutherby comment that under static SCC loading the crack is likely to come to a dormancy state, making the SCC term in the model negligible. They also note that the fatigue term alone does not take into account the effect of frequency, and the maximum stress intensity factor. Chen and Sutherby, therefore, modify the corrosion fatigue model to equation 2.4.

$$\frac{da}{dN} = A\left[\frac{\Delta K^{\alpha} K_{max}^{\beta}}{f^{\gamma}}\right]^{n} \quad \text{(Equation 2.4)}$$

Using this correlation, it is also possible to find the threshold stress that generates crack tip blunting and promotes crack dormancy, this threshold stress is environmentally dependent.

2.5.2.6.5 Later Stages of Crack Growth

Crack growth through crack coalescence is considered to be a crack growth mechanism for later stages of crack growth and crack extension prior to failure; Figure 2-7 is an example of crack coalescence Crack coalescence can occur not only in coplanar cracks that adjoin tips, but also in non-coplanar cracks that are displaced from each other in the hoop direction, in cases when they are sufficiently close. Coplanar cracks that are closely positioned to each other have high odds of interaction between their stress fields. Due to the mixed loading mode (Mode I and Mode II), the crack tips change direction and grow towards each other until they approach coalescence [27].

A condition for the coalescence separation distance is shown in Equation 2.5; this condition has been confirmed both in service and laboratory tests.

$$y \leq 0.14 * 2a \qquad \text{(Equation 2.5)}$$

Where *y* is the separation distance in the hood direction, *2a* is the average length of the adjacent cracks.

Figure 2-7: Cracks Coalescing [4]

2.5.2.6.6 Effect of Environment on Crack Growth

Johnson *et al.* estimated the effect of CO_2 and O_2 on crack propagation in near-neutral pH environments during cyclic growth tests. They performed experiments at OCP and found that increasing the CO_2 level increased the corrosion rate, hydrogen permeation into the steel, and accelerated cyclic crack growth; the most pronounced effect of crack growth was observed between 0% and 5% CO_2 [60]. A similar effect of increase of near-neutral pH SCC susceptibility with increase in CO_2 in solution was observed during SSR tests [61]. The increase in SCC susceptibility with higher CO_2 concentrations is attributed to the higher generation and permeation of hydrogen into the steel.

Egbewande *et al*. [62] studied the growth of surface cracks in near-neutral pH environments under disbonded coatings with an application of CP potential of -1.2 V (SCE) at the OM of the simulated disbondment (10 mm). In those tests, crack dormancy was observed for R ratios of 0.88 and 0.65, while crack growth was observed for R ratios of 0.65 and 0.4. The highest crack growth, and the ultimate rupture, was observed at the OM for both R ratios. The authors discuss the contribution of CP to the high crack growth rate at the OM; where the generated hydrogen could migrate to the most cathodic electrode with imposed CP for charge balance. Nonetheless, as the authors state themselves, pipelines in the field receiving CP current on the order of -1.2 V(SCE) are not likely to develop cracks. Additionally, tape coatings are known to shield CP, therefore, the pipe is very likely to operate in nearly OCP conditions for prolonged periods of time. Therefore, it is of interest to understand the effect of the environment alone in OCP conditions on crack behavior.

2.6 Environment under Disbonded Coatings

While many SCC and corrosion investigations are performed in bulk solutions, it is important to keep in mind that these integrity threats initiate due to coating deterioration and its disbondment from the pipeline. Corrosion of steel under disbonded coatings is considered to be a complex process, as many factors need to be taken into account to understand the formation of the localized environment: charge and mass transfer reactions, potential distribution inside the coating, and a possibility of concentration cells. Numerous laboratory studies and computer simulations have been performed to characterize the electrochemical conditions under disbonded coatings with the presence of CO_2 (representing the conditions for high pH and near-neutral pH SCC) [30, 26, 63-65].

Chen *et al.* showed that in a narrow crevice in aerobic conditions, hydrogen bubbles that were generated at high cathodic potentials inside the disbondment prevented the CP penetration to the bottom of the disbondment. Of particular interest are those experiments that were conducted in anaerobic conditions with CO_2 purging, as those are conditions that closely represent the near-neutral pH conditions on a pipeline [63].

Yan *et al.* simulated a narrow coating crevice with a gap distance of 0.5 mm with 5% CO_2. The presence of CO_2 promoted a near neutral pH environment at the crevice tip even with an application of CP; the crevice opening, on the other hand, formed an alkaline environment [64].

Yan *et al.* also showed that the cathodic current decreased towards the bottom of the disbondment (0.5 mm) by as much as 95% compared to the top in anaerobic conditions, with 5% CO_2 and an applied CP of -1000 mV (SCE) [65]. These tests showed that, similarly to Chen's test, the CP did not fully penetrate to the bottom of the disbondment, regardless of the applied potential (-0.85 V(SCE), -1.0 V(SCE), and -1.2 V(SCE)). Similar results were obtained through a mathematical model to simulate crevice corrosion of pipeline steel developed by Song and Sridhar [66] that showed that CP protection at the crevice bottom was insufficient.

In Yan's experiments [64], interruption of CP promoted a rapid decay to OCP at the opening and a decrease of pH to the near-neutral range in all the positions. A similar experimental setup was performed by the same authors under the same conditions, with a different soil solution [65]. The experimental results showed that even after the interruption of CP, the pH inside the disbondment remained in the alkaline range, despite the continuous purging with CO_2. This finding demonstrates the profound effect of the trapped water solution chemistry on the environment inside the crevice, and the ability of smaller gaps to maintain specific conditions at the steel surface, regardless of the chemistry of the bulk solution outside the crevice.

Additionally, Yan *et al.* [64] performed potentiodynamic polarization measurements and showed that the presence of CO_2 increased the corrosion rate of pipeline steel. Zhang *et al.* [18] obtained similar results showing that the corrosion rate of steel increases with CO_2 partial pressure, performing potenti-dynamic polarization measurements in aerobic conditions with various concentrations of CO_2. Those experimental results, however, did not show the effect of CO_2 partial pressure on the environment inside a disbondment.

Eslami *et al.* [34] showed that in a tensile test with a 10 mm shielding where CP was applied and anaerobic conditions were maintained with constant purging of 5% CO_2, pitting corrosion was most severe at the middle of the disbondment where the CP protection was insufficient, while regions without any CP showed the highest degree of general corrosion.

The fore-mentioned experiments estimating the environmental changes inside the disbondment were performed with an applied CP potential. However, in many cases in the field the CP is shielded by coatings (such as PE), and the corrosion processes happen in OCP conditions. As well, Chen's and Yan's experiments considered a crevice size of small dimensions, while the disbondment gap size between the coating and the steel in the field can be considerably larger.

As well, in order to study SCC, it is essential to incorporate a load component in the experiment to match the stress conditions on the pipe. Egbewande *et al.* studied the growth of SCC cracks in near-neutral pH environments in a setup that contained a disbondment imitation (10 mm disbondment gap size) [62]. However, his studies were more oriented towards understanding the effect of stress on the pipeline, rather than understanding the effect of the localized environment under the coating on crack development.

2.7 Research Objectives

Near-neutral pH SCC and corrosion under disbonded coatings both occure in the event of a coating failure, where the metal is exposed to the ground water solution. Near-neutral pH SCC occurs when cathodic protection does not reach the pipeline, and the pipeline often remains in OCP conditions. Near-neutral pH SCC occurs in dilute carbonate-bicarbonate solutions generated by the presence of CO_2 in the ground in anaerobic conditions.

Despite the wide study of the electrochemical conditions underneath disbonded coatings, little or no research has been previously performed to understand:

1) The corrosion rate under disbonded coatings in OCP conditions

2) The effect of the disbondment gap size on the localized environment under the coating
3) The effect of CO_2 concentration on the corrosion rate inside the disbondment
4) The correlation between the coating condition in the field and the corrosion rate on the underlying pipeline

The goals of this research are outlined as follows:

1. To study the corrosion under disbonded coatings
    a. Under various environmental conditions (CO_2 concentration)
    b. Under various coating deterioration conditions (disbondment gap size)
    c. With and without CP
2. To study the near-neutral pH SCC crack growth and morphology in the initial stage
    a. Under various environmental conditions (CO_2 concentration)
    b. Under various coating deterioration conditions (disbondment gap size)
3. To correlate the findings both for corrosion and near-neutral pH SCC to the processes in the field, through field dig-data analysis
4. To develop prediction-strategies for defects found in the field
5. To promote the knowledge on CP-application strategies

2.8 References

1. Cheng, Y. F. *Stress Corrosion Cracking of Pipelines*. Hoboken, New Jersey: John Wiley & Sons, 2013.
2. Canadian Energy Pipeline Association, n.d. Web. http://www.cepa.com/about-pipelines/why-pipelines
3. Marcus, S. Oil and gas pipeline in Canada, *J. Oil Gas* 2, 15, 2009.
4. *Stress Corrosion Cracking on Canadian Oil and Gas Pipelines,* Report of the Inquiry, National Energy Board (NEB), 1996.
5. Kiefner, J.F and Rosenfeld M.J. The Role of Pipeline Age in Pipeline Safety*, INGAA Foundation Report* No 2012.04, 2012.
6. *Stress Corrosion Cracking Recommended Practices*. Rep. 2nd ed. Canadian Energy Pipeline Association (CEPA). 2007.

7. Beavers, J. A. "Integrity Management of Natural Gas And Petroleum Pipelines Subject To Stress Corrosion Cracking." *Corrosion* 70.1 (2014)
8. Leeds, J. M., and S. S. Leeds. "Coating Properties and Test Procedures." *Pipeline and Gas* 237.3. 2010.
9. Papavinasam, S. *Corrosion Control in the Oil and Gas Industry*. Burlington: Elsevier Science, 2013.
10. *Dissecting Coating Disbondments*. Rep. no. 101131, Det Norse Veritas (DNV). 2009.
11. Baker, M. *Stress Corrosion Cracking Study- Final Report*. Rep, 2005.
12. Varughese, K. "Coatings and Cathodic Protection for Underground Pipelines - What a Corrosion Engineer Should Know." Review. DuPont Coatings. Web.
13. Callister, W. D., and Rethwisch D. G. *Fundamentals of Materials Science and Engineering: An Integrated Approach*. Hoboken, NJ: Wiley, 2012.
14. Beavers, J. A. and Thompson, N. "External Corrosion of Oil and Natural Gas Pipelines" *ASM Handbook*, Volume 13C, Corrosion: Environments and Industries (#05145)
15. Focus on Safety and Environment: A Comparative Analysis of Pipeline Performance 2000-2009. National Energy Board (NEB), 2009.
16. Sherar, B. W. A. *The Effect of the Environment on the Corrosion Products and Corrosion Rates on Gas Transmission Pipelines*. PhD Thesis. London, Ontario, 2011.
17. Rozenfeld I. L. *Corrosion Inhibitors*. McGraw Hill, New York, p. 161. 1981.
18. Zhang, L., Li, X.G., Du, C.W., and Cheng, Y.F. "Corrosion and Stress Corrosion Cracking Behaviour of X70 Pipeline Steel in a CO_2-Containing Solution." *Journal of Materials Engineering and Performance* 18.3 (2009): 319-23.
19. Yan, M., Wang, J., Han, E., and Ke, W. "Local Environment under Simulated Disbonded Coating on Steel Pipelines in Soil Solution." *Corrosion Science* 50.5 (2008): 1331-339.
20. Nesic, S. "Carbon Dioxide Corrosion of Mild Steel", *Uhlig's Corrosion Handbook, Third Edition*, Edited by R. Winston Revie, 2011.
21. Niu, L., and Cheng, Y.F. "Corrosion Behaviour of X-70 Pipe Steel in Near-Neutral pH Solution." *Applied Surface Science* 253 (2007) 8626–8631.

22. Fajardo, V., Brown, B., Young, D.S. “Study of the Solubility of Iron Carbonate in the Presence of Acetic Acid Using an EQCM”. *NACE International 2013*, 2452.
23. Nordsveen, M., S. Nešić, R. Nyborg, and A. Stangeland. "A Mechanistic Model for Carbon Dioxide Corrosion of Mild Steel in the Presence of Protective Iron Carbonate Films—Part 1: Theory and Verification." *Corrosion* 59.5 (2003): 443.
24. Jones, D. A. *Principles and Prevention of Corrosion*. Upper Saddle River, NJ: Prentice Hall, 1996. Print.
25. Jenney, C. L. O’Brien, A. *Welding Handbook, Volume 1 - Welding Science and Technology* (9th Edition). American Welding Society (AWS). Online version available at: p. 150. 2001.
26. Ahmad, Z. *Principles of Corrosion Engineering and Corrosion Control*. Boston, MA: Elsevier/BH, 2006.
27. Parkins, R.N. “A Review of Stress Corrosion Cracking of High Pressure Gas Pipelines.”*Corrosion 2000*, Paper 363, NACE, Houston, TX, 2000.
28. Asher, S. L., Leis, B., Colwell, J., Singh, P. M. “Investigating a Mechanism for Transgranular Stress Corrosion Cracking on Buried Pipelines in Near-neutral pH Environments”. *Corrosion* 63, 932–939. 2007.
29. Parkins, R.N. “Factors Influencing Stress Corrosion Crack Growth Kinetics.” *Corrosion*. Vol. 43. pp. 130-138. 1987.
30. Been, J., King, F., Yang, L., Song, F., Sridhar, N. “The Role of Coatings in the Generation of High- and Near-neutral pH Environments that Promote Environmentally Assisted Cracking.” *Corrosion 2005*, Paper 05167, NACE, Houston, TX, 2005.
31. Van Boven, G., Chen, W., Rogge, R. “The Role of Residual Stress in Neutral pH Stress Corrosion Cracking of Pipeline Steels: I. Pitting and Cracking Occurrence.” *Acta Mater*. 55, 29–42, 2007.
32. Van Boven, G., Chen, W., Rogge, R. “The Role of Residual Stress in Neutral pH Stress Corrosion Cracking of Pipeline Steels: Part II. Crack Dormancy.” *Acta Mater*. 55, 43–53, 2007.

33. Sutherby, R., Jack, T., Van Boven, G., and Wilmott, M. "CEPA Study on Characterization of Pipeline Pressure Fluctuations in Terms Relevant to Stress Corrosion Cracking." *Proc. IPC/2000*, Calgary, Canada, 2000.
34. Eslami, A., Kania, R., Worthingham, B., Van Boven, G., Eadie, R., and Chen, W. "Effect of CO_2 and R-ratio on Near-neutral pH Stress Corrosion Cracking Initiation under a Disbonded Coating of Pipeline Steel." *Corros. Sci*. 53, 2318–2327, 2011.
35. Fang, B., Eadie, R., Chen, W., and Elboujdaini, M. "Pit to Crack Transition in X-52 Pipeline Steel in Near-neutral pH Environment: 1. Formation of Blunt Cracks from Pits under cyclic loading, *Corros. Eng. Sci. Technol*. 45, 302–312, 2010.
36. Parkins, R.N. , Blanchard, W. K., Delanty, B. S. "Transgranular Stress Corrosion Cracking of High Pressure Pipelines in Contact with Solutions of Near-neutral pH." *Corrosion 50, 394–408*, 1994.
37. Jack, T.R., B. Erno, K. Krist, and R.R. Fessler. "Generation of Near Neutral pH and High pH SCC Environments on Buried Pipelines". *NACE International Corrosion 2000*. Paper No. 00362.
38. Delanty, B. and O'Beirne, J.. "Major Field Study Compares Pipeline SCC with Coatings," *Oil & Gas Journal*, 90 (24), pp. 39-44. 1992
39. Cheng, Y.F. "Fundamentals of Hydrogen Evolution Reaction and Its Implications on Near-neutral PH Stress Corrosion Cracking of Pipelines." *Electrochimica Acta* 52.7: 2661-667. 2007.
40. Delanty, B.S., and Marr, J.E. " Stress Corrosion Cracking Severity Rating Model". *Proc. International Conference on Pipeline Reliability*, CANMET, Ottawa, Ontario, Canada, 1992.
41. Capelle, J., Dmytrakh, I., and Pluvinage, G. "Comparative Assessment of Electrochemical Hydrogen Absorption by Pipeline Steels with Different Strength." *Corros. Sci. 52*, 1554–1559, 2010.
42. Chu, R., Chen, W., Wang, S. H., King, F., Jack, T. R., and Fessler R.R. "Microstructure Dependence of Stress Corrosion Cracking Initiation in X-65 Pipeline Steel Exposed to a Near-neutral pH Soil Environment." *Corrosion* 60, 275–283, 2004.

43. Liu, Z. Y., Li, X.G., Cheng, Y.F. " In-situ Characterization of the Electrochemistry of Grain and Grain Boundary of an X70 Steel in a Near-neutral pH Solution." *Electrochem. Commun.*12, 936–938, 2010.
44. Elboujdaini, M., Wang, Y. Z., Revie, R.W., Parkins, R.N., and Shehata, M.T. " Stress Corrosion Crack Initiation Processes: Pitting and Microcrack Coalescence". *Corrosion 2000*, Paper 00379, NACE, Houston, TX, 2000.
45. Jin, T.Y., Cheng, Y.F. "In-situ Characterization by Localized Electrochemical Impedance Spectroscopy of the Electrochemical Activity of Microscopic Inclusions in an X100 Steel." *Corros. Sci.* 53, 850–853, 2011.
46. Kushida, T., Nose, K., Asahi, H., Kimura, M., Yamane, Y., Endo, S., and Kawano, H. "Effects of Metallurgical Factors and Test Conditions on Near-neutral pH SCC of Pipeline Steels." *Corrosion 2001*, Paper 01213, NACE, Houston, TX, 2001.
47. Qin, Z., Demko, B., Noel, J., Shoesmith, D., King, F.,Worthingham, R., and Keith, K. "Localized Dissolution of Mill Scale-covered Pipeline Steel Surfaces." *Corrosion 60*, 906–914, 2004.
48. Chen, W., Kania, R., Worthingham, R. and Van Boven, G. "Transgranular Crack Growth in the Pipeline Steels Exposed to Near-neutral pH Soil Aqueous Solutions: The Role of Hydrogen." *Acta Materialia* 57: 6200-6214, 2009.
49. King, F., Jack, T., Chen, W., Wilmott, M., and Fessler, R. "Mechanistic Studies of Initiation and Early Stage Crack Growth for Near-neutral pH SCC on Pipelines." *Corrosion 2000*, Paper No. 00361, 2000.
50. W. Chen, F. King, E. Vokes, Characteristics of near-neutral-pH stress corrosion cracks in an X-65 pipeline, Corrosion 58 (2002) 267–275.
51. Asher, S., Singh, P.M. "Hydrogen Production and Permeation of X-65 Pipeline Steel in Near-neutral pH Environments." *Corrosion 2008*, NACE International, Houston, Paper No. 08411, 2008.
52. Lu, B.T., Luo, J.L., Norton, P.R., and Ma, H.Y." Effect of Dissolved Hydrogen and Elastic and Plastic Deformation on Active Dissolution of Pipeline Steel in Anaerobic Groundwater of Near-neutral pH." *Acta Mater*. 57: 41–49, 2009.

53. Lu, B.T., Luo, J.L., and Norton, P.R. “Environmentally Assisted Cracking Mechanism of Pipeline Steel in Near-neutral pH Groundwater.” *Corros. Sci.* 52: 1787– 1795, 2010.
54. Wang, R., “Effects of Hydrogen on the Fracture Toughness of a X70 Pipeline Steel.” *Corros. Sci.* 51: 2803–2810, 2009.
55. Lu, B.T.,Qiao, L.J., Luo, J.L., Gao,K.W., *Philosophical Magazine, 91(2)(2011)208–228*
56. Gangloff, R.P. “Hydrogen-assisted Cracking, in: Milne, I., Ritchie, R.O., Karihaloo, B., (Eds.), *Comprehensive Structure Integrity, volume 6: Environmentally-Assisted Fracture*, Elsevier, Oxford, pp. 31–34, 2003.
57. Gu, B., Luo, J., and Mao, X. “Hydrogen-Facilitated Anodic Dissolution-Type Stress Corrosion Cracking of Pipeline Steels in Near-Neutral pH Solution.” *Corrosion*: January 1999, Vol. 55, No. 1, pp. 96-106, 1999.
58. Zhang, X.Y. , Lambert, S.B., Sutherby, R., and Plumtree, A. “Transgranular Stress Corrosion Cracking of X-60 Pipeline Steel in Simulated Ground Water”, *Corrosion*. Vol. 55. pp. 297-305, 1999.
59. Chen, W., and R. L. Sutherby. "Crack Growth Behavior of Pipeline Steel in Near-Neutral PH Soil Environments." *Metallurgical and Materials Transactions A* 38.6: 1260-268, 2007.
60. Johnson, J. T., Beavers, J. A., Durr, C. L., and Delanty, B. S. “ Effects of O_2 and CO_2 on Near-Neutral-pH and Stress Corrosion Crack Propagation”. *NACE International*, 2000.
61. Parkins, R.N. “Transgranular Stress Corrosion Cracking of High-Pressure Pipelines in Contact with Near Neutral pH Solutions,” *8th Symp. Line Pipe Research*, Catalog no. L51680 (Washington, DC: American Gas Association, 1993), p. 16-1.
62. Egbewande, A., Eslami, A., Chen, W., Worthingham, R., Kania, R., VanBoven, G. “Growth of Surface Cracks in Near-neutral pH Environments under Disbonded Coatings”, *Proceedings of IPC 2010*, Calgary, 2010.
63. Chen, X., Du, C., Li, X., and Huang, Y. “Effects of Cathodic Potential on the Local Electrochemical Environment under a Disbonded Coating.” *J Appl Electrochem* 39: 697-704, 2009.

64. Yan, M., Wang, J., Han, E., and Ke, W.”Local Environment under Simulated Disbonded Coating on Steel Pipelines in Soil Solution”. *Corrosion Science*, 50 (5), pp. 1331—1339, 2008.
65. Yan, M.C., Wang, J. Q., Han, E. H., and Ke, W. “Electrochemical Measurements Using Combination Micro-Electrodes in Crevice Simulating Disbonded of Pipeline Coatings under Cathodic Protection”, *Corrosion Engineering Science and Technology*, 42-1, 42-49, 2007.
66. Song, F.M., and N. Sridhar. "Modeling Pipeline Crevice Corrosion under a Disbonded Coating with or without Cathodic Protection under Transient and Steady State Conditions." *Corrosion Science* 50.1: 70-83, 2008.

CHAPTER 3 : EXPERIMENTAL METHODS

This chapter outlines the experimental methods used for obtaining the results discussed in Chapter 4 and Chapter 7. Chapter 4 discusses the experimental study performed to understand the corrosion process under a disbonded coating, and Chapter 7 discusses the experimental study performed to enhance the understanding on shallow crack growth in near-neutral pH conditions under a disbonded coating. As Chapter 5 and Chapter 6 focus on the statistical analysis on field data, the approach and methods utilized in those chapters are described within them, and will not be provided in this chapter.

3.1 Understanding Anaerobic Corrosion under Disbonded Coatings (Chapter 4)

The objective of this study was to understand the corrosion process under disbonded coatings in various environmental settings and under various coating conditions. In particular, it was of interest to understand the differences in corrosion rate at different positions from the Open Mouth (OM) of the coating, to check for a possibility of a concentration cell formation. The corrosion rate assessment was performed by employing the weight loss method, described below.

An additional goal of this experiment was to understand the effect of the underground environment on the corrosion process. Therefore, the test environment remained isolated throughout the duration of the test to maintain constant environmental conditions similar to the environment to which buried pipelines are exposed.

3.1.1 Corrosion Rate Measurement

Assessment and verification of a specimen’s corrosion rate can be performed through weight-loss testing, where a specimen is exposed to the test environment for a certain period of time, and its weight loss is calculated upon its removal from the test environment. Thus, the corrosion rate obtained through weight loss calculations represents the average corrosion rate of the specimen during its exposure time to the test environment, and is expressed in units of mils/year (mpy) or mm/y.

Corrosion rate assessment through weight loss is considered to be a reliable technique, commonly used both in the field and in the lab. This technique was derived from Faraday's law, and uses Equation 3.1.

$$CR = \frac{W_2 - W_1}{t * \rho * A} \qquad \text{(Equation 3.1)}$$

where W_2 and W_1 are the initial and final weights, respectfully; t is the time, ρ is the density of the metal, and A is the area of the coupon exposed to the solution [1].

In this study, the initial and final weight of the metal coupons were measured carefully after cleaning the coupons from dirt particles in ethanol in an ultrasonic bath.

3.1.2 Simulation of the Underground Pipeline Environment

A near-neutral pH underground pipeline environment, characteristic of sites where SCC and corrosion were found, was simulated with the use of a C2 synthetic soil solution [2]. The C2 solution composition is provided in Chapter 4 in Table 4-2. The solution was purged with 5% CO_2- N_2 for at least 48 hours prior to testing while its pH reached a stable value of 6.3.

The soil adjacent to the pipeline is known to contain various concentration of CO_2 from decayed organic matter; the CO_2 concentration varies seasonally and regionally, typically between 4%-23% CO_2 [3].

In this experiment, the C2 soil solution was continuously purged with different CO_2 concentrations for each set of tests: 2% CO_2- N_2, 5% CO_2-N_2, and 20% CO_2-N_2. 2% CO_2 and 20% CO_2 were used to simulate the lower and the upper bound of the CO_2 concentration in the ground, and 5% CO_2 was used to imitate the average concentration. A concentration of 20% CO_2 in the ground is not commonly observed and corresponds to an extreme concentration of CO_2 (upper bound).

3.1.3 Imitation of a Coating Disbondment on a Pipeline for Corrosion Tests

Sealed corrosion cells were used for generation of an isolated environment from oxygen. The coating conditions on a pipeline were simulated by placing a plastic shielding plate over metal, imitating a coating disbondment. The corrosion rate of the metal was assessed through the weight-loss technique; therefore, the metal that was used in the experiment was cut into square coupons, for weight loss measurements. The plastic assembly containing the metal coupons was referred to as “coupon holder”. Each of the cell components is described below.

3.1.3.1 Corrosion Cell

The design of the corrosion cell included a solid Poly Methyl Methacrylate (PMMA) cell body containing the test ground water solution and the coupon holder, with a gas inlet and an outlet opening. A schematic of the cell assembly is shown in Figure 3-1.

From Figure 3-1 it can be seen that the cell had multiple inlets and outlets. The opening at the top on the lid of the cell served as a removable plug to collect small-volume solution samples and to insert micro-electrodes into the cell for in-situ pH measurements. The gas inlet tube extended to the bottom of the cell to insure that bubbling occurred from the bottom of the cell and that the solution in the cell was saturated with the bubbling gas at all the positions. The coupon holder was inserted into a cell prior to filling it with the test solution. The test solution was poured into the cell through the gas inlet tube in a manner that avoided oxygen contamination after the cell was sealed with silicone to maintain an anaerobic environment.

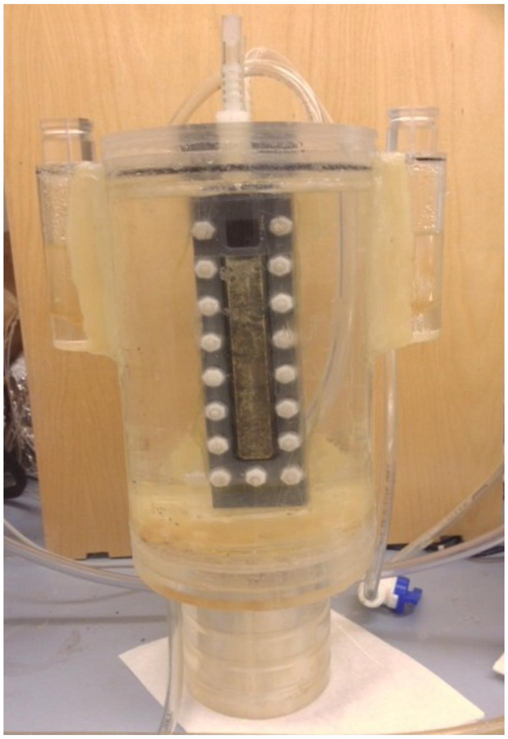

Figure 3-1: PMMA Corrosion Cell Used in the Experiment

3.1.3.2 Coupon Holder

The “coupon holder’ assembly was designed to imitate a coating adhesion failure where a coating disbondment gap was created between the pipeline material and the delaminated coating [4]. Such coating failures are characteristic of tape coatings in the field. The coupon holder contained metal coupons that were used to characterize the corrosion of the metal under a disbonded coating. As well, the design of the coupon holder permitted the characterization of the electrochemical conditions (pH, conductivity) inside and outside the disbondment, as well as elemental analysis.

The design of the coupon holder incorporated seven coupons: six coupons located under a shielding imitating a delaminated coating, and one unshielded coupon. The unshielded coupon was fully exposed to the bulk solution, imitating the location of a coating holiday on a pipeline where the metal is exposed to the environment of the underground soil. The shielded coupons imitated the pipeline location subjected to trapped water solution under a disbonded coating. The coating disbondment gap sizes varied between 2 mm, 5 mm, 10 mm, and no shielding, to explore the conditions under smaller gap sizes, and compare them to medium, and infinitely large (no shielding) gap sizes.

The coupon holder, shown schematically in Figure 3-2, is comprised of a solid PMMA back, a PMMA part with seven square openings, and a shielding plate with an opening at the top, held together with acetal rods and nuts. In an unpublished study, PMMA was found similar to High Density Polyethylene (HDPE) and Low Density Polyethylene (LDPE) coatings in their low CO_2 permeability and high electrical resistivity.

The gap between the coupon holder and the shielding plate varied from 10 mm to 2 mm, simulating a coating de-cohesion (the holiday) and a disbondment (the shielded area) on the pipe surface. Due to the low gas permeability of the PMMA shielding, the gas entrance to the disbondement was only via the opening at the top of the coupon holder, representing the OM (only one face of each specimen was exposed to the solution in the gap (exposed area 1.9 cm^2).

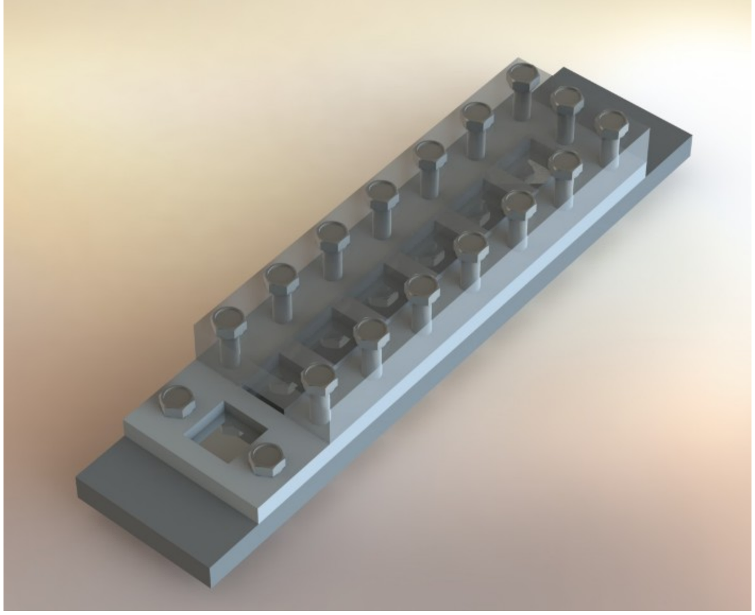

Figure 3-2: Coupon Holder Assembly

3.1.3.3 Metal Coupons

In each experiment, seven X-65 square coupons with a 1.9 cm side and a 2 mm thickess were used. The chemical composition of X-65 pipeline steel is presented in Chapter 4 in Table 4-1. The coupons were machined from sections of X-65 pipeline steel from failed pipeline sections obtained from the field, ground to 600 grit, immersed into an ethanol ultrasonic bath for 2 minutes, and quickly dried with air.

Since the corrosion analysis is based on the weight loss method, the initial weight of the coupons was recorded prior to their placement in the coupon holder; the coupons placed in the coupon holder were connected to each other. After the coupons' initial weight was recorded, they were placed into the coupon holder connected to each other.

3.1.4 Sample Preparation for SEM Characterization

Scanning Electron Microscopy (SEM) analysis was performed to explore the corrosion effect on the surface of the specimens at different positions from the OM of the disbondment. For the SEM characterization, the samples were immersed in an ultrasonic bath with a rust-removing solution for a duration of 2 minutes, after which they were immersed into an ethanol bath for 3 minutes to clean off the rust-removing solution. The chemical composition of the rust-removing solution was as follows: 100 ml H_2O, 4 ml Cis-2-butene-1,4-diol, and 3 ml HCl.

3.1.5 Electrochemical Characterization

In order to characterize the conditions under a coating disbondment, pH and solution resistivity measurements were performed. The pH was measured at the OM, middle, and bottom of the disbondment, by immersing the measuring electrode inside the disbondment.

3.1.5.1 pH Measurements

A common way to measure the pH of an electrolyte is with a use of an electrochemical cell consisting of a measuring electrode and a reference electrode. The potential of the measuring electrode is directly proportional to the pH of the electrolyte, while the potential of the reference electrode if independent of pH. Commonly, the system is first calibrated by placing the electrodes in a buffer solution with a known pH, obtaining the voltage of the cell. Since the cell voltage is a linear function of pH, only two calibrations are required in two solutions with different pH. Following the calibration, the cell voltage of the desired solution is measured, and its pH value is obtained from the pH-voltage calibration curve.

pH characterization was performed with the use of combination microelectrodes, that combine measuring and reference cells in a single probe. The calibration micro-electrodes had a diameter less than 1.6 mm, and a response time shorter than 10 sec. The measurements were all performed at room temperature ±3°C; therefore, the temperature effect on the obtained results is estimated to be negligible. Two common sources of error may be related to the entry of oxygen into the solution during the measurement, and mixing of the solution at the different positions inside the disbondment gap (top, middle, and bottom) as the electrode was inserted into the disbondment. Figure 3-3 shows the combination microelectrodes immersed into a KCl storage solution.

3.1.5.2 Resistivity Measurements

The resistivity measurements were performed with an Accumat conductivity probe calibrated in a commercial Fisher Scientific solution with a known resistivity, and immersed into the solution of interest. Figure 3-4 shows the Accumat electrode for resistivity measurements.

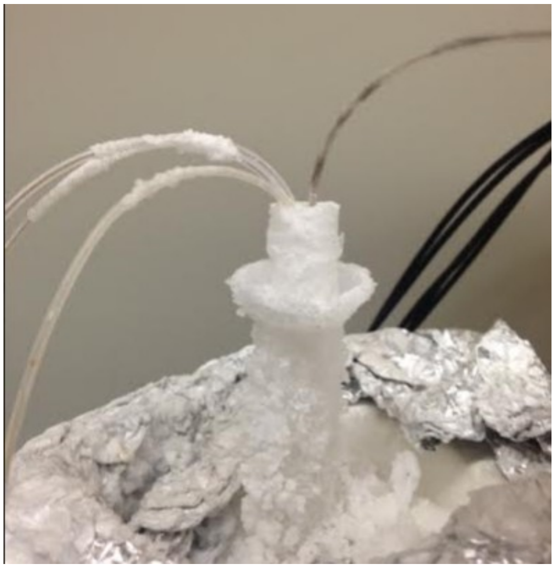

Figure 3-3: Combination Microelectrodes Immersed into a KCl Storage Solution

Figure 3-4: Accument Electrode for Resistivity Measurements [4]

3.2 Understanding Surface Crack Morphologies under Disbonded Coatings (Chapter 7)

The objective of this experimental setup was to study the environment under a disbonded coating (in particular the effect of corrosion) on the crack morphology under disbonded coating, rather than the effect of mechanical loading parameters. Therefore, the chosen mechanical loading parameters were mild, and were not expected to promote fast crack propagation. The isolation of the experimental environment was performed in the same manner described in Section 3.1, with the use of a corrosion cell. The design of the corrosion cell, with the various cell components, is shown in Chapter 6 in Figure 6-1.

The environment in this setup was similar to the one described in section 3.1.2, where a C2 simulated ground water solution was used, and purged with 5% CO_2.

3.2.1 Imitation of a Coating Disbondment on a Pipeline for Tensile Tests

The corrosion cell used in this set of experiments contained a PMMA shielding imitating a coating disbondment with a gap between the coating and the metal specimen; the gap size varied between 2 mm (narrower coating disbondment gap) and 10 mm (wider coating disbondment gap). The shielding was firmly attached to the bottom of the cell with acetal screws, which enabled solution and gas penetration into the disbondment gap only from the top of the disbondment (OM). The solution outside the disbondment, between the shielding and the metal specimen, imitated trapped water solution, while the solution in the cell imitated bulk ground water in the soil.

3.2.2 Sample Preparation for the Experiment

The tensile specimens were machined out of X60 pipeline sections taken from the field after experiencing a service failure; only undamaged sections were used for specimen fabrication. The tensile specimens had three reduced sections (gauges); the samples were designed to have three gauge sections to understand the crack behavior in three locations under a disbonded coating: top (OM), middle, and bottom. The gauge width was 23 mm, and its initial thickness was 6.4 mm, and a gauge area of 147 mm^2.

4.8 mm Electrical Discharge Machining (EDM) semi-circular notches were machined in the middle of each gauge to facilitate pre-crack initiation, the circle diameter was 2.4 mm. The combined length of the pre-fatigue cracks from both sides of the machined notch was 1.6 mm.

After the pre-fatigue cracks were produced, the front surface of the tensile specimen was machine-ground until the machined EDM notch were completely ground off. The sample thickness after grinding the machined notches was ~5.3 mm. The pre-cracks' lengths were estimated with the use of an optical microscope, and varied between different locations on a tensile specimen and different tensile specimens. The specimen design before and after grinding of the front face is shown in Chapter 6 in Figure 6-2.

The back of the specimen was coated with epoxy to simulate realistic field conditions, where only one face of the pipeline is exposed to the corrosive underground environment.

3.2.3 Sample Preparation for SEM Characterization

After the experiment ended and the specimen was extracted from the corrosion cell, it was cut into smaller sections that contained the gauges and the cracks (top, middle, and bottom), in order to be able to fit the sample into the Scanning Electron Microscope (SEM) to observe the sample surface. The following images were taken:

1) **The cracks' front surface after cleaning the sample in a rust-remover solution**

   In order to observe the morphology of the crack surface to compare the extent of corrosion at the different position from the OM, the oxides adhering to the metal surface were removed. The cut gauges were immersed into an oxide remover solution (with 100 ml water/4 ml Cis-2-butene-1,4-diol/3 ml HCl) for 3 minutes in an ultrasonic bath, followed by an ethanol ultrasonic bath, then they were dried with hot air.

2) **The cracks' front surface after polishing**

   In order to observe the crack morphology (width and length), the samples were polished to a mirror finish. The sample was polished with 6 µm, 3 µm, 1 µm oil-based silica, and with 0.05 µm silica polishes. Afterwards, the samples were immersed into an ethanol ultrasonic bath for 10 minutes, to extract the polishing residue out of the crack, and thoroughly dried with hot air.

3) **The cracks' front surface after etching the polished surface**

   In order to observe the crack morphology and reveal the microstructure of the material, the sample surface was etched with 3% Nital solution (3% Nitric acid- balance ethanol) for ~15 sec. After etching, the sample was washed in ethanol and dried.

4) **The cracks' cross-sectional surface after polishing**

   In order to observe the crack morphology in the depth direction, the sample was sectioned vertically in the middle of the gauge section with the use of the wire EDM technique. The depth surface was polished in a similar manner described for the front surface polishing in 3.

5) The cracks' depth surface after etching the polished surface

In order to observe the crack morphology and reveal the microstructure of the material in the depth direction, the polished depth surface was etched with 3% Nital, in a similar manner described for the front surface in 3.

6) The cracks' morphology of the fractured surface

In order to obtain a micrograph of the fracture surface and provide a morphological characteristic of it, the samples were fractured by immersing them into liquid nitrogen for at least 20 minutes, and fracturing them by applying force with a hammer on the back of the sample.

In order to fracture the specimens with the shallow crack, a special assembly was designed to place and hold the specimen. The specimen was hit at a 45˚ angle at the corner opposite to the crack. The cross-sectional area of the specimen was reduced by filing the edges of the specimen on the opposite side of the crack to facilitate the fracture of the specimen.

3.2.4 Electrochemical Characterization

The electrochemical characterization, in terms of pH and resistivity analysis, was performed at the end of the test to avoid test disturbance and oxygen penetration into the system.

3.2.4.1 pH Measurement

The pH at the different positions inside the disbondment was measured in the same manner described in Section 3.1.4.2; however, instead of inserting the electrodes into the cell, the solution from the positions of interest inside the disbondment was extracted with a pipette and its pH was measured with the electrodes outside the cell.

3.3 References

1. Schweitzer, P.A. *Corrosion and Corrosion Protection Handbook*. New York: Dekker, 1989

2. Chen, W., and R. Sutherby. "Crack Growth Behavior of Pipeline Steel in Near-Neutral PH Soil Environments." *METALLURGICAL AND MATERIALS TRANSACTIONS A* 38A.June 2007 (n.d.): 1260-268.
3. Delanty, B. and O'Beirne, J. “Major Field Study Compares Pipeline SCC with Coatings,” Oil & Gas Journal, 90 (24), pp. 39-44, 1992.
4. Eslami, A. "Near-neutral PH Stress Corrosion Crack Initiation under Simulated Coating Disbondment." Thesis. University of Alberta, 2012
5. Agbewande, A. “Growth Behavior of Surface Cracks in Pipeline Steels Exposed to Near-neutral pH Environments.” Thesis. University of Alberta, 2013.

CHAPTER 4 : UNDERSTANDING ANAEROBIC CORROSION UNDER DISBONDED COATINGS

4.1 Introduction

Underground pipelines are protected from environmental corrosion by a dual defense line, where a non-metallic coating is the primary protection system, and Cathodic Protection (CP) is the secondary. The role of a protective coating is to protect the pipeline steel from a corrosive soil environment while reducing CP current requirements. Coating failure may result in the pipeline's exposure to the ground water electrolyte and corrosive species; in that event, CP becomes the primary protection system. However, the effectiveness of the CP can be limited by highly insulating CP-shielding coatings (usually tape coatings), or high resistivity ground water solutions [1-3].

Two main coating failure types are loss of cohesion and loss of adhesion. Loss of cohesion refers to tearing of the coating by cracking and breaking off the pipeline surface. Loss of cohesion occurs more commonly in brittle coatings (e.g. asphalt and coal tar) that have good adhesion to the substrate. Loss of adhesion refers to the coating's delamination from the pipeline, promoted by degradation of the organic components in the coating, permeation of water and other species under the coating. The extent of the coating disbondment from the pipeline is determined by the conditions in the field (pH, CP, cyclic wetting and drying, temperature, ground water composition) and the nature of the coating itself [4]. Additionally, coating disbondments on the pipeline can exist prior to the pipe's placement in the field due to improper surface preparation or resulting from the geometry of the wrapped coating at the welds ("tenting") [5]

In an event of coating failure, when the CP protection is insufficient, the integrity of the pipeline in contact with the ground water electrolytes may be compromised through various types of corrosion and Stress Corrosion Cracking (SCC). Due to the shielding of CP, a failure of coating rupture prior to disbondment (loss of cohesion) is generally preferred, where the CP can reach the exposed steel. This statement is supported by the fact that SCC is not commonly found in areas of large coating disbondments and holidays. It is, however, found close to longitudinal seam welds and girth welds where coating tenting generates small disbondments (less than 10 cm wide) and other areas of minor disbondment along the pipe [6].

SCC is believed to be initiated and developed under the combined effect of stress, material, and environment [5]. Two forms of SCC were identified in pipeline steel classified based on the environment in which they develop. High pH SCC initiates in concentrated carbonate-bicarbonate solutions in an electrolyte pH range of 8.5 to 10.5, while near-neutral pH SCC initiates in dilute carbonate solutions with dissolved CO_2 in the soil (4%-23%), in a pH range of 5.5 to 7.5 [5-7]. Corrosion plays an important part in SCC, as it may affect the initiation, propagation, and arrest of SCC cracks, through pit formation (crack initiation sites) [5], hydrogen generation (crack tip embrittlement), and crack tip dissolution (crack tip blunting) [8]. CO_2 concentration has been found to have an effect on the corrosion rate and SCC crack growth [9, 10].

Since coatings are the first line of defense which determines the CP requirements and the magnitude of expenditures associated with maintaining the pipeline integrity, understanding the consequences of their disbondment (in terms of the generated environment and corrosion mechanisms and rate) is important. Numerous laboratory studies and computer simulations have been performed to characterize the electrochemical conditions under disbonded coatings with the presence of CO_2 [3, 11-13]. Yan *et al.* [12] showed that in aerated conditions with 5% CO_2, the presence of CO_2 promoted a near neutral pH environment at the crevice tip even with an application of CP. They also showed through potentiodynamic polarization measurements that the presence of CO_2 increased the corrosion rate of pipeline steel; similar results were obtained by Zhang *et al.* [14].

The experiments mentioned above were performed in aerobic conditions, whereas near-neutral pH SCC and anaerobic corrosion occurs in de-aerated conditions [3]. Several investigations focused on understanding the conditions under disbonded coatings in anaerobic conditions. Yan *et al.* [11] showed that the cathodic current decreased towards the bottom of a disbondment by as much as 95% compared to the top in anaerobic conditions, with 5% CO_2 and an applied CP of -1000 mVSCE. Eslami *et al.* [2] showed that with an application of CP in anaerobic conditions with 5% CO_2, pitting was most severe at the middle of the disbondment where the CP protection was insufficient, while regions without any CP showed the highest degree of general corrosion. Despite the wide study of the electrochemical conditions underneath disbonded coatings, little information has been provided regarding the correlation between the disbondment gap size the corrosion rate and location underneath disbonded coatings. The objective of this study was to evaluate the corrosion rate under disbonded tape coating gaps of various sizes and understand the possible corrosion mechanism in anaerobic conditions.

One of the main objectives of this study is to develop an understanding of the correlation between near-neutral pH SCC and corrosion under disbonded coatings. Therefore, the experimental conditions in this study were closely correlated to conditions relating to near-neutral pH SCC. The corrosion evaluation was performed at OCP conditions with different concentrations of CO_2, simulating soils with various concentrations of carbon dioxide (2% CO_2 to 20% CO_2) (characteristic to different seasons and environments) [15]. The choice to perform the experiments in OCP conditions was based on the fact that tape coatings (under which SCC and general corrosion are commonly found) often shield CP.

4.1.1 Objective

Despite the wide study of the electrochemical conditions underneath disbonded coatings, little information has been provided regarding the correlation between the disbondment gap size the corrosion rate and location underneath disbonded coatings. The objective of this study was to evaluate the corrosion rate under disbonded tape coating gaps of various sizes and understand the possible corrosion mechanism in anerobic conditions. Specifically, it was of great interest to understand the mechanism behind corrosion under tape wrinkles where deep corrosion regions are found closely adjacent to uncorroded regions, as the one shown in Figure 4-1. One of the main objectives of this study is to develop an understanding of the correlation between near-neutral pH SCC and corrosion under disbonded coatings. Therefore, the experimental conditions in this study were closely correlated to conditions relating to near-neutral pH SCC. The corrosion evaluation was performed in OCP conditions with different concentrations of CO_2, simulating soils with various concentrations of carbon dioxide (2% CO_2 to 20% CO_2) (characteristic to different seasons and environments). The choice to perform the experiments in OCP conditions was based on the fact that tape coatings (under which SCC and general corrosion are commonly found) shield CP.

Figure 4-1: Corrosion under a Disbonded Coating

The experiments were performed inside corrosion cells, where a plastic coupon holder containing metal coupons was inserted; the coupon holder simulated a location on a buried pipeline surface where coating failure has occurred. Each of the cell components is described below.

4.2 Experimental Setup

4.2.1 Corrosion Cell

In the experiments, Poly Methyl Methacrylate (PMMA) corrosion cells were used. The design of the cell included a solid Poly Methyl Methacrylate (PMMA) cell body where the coupon holder was inserted, with a gas inlet and an outlet opening. The cell assembly is shown in Figure 4-2.

The cell had an opening at the top with a removable plug to collect small-volume solution samples and to insert micro-electrodes into the cell for in-situ pH measurements. The gas inlet tube extended to the bottom of the cell to insure that the solution in the cell is saturated with the bubbling gas at all the positions. The coupon holder was inserted into a cell without any solution inside. After the cell was thoroughly sealed with silicone to ensure an anaerobic environment inside the cell, ground water solution was inserted into the cell through the gas inlet tube in a manner that avoided oxygen contamination.

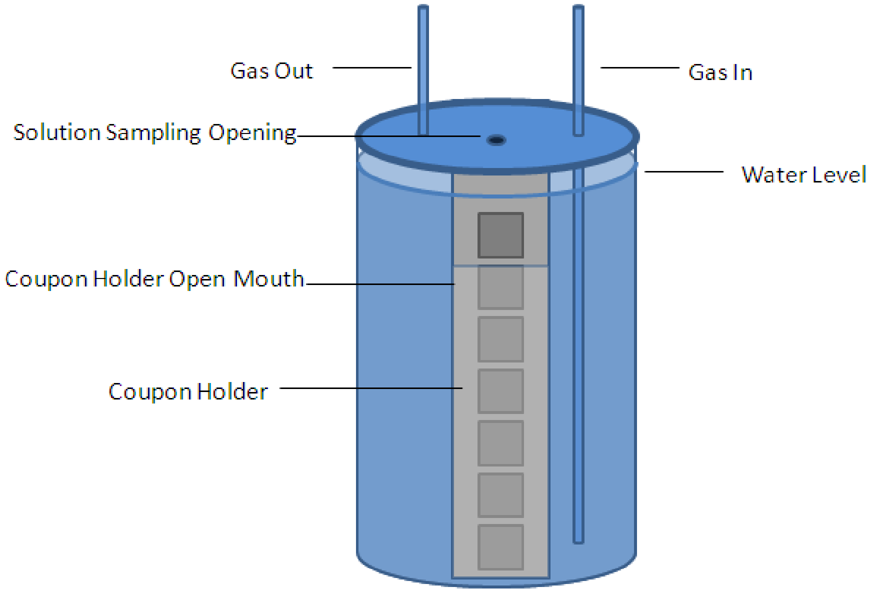

Figure 4-2: PMMA Corrosion Cell Design

4.2.2 Coupon Holder

4.2.2.1 Design Principle of the Coupon Holder

The experimental component termed "coupon holder" refers to an assembly intended to imitate a coating adhesion failure that creates a disbondment gap between the pipeline material and the delaminated coating, characteristic to tape coatings in the field. The main purpose of the assembly is to characterize the corrosion of the metal under a disbonded coating, in terms of rate (weight loss), deposits, and the developed electrochemical conditions (pH, conductivity) inside and outside the disbonded coating.

The design of the coupon holder incorporated six coupons located under a shielding imitating a delaminated coating, and a single unshielded coupon. The unshielded coupon imitated the location of a holiday (hole in the coating) on a pipeline, where the metal is fully exposed to the underground soil. This unshielded coupon also signified a location outside, but adjacent to, the electrochemical environment created by the disbondment gap. The coupon adjacent to the unshielded coupon imitated the location of the open mouth (OM) of the coating disbondment, closely adjacent to a holiday, which may be affected both by the electrochemical conditions inside the disbondment gap (trapped water) and in the bulk solution (soil and groundwater solution surrounding the pipeline).

Since this study was aimed to correlate corrosion with SCC, it was of interest to study smaller coating disbondment gaps (up to 10 mm), as SCC is commonly not found in areas of large coating disbondments gaps. The coating disbondment gap sizes on the coupon holder varied between 2 mm and 10 mm.

The coupon holder, shown in Figure 4-3, is comprised of a solid PMMA back, a PMMA part with seven square openings, and a shielding plate with an opening at the top. The gap between the coupon holder and the shielding plate varied from 1 cm to 2 mm, simulating a coating de-cohesion (the holiday) and a disbondment (the shielded area) on the pipe surface. Due to the low gas permeability of the PMMA shielding, the gas entrance to the disbondement was only via the Open Mouth (OM).

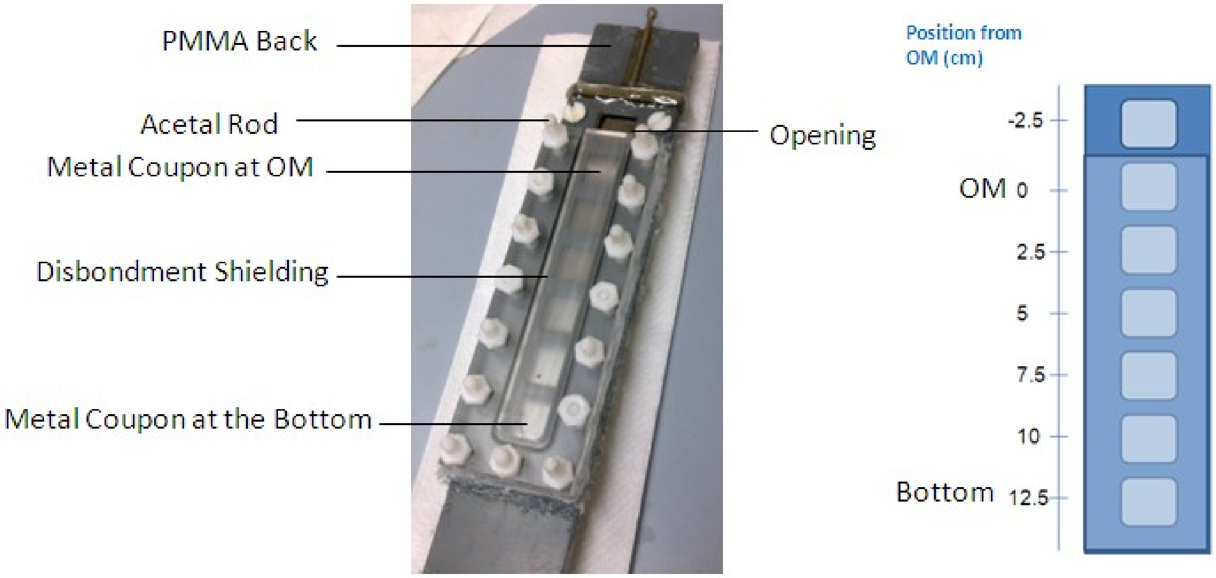

Figure 4-3: Coupon Holder Assembly

4.2.2.2 Components and Design of the Coupon Holder

The shielding material used in this experiment was made out of PMMA. This is justified by experimental findings that show that the electrochemical conditions generated under PMMA coatings are not significantly different from the ones formed under high density polyethylene (HDPE) and low density polyethylene (LDPE) coatings. Both types of PE coatings and PMMA have a low CO_2 permeability, and a high electrical resistivity [15].

To analyze the effect of the coating disbondment size on the corrosion rate, four scenarios were tested:

a. No shielding (where the steel coupons were exposed to the bulk solution)
b. 1 cm gap distance (large disbondment)
c. 5 mm gap distance
d. 2 mm gap distance

In each experiment, seven X-65 square coupons with a 1.9 cm side and 2 mm thickness were used. The chemical composition of X-65 pipeline steel is presented in The surface of the coupon prior to the test is shown in Figure 4-4.

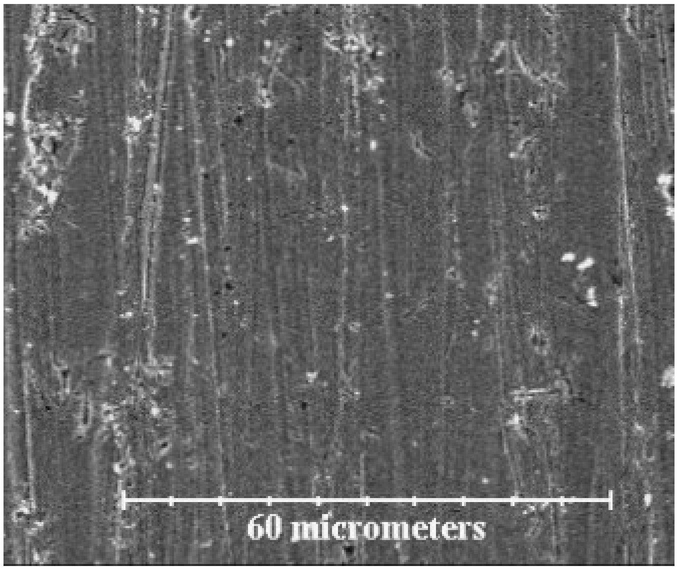

Figure 4-4: X-65 Coupon Surface Prior to the Test

After the specimens' initial weight was recorded, the coupons were placed into the coupon holder connected to each other. The coupon holder was attached to the shielding plate with acetal rods and nuts, and the sides and the bottom of the coupon holder were sealed with silicone and epoxy to ensure that CO2 penetrates into the disbondment only from the top opening. Only one face of each specimen was exposed to the solution in the gap (exposed area 1.9 cm2). The position above the OM, represented by the top coupon, was not shielded.

Table 4-1. The specimens were machined from sections of X-65 pipeline steel from pipes taken from the field. The specimens were ground to 600 grit, immersed into an ethanol ultrasonic bath for 2 minutes, and quickly dried with air. The surface of the coupon prior to the test is shown in Figure 4-4.

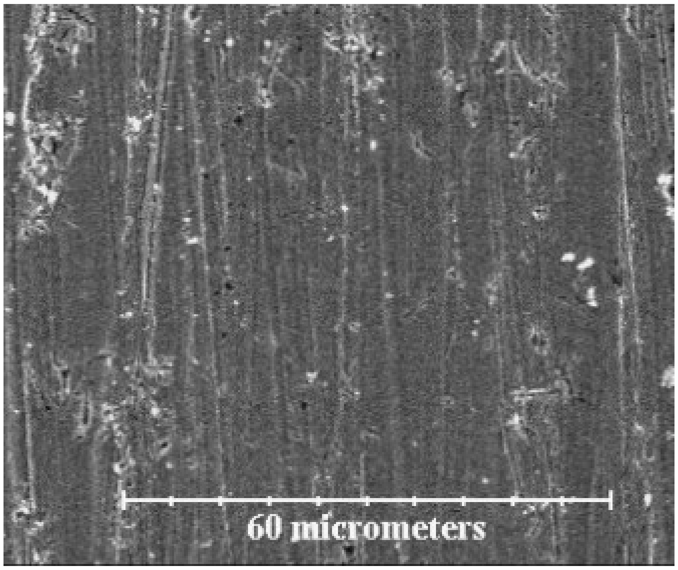

Figure 4-4: X-65 Coupon Surface Prior to the Test

After the specimens' initial weight was recorded, the coupons were placed into the coupon holder connected to each other. The coupon holder was attached to the shielding plate with acetal rods and nuts, and the sides and the bottom of the coupon holder were sealed with silicone and epoxy to ensure that CO_2 penetrates into the disbondment only from the top opening. Only one face of each specimen was exposed to the solution in the gap (exposed area 1.9 cm^2). The position above the OM, represented by the top coupon, was not shielded.

Table 4-1: X-65 Pipeline Composition

\

Element	Composition, wt%
C	0.12
Mn	1.5
P	0.017
S	0.0046
Si	0.26
Cu	0.014
Ni	<0.02
Cr	0.065
Mo	<0.03
V	<0.01
Nb	0.049
Ti	<0.005
Al	0.029
Sn	0.0016
Ca	0.0012
B	<0.0005
Pb	<0.01
Zr	<0.002
Co	0.004

4.2.3 Electrolyte

C2 solution with a composition similar to the one found on sites where SCC was found was used as the electrolyte in the corrosion cell [16]. The C2 solution chemistry is presented in Table 4-2. The solution was purged with 5% CO_2- N_2 for at least 48 hours prior to testing while its pH reached a stable value of 6.3.

Table 4-2: C2 Solution Composition

Component	Concentration (g/l)
$MgSO_4*7H_2O$	0.0274
$CaCl_2$	0.0255
KCl	0.0035
$NaHCO_3$	0.0195
$CaCO_3$	0.0606

The corrosion cell was continuously purged with different CO_2 concentrations for each set of tests: 2% CO_2- N_2, 5% CO_2-N_2, and 20% CO_2-N_2 to imitate the lower and the upper values of the dissolved CO_2 in soil found in the field (4% to 23% CO_2) [6]. It is important to note that a concentration of 20% CO_2 in the ground is an extreme condition which is not frequently observed. The choice to perform tests at a high concentration of 20% CO_2 was to illustrate an extreme situation of CO_2 concentration in the ground.

4.2.4 Cathodic Protection (CP)

Due to the shielding effect of the tape coating, the applied CP often doesn't reach the pipeline and cannot provide it the necessary protection. To imitate this situation, the tests were performed at Open Circuit Potential (OCP), without an application of CP.

4.2.5 Test Duration

The duration of the test was established based on a previous study performed by Chen and Sutherby on X-65 coupons suspended in different ground water solutions for a duration of 25 days. This study showed that the corrosion rate of X-65 steel in C2 solution became constant after ~3 days [17]. The extension of the test to 30 days was to insure the accuracy of the obtained corrosion rate, and decrease the experimental error associated with the sensitivity of the corrosion rate measurement method.

4.2.6 Corrosion Rate Measurement

After ~30 days (±1), the specimens were taken out of the solution, quickly dried, cleaned with ethanol, and weighed. The corrosion rate (CR) of each coupon was calculated based on its weight loss during the experiment (initially derived from Faraday's law) using Equation 4-1:

$$CR = \frac{W_2 - W_1}{t * \rho * A} \qquad \text{(Equation 4-1)}$$

Where W_2 and W_1 are the initial and final weights, respectively; t is the time, ρ is the density of the metal, and A is the area of the coupon exposed to the solution.

4.2.7 pH and Conductivity

Due to the sensitivity of the test, the pH inside the gap was not measured during the test to avoid oxygen penetration while the microelectrodes were inserted into the disbondment and mixing inside the disbondment by the electrodes.

At the end of the test, the pH inside the gap at three distinct locations: OM, middle, and bottom, was measured using commercial combination micro-electrodes. The diameter of the microelectrodes was smaller than 1.6 mm; they were calibrated carefully in buffer solutions of pH 4 and 7 prior to each measurement. As well, the conductivity of the solution inside the shielding and outside the shielding was measured with the use of the Accumet XL60 Dual Channel Meter, after extracting the solution out of the disbondment.

4.3 Experimental Results

4.3.1 Corrosion Rate under Coating Disbondments

The corrosion rate of the pipeline steel at different positions from the OM (consistent with the positions shown in Figure 2) was obtained for various CO_2 concentrations: 2% CO_2, 5% CO_2, and 20% CO_2 shown in Figure 4-5, Figure 4-6, Figure 4-7, respectively. The results represent the average corrosion value and the associated error, obtained from at least two test repetitions; tests that exhibited a higher scatter in the results had a higher number of repetitions. The error bars represent the standard deviation between the results of the repeated experiments.

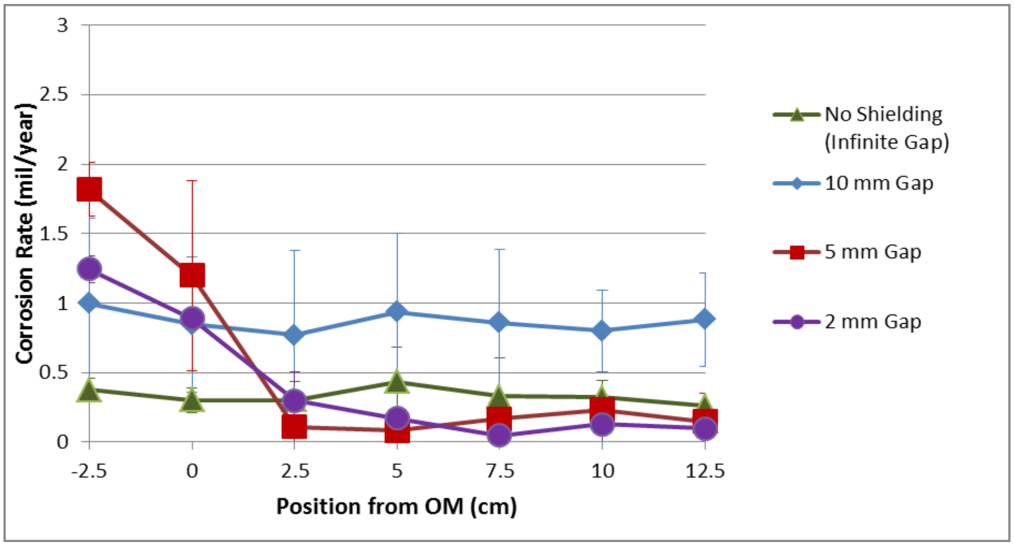

Figure 4-5: Corrosion Rate in Deaerated C2 Ground Water Solution at Various Positions from the OM for a Solution Purged with 2% CO_2, Determined Based on 30-Day Tests Through Weight Loss Analysis

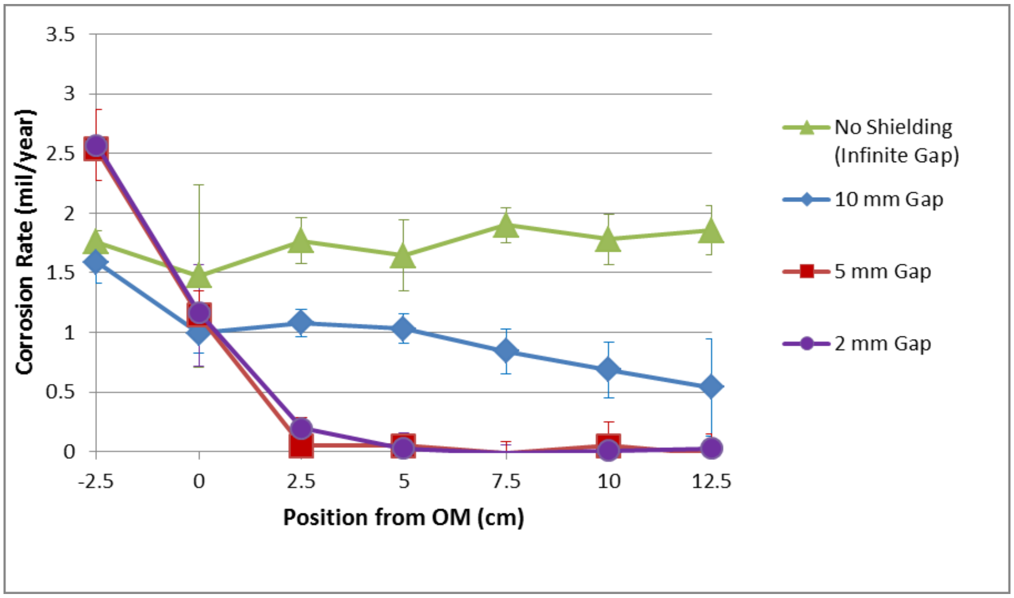

Figure 4-6: Corrosion Rate in Deaerated C2 Ground Water Solution at Various Positions from the OM for a Solution Purged with 5% CO_2, Determined Based on 30-Day Tests Through Weight Loss Analysis

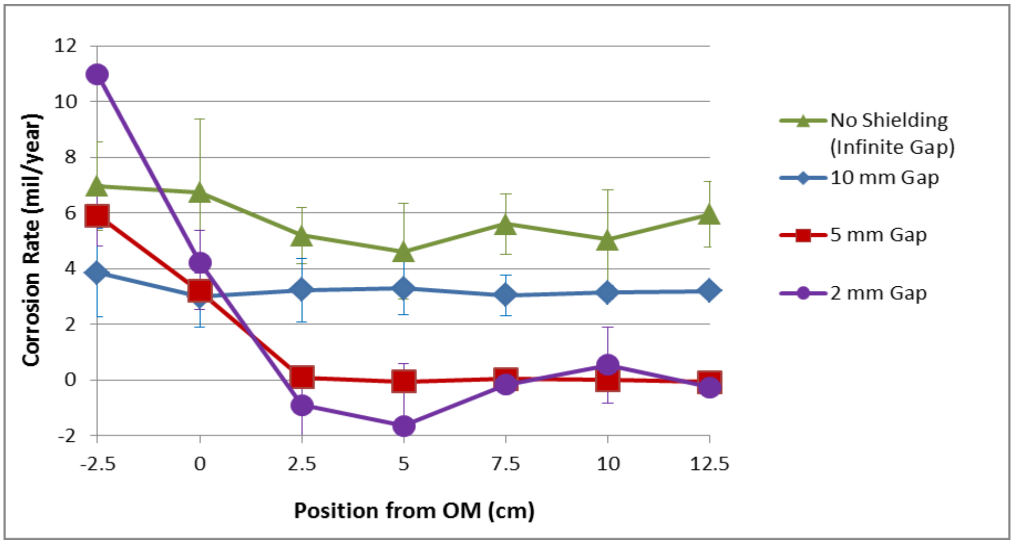

Figure 4-7: Corrosion Rate in De-aerated C2 Ground Water Solution at Various Positions from the OM for a Solution Purged with 20% CO_2, Determined Based on 30-Day Tests Through Weight Loss Analysis

From analyzing Figure 4-5 to Figure 4-7, it can be seen that the corrosion rate was lower at all the positions for the test purged with 2% CO_2 compared to 5% CO_2, and almost three times higher for the test purged with 20% CO_2.

For all the tests it can be seen that the corrosion rate in the test without the shielding imitating a holiday or a large coating disbondment is constant at all the coupon positions inside the disbondment. Similar results were observed for the test with a 10 mm gap for 2% CO_2 and 20% CO_2. However, for 5% CO_2, for the 10 mm gap, the corrosion rate appeared to be the highest at the OM, and decreased towards the bottom of the disbondment.

For smaller disbondment sizes (2 mm and 5 mm), the corrosion rate at the OM is higher than the corrosion rate of the tests with larger disbondments, but at the bottom of the disbondment there is almost no corrosion (the corrosion rate is close to zero). For 20% CO_2 for 2 mm gap, there appears to be a negative corrosion rate, indicating of weight gain, which is likely an experimental error associated with the oxidization of the surface during coupon extraction at the end of the experiment.

For all the CO_2 concentrations, it can be seen that the standard deviation between the repeated results under the 10 mm disbondment gap and the infinite gap is much higher at all the positions compared to the standard deviation under the 2 mm and 5 mm disbondment gaps.

For the 2 mm and 5 mm disbondment gap sizes, it is important to note that the shape of the obtained curves and the region of transition from higher corrosion rates to lower corrosion rates at the bottom of the disbondment are based on the size of the coupons. Had the experiment been performed with the same length of the disbondment but with smaller coupons, the transition to low corrosion rates would've been expected to be more gradual.

4.3.2 Surface SEM Analysis of Corroded Coupons

In order to confirm the observed corrosion rate calculations shown in the previous section, SEM surface images were obtained for coupons in different positions for each experimental setup. A comparison of the coupons at the position above the OM, the middle of the disbondment, and the bottom of the disbondment is shown in Figure 4-9, Figure 4-8, Figure 4-10, and Figure 4-11 for 5% CO_2, 2 mm, 5 mm, 10 mm disbondment gap, and infinite disbondment gap, respectively. Similar images were obtained for 2% and 20% CO_2, shown in Appendix A.

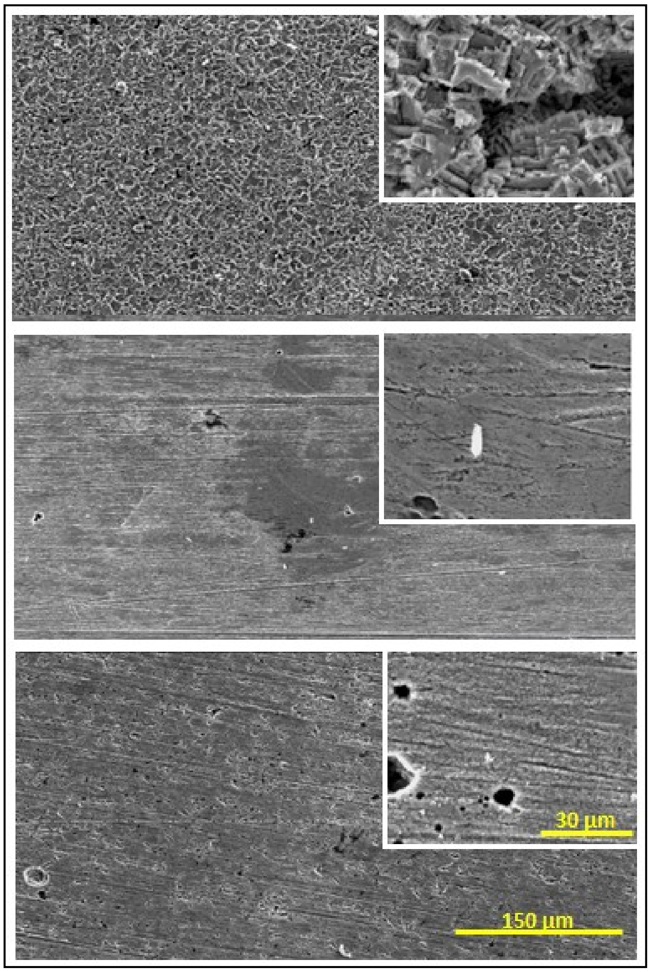

Figure 4-9: Sample Surface at the Top, Middle, and Bottom for 5% CO2, 2 mm Gap

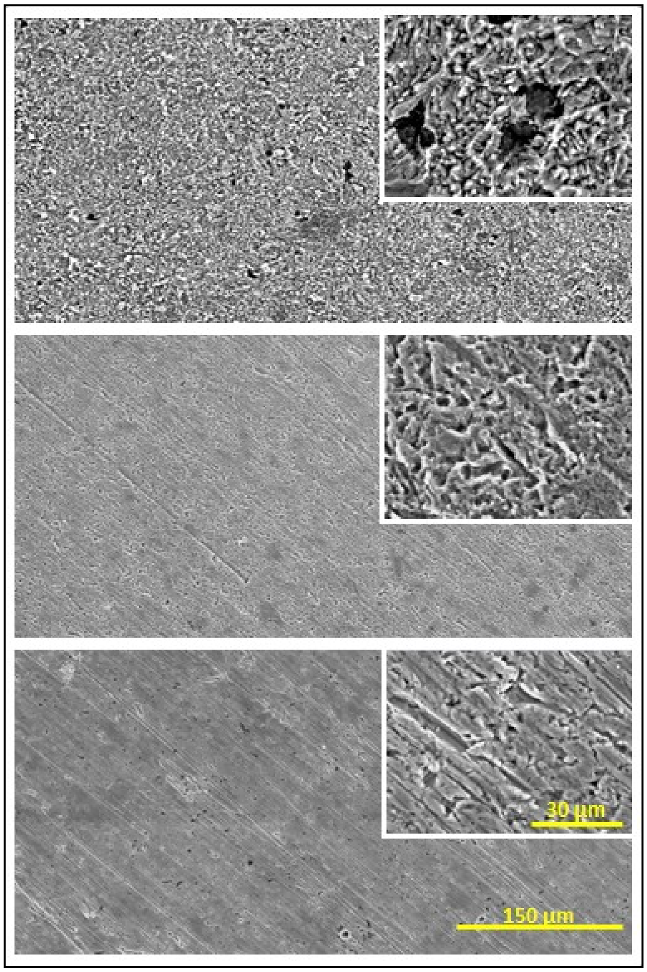

Figure 4-8: Sample Surface at the Top, Middle, and Bottom for 5% CO2, 5 mm Gap

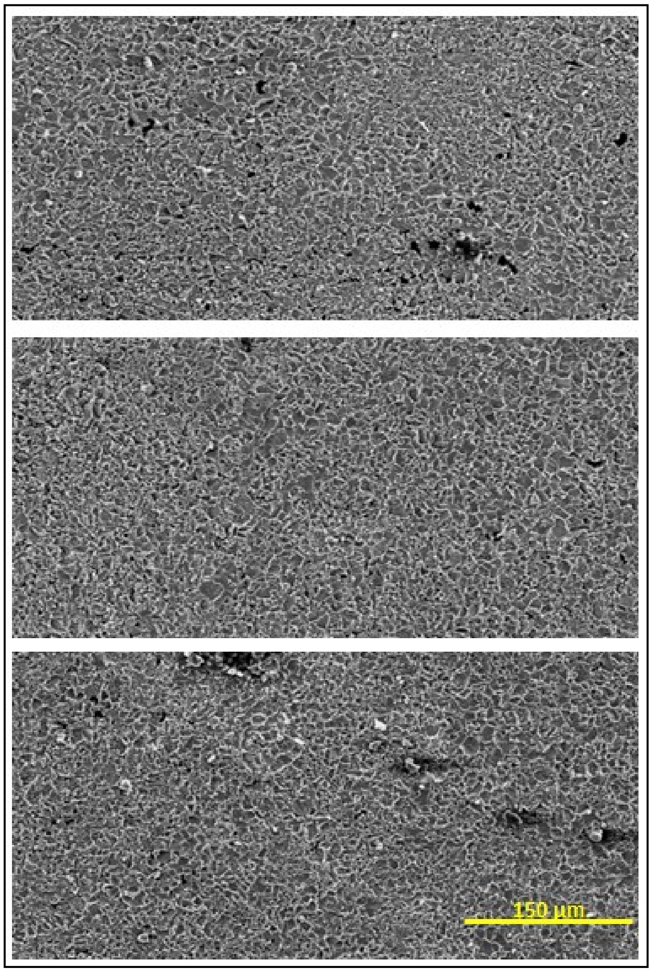

Figure 4-11: Sample Surface at the Top, Middle, and Bottom for 5% CO2, 10 mm Disbondment Gap

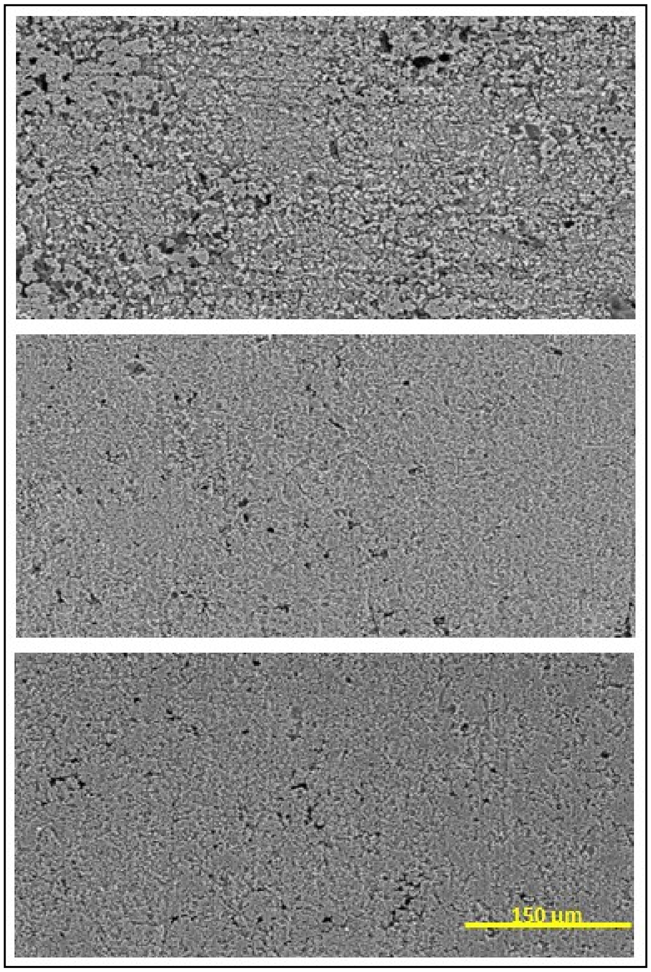

Figure 4-10: Sample Surface at the Top, Middle, and Bottom for 5% CO2, Infinite Disbondment Gap

4.3.3 Electrochemical Conditions

4.3.3.1 pH

The pH of the C2 solution after purging with 5% CO_2 for two days was approximately 6.3. The measured range of the pH at the different positions inside the shielding at the end of the test (~30 days) was in the neutral pH region (between 5.9 and 8), indicating that no high pH environment (pH 9-11) was formed. This demonstrates that the observed variation in the corrosion rate is most likely not associated with the formation of a passive film on the surface of the coupons typical to alkaline environments.

In narrower disbondment gaps (2 mm and 5 mm), the pH at the top of the disbondment, where the higher corrosion rates were observed, was found to be lower than the pH in the bottom of the disbondment. This is consistent with the fact that iron oxidation results in a pH reduction, and the highest degree of iron oxidation occurred at the OM and above the OM of narrower disbondment gaps. As well, at the OM the solution has a higher concentration of CO_2, compared to the bottom of the disbondment, which also promotes a lower pH.

4.3.3.2 Conductivity

The conductivity of the solution was found to be in the range of 180-250 μS/cm. No consistent values or trends could be obtained for the conductivity values of the solution inside various gaps. This is most likely related to the solution extraction method, where the volume of solution obtained from inside the disbondment is fairly small, and it can quickly oxidize during the resistivity analysis, providing inconsistent results.

4.3.4 Solution Metal Ion Concentration

It was observed that the solutions extracted for conductivity measurements from inside the disbondment and from the bulk for smaller gap disbondments (2 mm and 5 mm) reacted differently when left exposed to open air for ~20 minutes inside a glass vial. The solution from inside the disbondment had a stronger yellow color when exposed to oxygen compared to the solution from the bulk, as shown in Figure 4-12. This indicated that the solution from inside the disbondment had a higher metal ion concentration, which upon reaction with oxygen produced a stronger yellow color.

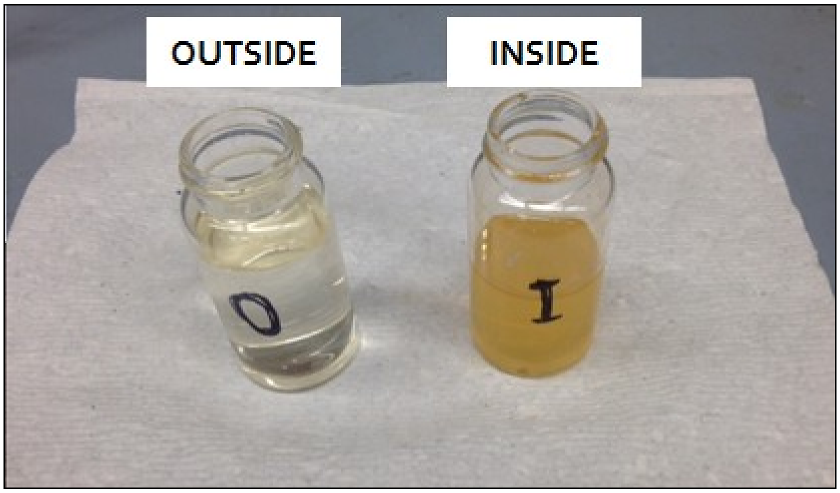

Figure 4-12: Solutions Taken from Inside the Disbondment and Outside the Disbondment after ~20 Minutes of Exposure to Oxygen

4.4 Experimental Analysis

Several important observations were obtained from studying the corrosion rate under coating disbondments. First, as the CO_2 concentration increased (and the pH of the bulk solution decreases), the corrosion rate at the OM and outside the OM increased for smaller disbondment gaps, and the corrosion rate inside and outside the disbondment increased for larger disbondment gaps. Comparing the results of 20% CO_2 and 5% CO_2, the corrosion rate increased up to 4 times as the CO_2 concentration increased.

Second, as the coating disbondment gap size decreased, the corrosion rate inside the coating decreased. For the 2 mm and 5 mm disbondment gaps, the corrosion rate inside the coating was close to zero, regardless of the CO_2 concentration of the bulk solution. For 10 mm gap, the corrosion rate appeared to be fairly uniform inside and outside the disbondment, similar to a situation when the shielding was removed.

Third, for smaller disbondment gap sizes (2 mm and 5 mm), the corrosion rate at the OM and above the OM significantly varied from the corrosion rate at the bottom of the disbondment (close to zero), regardless of the CO_2 concentration of the bulk solution. This observation suggests that the existed a concentration cell between the OM and the bottom of the disbondment, where the coupons at the OM and above the OM served as anodes, and the coupons inside the disbondment serves as cathodes.

4.4.1 Electrochemical Reactions

Prior to discussing the experimental results, it is important to understand the reactions involved in the corrosion process in the system. In the experimental setup, the cells were sealed from oxygen and continuously purged with different concentrations of CO_2: 2%, 5%, and 20% CO_2. Continuous purging with CO_2 generated carbonic acid through the carbon dioxide hydration reaction (Reaction 1) [5].

$$CO_2 + H_2O \rightarrow H_2CO_3 \qquad \text{(Reaction 1)}$$

The carbonic acid further dissociated into bicarbonate (Reaction 2) and carbonate (Reaction 3) in a two-step process:

$$H_2CO_3 \rightarrow H^+ + HCO_3^- \qquad \text{(Reaction 2)}$$

$$HCO_3^- \rightarrow H^+ + CO_3^{2-} \qquad \text{(Reaction 3)}$$

In the pH range of 6-7, Reaction 2 is prevalent.

The corrosion of the steel occurs through the iron dissolution reaction (Reaction 4).

$$Fe \rightarrow Fe^{2+} + 2e^- \qquad \text{(Reaction 4)}$$

In the pH range of 6-7, in room temperature, passivation of the steel through formation of $FeCO_3$ does not occur.

The overall corrosion reaction induced by the presence of CO_2 is (Reaction 5):

$$Fe + CO_2 + H_2O \rightarrow Fe^{2+} + CO_3^{2-} + H_2 \qquad \text{(Reaction 5)}$$

4.4.2 Corrosion Rate under Coating Disbondments

For the aqueous solution with the same chemical composition, the corrosion rate can be correlated with the CO_2 level in the environment, as the presence of CO_2 facilitates the hydrogen evolution in the water through Reactions 2 and 3. The increase in the corrosion rate due to an increase in the CO_2 partial pressure in an aqueous solution has been previously reported in the literature [89, and is consistent with the results of these experiments.

The geometry of the disbondment in the experiment allows CO_2 penetration into the disbondment only from the top opening. Smaller disbondments (2 mm and 5 mm) limit the mass-transport of CO_2, carbonic acid, and carbonate species into the disbondment.

For the 10 mm disbondment gap in 5% CO_2, the decrease in the corrosion rate towards the bottom of the disbondment is gradual (almost linear). This indicates that there may exist a concentration gradient in CO_2 and CO_2-related species that results from the slightly larger disbondment gap that facilitates the mass-transport of CO_2 into the gap. For 2% CO_2 and 20% CO_2, the corrosion rate under the 10 mm disbondment appears consistent in all the positions, which strengthens the argument that the mass-transport of CO_2 into the disbondment is facilitated by larger gaps. For larger gap sizes, the concentration gradient of CO_2 inside the disbondment decreases, which also decreases the corrosion rate differences between the coupons at various positions. An extreme case of this scenario is demonstrated with an infinite gap size where the CO_2 concentration was equal at all the coupon position; in these conditions, the corrosion rate of the coupons in all the positions is constant.

The observation where the CO_2 and CO_2-related species gradient-change affects the corrosion rate may lead to an erroneous assumption that a CO_2 concentration cell promotes the corrosion rate differences, similar to a case of a differential oxidation cell. Application of the Nernst

Equation 4-2 on the overall corrosion reaction shows an opposite effect of the one observed in the experiment: with a higher CO_2 partial pressure, a higher E would be expected, thus indicating that the location with the higher CO_2 partial pressure is cathodic and would not corrode. Therefore, the experimental results cannot be explained by a formation of a CO_2 concentration cell.

$$E = E^0 - \frac{0.0592}{n} * log\frac{[H^+] * [HCO_3^-]}{P_{CO_2}} \quad \text{(Equation 4-2)}$$

As well, since a passivating $FeCO_3$ film cannot form in a dilute carbonate-bicarbonate environment in the pH range of 6-7 in room temperature, the lower corrosion rates observed at the bottom of the disbondment in 2 mm and 5 mm disbondment sizes cannot be related to a passive film deposition.

The concentration cell effect observed in the narrower disbondments can be explained by a formation of a metal ion concentration cell, through a two-stage process.

Stage 1

At the start of the test, the solution that is poured into the corrosion cell and filled the disbondment gap was previously purged with 5% CO_2-Nitrogen for a duration of a least 48 hours; therefore, the disbondment gap is not entirely depleted of CO_2. At the start of the experiment, dissolution can occur equally within the disbondment because the steel surface is exposed to the same groundwater electrolyte.

At the start of the experiment, in the presence of CO_2 and carbonic acid, slight metal dissolution can occur both inside the disbondment and outside the disbondment, as the steel surface is exposed to the same groundwater electrolyte. This is consistent with the fact that the corrosion rate of the coupons inside the disbondment is not strictly zero.

The metal dissolution rate inside the disbondment decreases with time, as the solution gets slowly depleted of CO_2. The metal outside the disbondment and at the OM is exposed to the constantly-purged bulk solution, where the concentration of CO_2 remains at the same level, and the dissolution proceeds at the same rate. The higher concentration of reductant-species (carbonic acid), results in a higher dissolution rate.

The first stage results in formation of ferrous ions Fe^{2+} at the OM and inside the disbondment. The ferrous ions at the OM transport through convection both into the disbondment and into the bulk solution. However, mass-transport of ions from inside the disbondment into the bulk solution can be limited because the concentration of ferrous ions increases closer to the OM due to a higher dissolution rate induced by the presence of CO_2.

Stage 2

The restricting geometry of the disbondment limits the mass-transport of ferrous ions outside the disbondment, creating a situation where the concentration of metal ions inside the disbondment is higher than its concentration outside the disbondment. This results in the metal coupons inside the disbondment and at the OM of the disbondment acquiring different electric potentials, leading to a formation of a metal-ion concentration cell.

In this concentration cell, the metal at the OM and above the OM is the anodic and proceeds to corrode, and the metal inside the disbondment is the cathodic and does not undergo further dissolution. This hypothesis can explain why a large section of disbonded area was not corroded and accelerated corrosion was only limited to the first two coupons at the OM and above the OM.

This hypothesis is supported by Nernst equation (Equation 4-3) that shows a positive potential when the concentration of ferrous ions at the cathode exceeds the concentration of ferrous ions at the anode.

$$E = E^0 - \frac{0.0592}{n} * log\frac{[Fe^{+2}]_{anode}}{[Fe^{+2}]_{cathode}} \quad \text{(Equation 4-3)}$$

As the metal at the OM and above the OM proceeds to corrode, more metal ions transport into the disbondment, and the concentration cell proceeds to exist. Moreover, as the metal at the OM and above the OM corrodes, its surface roughness increases, which increases its dissolution rate even more. Both of these factors suggest that anaerobic corrosion at the OM of disbonded coatings is a self-perpetuating process.

4.4.3 OCP Conditions- Concentration Cell Effect

To illustrate the effect of CO_2 concentration on the corrosion rate, the corrosion rate for the 2 mm, 5 mm, and 10 mm disbondment gap sizes was normalized by dividing the highest corrosion rate at the OM (Figure 4-13), and above the OM (Figure 4-14) by the average corrosion rate obtained for the infinite disbondment gap (where the concentration effect was eliminated).

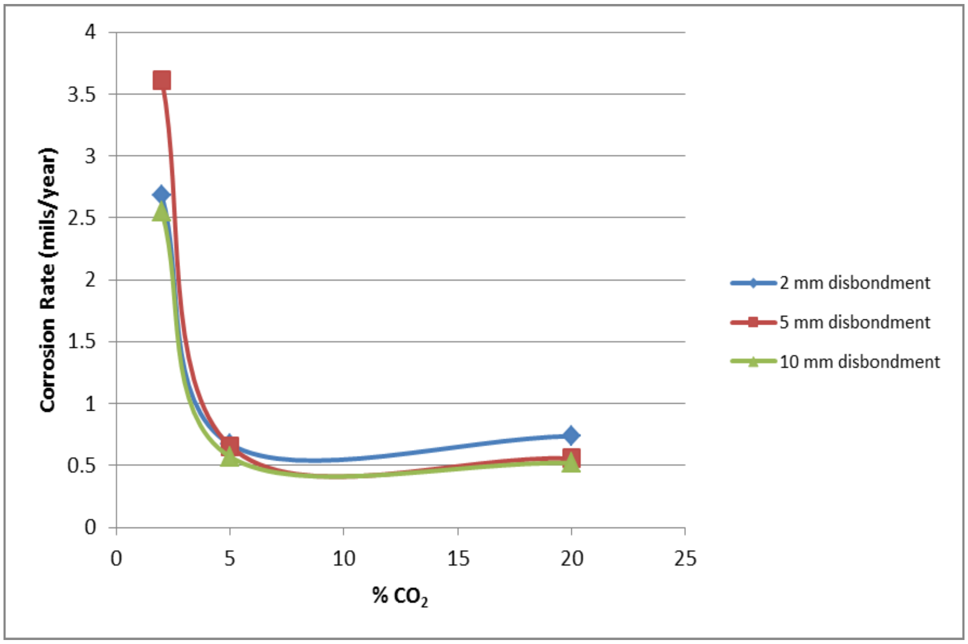

Figure 4-13: Normalized Corrosion Rate Illustrating the Concentration Cell Effect for the Position Above the OM

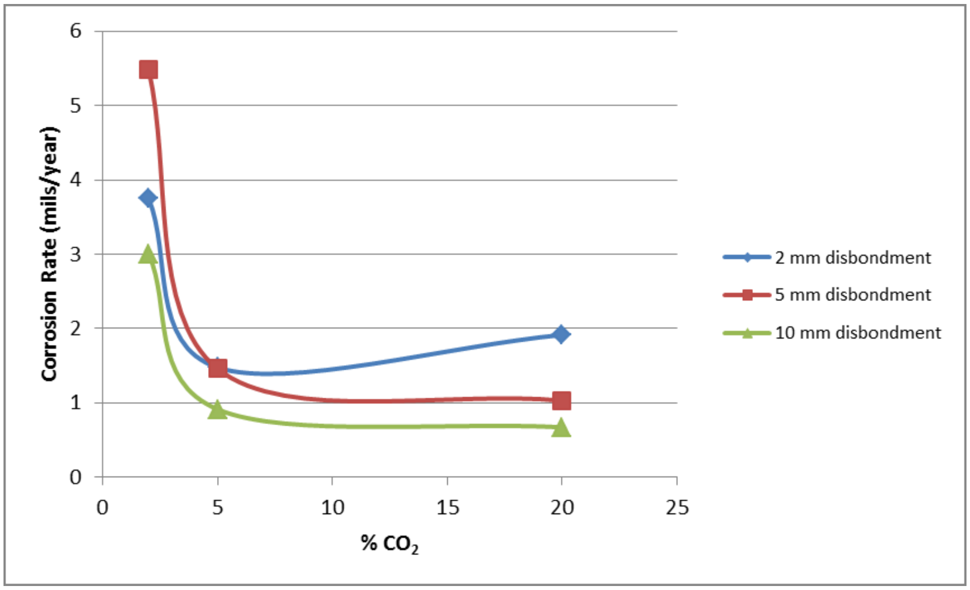

Figure 4-14: Normalized Corrosion Rate Illustrating the Concentration Cell Effect for the Position at the OM

The trends for the position at the OM and above the OM of the imitated disbondment appear to be consistent among themselves, showing that the highest concentration cell effect was observed at a low CO_2 concentration of 2%. It is also apparent that the concentration cell effect for the 5 mm disbondment gap is larger than the concentration cell effect for 2 mm gap. At 5% CO_2, the 2 mm gap and the 5 mm gap have a similar concentration cell effect, which changes with an increase of CO_2 to 20%, where the concentration cell effect of the 2 mm gap enhances. In all the cases, the concentration cell effect of the 10 mm gap is the lowest.

4.4.3.1 Effect of Coating Disbondment Gap at Lower CO_2 Concentrations (2% CO_2)

When the metal inside the disbondment is initially exposed to the C2 solutions previously purged with CO_2, dissolution of iron occurs equally inside the disbondment and at the OM. As the disbondment gets depleted of carbonic acid (contributing to the cathodic reaction in the iron corrosion), the corrosion rate inside the disbondment decreases, and is controlled by mass-transport of CO_2 and carbonic acid into the disbondment.

The mass-transport of Fe-ions out of the disbondment from the bottom of disbondment to the open mouth can be limited because the concentration of Fe-ions is actually higher as it gets closer to the open mouth, except for the steel surface near the open mouth, where mass-transport of Fe-ions to the open mouth could be possible. This could lead to a zone of disbondment with uniform concentration of Fe-ions in the bottom part of the disbonment. With an increase of exposure time, ferrous ions build up inside the disbondment, which decreases further dissolution by a formation of a metal ion concentration cell, where the coupons at the bottom of the disbondment serve as a cathode site (with a relatively large area).

When gap size is small (2 mm gap), the build-up of ferrous ions deep in the disbondment is slow and the concentration of ferrous ions is low. Therefore, a weak concentration cell is formed.

When gap size is very large, for example, with a gap size at 10 mm or larger, the dissolved ferrous ions could also transport (through convection) in the direction perpendicular to the steel surface, which could reduce the concentration of Fe^{2+} ions at the steel surface, forming a weak concentration cell. The larger gap size also enhances the mass-transport of Fe^{2+} ions to the open mouth.

A 5-mm gap forms a strong concentration cell because of 1) increased access of species resulting from CO_2 dissolution in water to the bottom of the disbondment, which leads to more dissolution of Fe, and 2) restricted mass-transport of Fe^{2+} to the open mouth, 3) limited dilution of Fe^{2+} ions in the direction perpendicular to the steel surface.

Another contributing factor to the strong concentration cell effect observed for experimental setups with 2% CO_2 is the fact that the general corrosion rate at these concentrations is relatively low. The coupons in the system of the infinite disbondment gap (used as a normalizing factor to illustrate the concentration cell effect) corrode only through general corrosion, and their corrosion rate, as shown in Figure 4, is relatively low.

4.4.3.2 Effect of Coating Disbondment Gap at Higher CO_2 Concentrations (20% CO_2)

This scenario is very similar to the one described above for 2% CO_2 in its initial stages. The main difference between the two systems is the fact that the abundance of CO_2 in the bulk solution (which increases the metal dissolution rate) and higher mass-transport of CO_2 and carbonic acid into the disbondment allow a creation of a strong metal ion concentration cell for both the 2 mm gap and the 5 mm gap.

For the 2 mm gap, a smaller opening of the disbondment at the OM may result in a lower mass-transport of ferrous ions from the disbondment into the bulk solution, retaining the metal ions inside the disbondment. The lower volume of the 2 mm disbondment gap, and the higher metal ion retention may result in a stronger concentration cell, compared to the 5 mm gap.

4.4.4 OCP Conditions- Cumulative Results

In order to understand the correlation between the highest corrosion rate under various disbondment sizes, Figure 4-15 was plotted. Figure 4-15 shows the corrosion rate at the OM (the location of the highest corrosion rate) for various gap sizes obtained for 2% CO_2, 5% CO_2, and 20% CO_2 concentrations. The corrosion rate under non-disbonded coatings (disbondment size=0) is expected to be null; however, in the field it is often found to be within 1 mil/year due to coating permeability to moisture and gases.

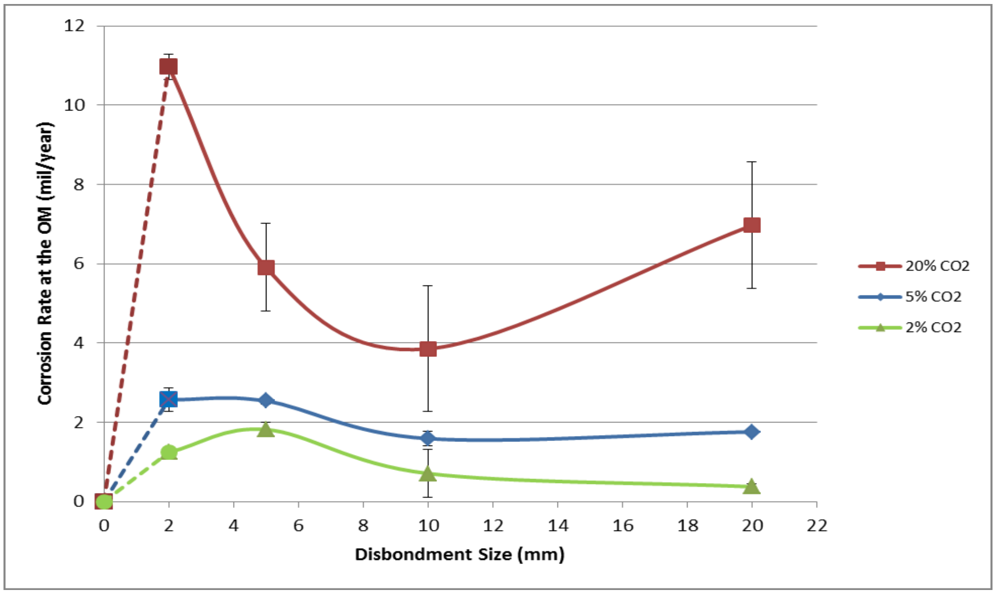

Figure 4-15: Corrosion Rate as a Function of Disbondment Size for Various CO_2 Concentrations

Analyzing Figure 4-15, it can be seen that the corrosion rate at the OM decreases with increasing disbondment size for all the CO_2 concentrations. The importance of these results lays in the fact that it indicates that pipeline material under smaller tape coating disbondment gaps has a higher corrosion susceptibility in near-neutral pH conditions, compared to larger tape coating disbondments. To confirm this experimental observation, corrosion field data was analyzed, and is discussed in Chapter 5.

4.5 Relation to Field Findings

The findings in this study show that a formation of a metal ion concentration cell can have a significant effect on corrosion and passivation under disbonded coatings. Regions under wrinkled or disbonded coatings with narrower disbondments may be protected from corrosion, while regions at the OM or a holiday can experience self-perpetuating corrosion, enhanced through continuous metal dissolution which strengthens the concentration cell and increases the surface roughness. This finding explains the situation presented in Figure 4-1, where deep corrosion under a wrinkled coating may have occurred at a site close to the OM of that coating, while the other sites further away from the OM were protected from dissolution due to the metal ion concentration difference under the wrinkle.

It is generally recognized that well-drained soils are less corrosive, due to low retention of soil moisture and decrease in electrolyte resistivity. The finding of this study can support and enhance this explanation, by arguing that better drainage can support the removal of dissolved ferrous ions with the solution from inside the coating disbondment, and thus decreasing the metal ion concentration cell effect.

The findings may also suggest an additional correlation between SCC and corrosion, by proposing that a metal ion concentration cell may also exist between the environment inside the crack and the bulk solution or trapped water solution, promoting or decreasing crack tip dissolution.

4.6 Experimental Conclusions

This study suggests that the gap size of coating disbondments from a pipeline is an important factor that can determine both the corrosion rate and the location of the highest corrosion on pipeline steel. Smaller coating disbondment gaps promote the formation of a metal ion concentration cell, which may be responsible for an enhanced corrosion rate at the OM of the disbondment, and a decreased corrosion rate towards the bottom of the disbondment. Larger coating disbondment gaps are prone to a more uniform corrosion rate inside the disbondment.

4.7 References

1. Perdomo, J. J., Chabica, M. E., and Song, I. "Chemical and electrochemical conditions on steel under disbonded coatings: the effect of previously corroded surfaces and wet and dry cycles," *Corrosion Science* 43 (2001) 515-532.
2. Eslami, A., Fang, B., Kania, R., Worthingham, R., Been, J., Eadie, R. and Chen. W. "Stress corrosion cracking initiation under the disbonded coating of pipeline steel in near-neutral pH environment," Corrosion Science 52 (2010) 3750-3756.
3. Been, J., King, F., Yang, L., Song, F., and Sridhar, N. "The role of coatings in the generation of high- and near-neutral pH environments that promote environmentally assisted cracking," *Corrosion/2005*, NACE International, Houston, TX: Paper 05167.
4. Papavinasam, S. Corrosion control in the oil and gas industry. Burlington: Elsevier Science. 2013.
5. Baker, M. "Stress corrosion cracking study- final report". January 2005.
6. Delanty, B. and O'Beirne, J. "Major Field Study Compares Pipeline SCC with Coatings," Oil & Gas Journal, 90 (24), pp. 39-44, 1992.
7. "Stress corrosion cracking on Canadian oil and gas pipelines," MH-2-95, *National Energy Board* (Calgary, Alberta, 1996).
8. Chen, W., Kania, R., Worthingham, R. and Van Boven, G. "Transgranular Crack Growth in the Pipeline Steels Exposed to Near-neutral pH Soil Aqueous Solutions: The Role of Hydrogen." Acta Materialia 57: 6200-6214, 2009.
9. Egbewande, A., Chen, W., Eadie, R., Kania, R., Van Boven, G., Worthingham, R and Been, J. Unpublished work. "Transgranular crack growth in the pipeline steels exposed to near-neutral pH soil aqueous solutions: Discontinuous crack growth mechanism." Currently revised for Corrosion Science.
10. Johnson, J. T., Beavers, J. A., Durr, C. L., and Delanty, B. S. " Effects of O_2 and CO_2 on Near-Neutral-pH and Stress Corrosion Crack Propagation". NACE International, 2000.

11. Yan, M. C., Wang, J. Q., Han, E. H., and Ke. W. “Electrochemical measurements using combination microelectrode in crevice simulating disbonded of pipeline coatings under cathodic protection”, *Corrosion Engineering, Science and Technology*, 42 (1), pp. 42-49, 2007.
12. Yan, M., Wang, J., Han, E. and Ke, W. “Local environment under simulated disbonded coating on steel pipelines in soil solution”, *Corrosion Science*, 50 (5), pp. 1331—1339, 2008.
13. Chen, X., Du, C., Li, X., and Huang, Y. “Effects of cathodic potential on the local electrochemical environment under a disbonded coating,” *Journal Appl Electrochem* (2009) 39: 697-704, 2009.
14. Zhang, L., Li, X. G., Du, C. W., and Cheng, Y. F. “Corrosion and stress corrosion cracking behavior of X70 pipeline steel in a CO_2-containing solution”, *Journal of Materials Engineering and Performance* 18 319-323 , 2009.
15. Eslami, A. *Near-neutral PH Stress Corrosion Crack Initiation under Simulated Coating Disbondment.* Thesis. University of Alberta, 2012. N.p.: n.p., n.d.
16. Chen, W., and Sutherby, R. L. “Crack Growth Behavior of Pipeline Steel in Near-neutral PH Soil Environments.” *Metallurgical & Material Transections* A, 2007. 38A, pp. 1260-1268.

CHAPTER 5 - ANALYZING ANAEROBIC CORROSION UNDER DISBONDED COATINGS THROUGH FIELD DATA

5.1 Introduction

The safety and integrity of pipelines are issues of major importance, as the substances transported by the pipelines are hazardous and impose a risk to human life, property, and environment in an event of failure. One of the major challenges faced by pipeline operators is operating aged pipelines that have been subject to fatigue and coating degradation during their long period of operation. In fact, almost 50% (by mileage) of the pipelines regulated by the National Energy Board (NEB) in Canada in 2011 were 30 years or older, with 13% being older than 50 years [1]. According to a report provided by The Interstate Natural Gas Association of America (INGAA), pipeline age is not a leading cause of pipeline accidents, and incidents can be prevented through successful risk mitigation programs and periodic integrity assessments [5].

The first line of defence for pipeline integrity maintenance is a protective external coating whose primary role is to form a barrier between the pipeline steel and the corrosive soil environment. In an event of coating failure, the second line of defence is cathodic protection (CP), which provides protection through electrochemical means. As well, pipeline operators have pipeline safety maintenance programs, called “Pipeline Integrity Management Programs” (PIM), which were developed for pipeline integrity implementation and management through risk assessment, mitigation, and prevention, in order to achieve the lowest feasibly-acceptable level of risk [3]. Common methods for integrity assessment are hydrostatic testing, in-line inspection (ILI), and direct assessment (DA) [3]. DA methods can be used for pipelines that cannot accommodate ILI tools for location of external corrosion, internal corrosion, and Stress Corrosion Cracking (SCC). The assessment incorporates historical evaluation of the operation, maintenance, and environment around the assessed pipeline segment, as well as field excavations for manual evaluation of the defects on the pipeline and their severity.

It is important to note that external defect development on pipelines is strongly associated with coating failure and the coating condition. Although CP is considered to be an effective means for pipeline protection, oftentimes CP cannot fully reach the pipeline due to coating shielding, or high resistivity of the underground electrolyte to CP currents. In an event of coating failure and CP shielding, the pipeline may be susceptible to threats promoted by the external soil environment, such as corrosion and SCC.

Three major modes of coating failure are 1) loss of adhesion, 2) loss of cohesion, and 3) water and/or air permeation [5, 6]; Figure 5-1 is a schematic for cohesive and adhesive failures. Loss of adhesion refers to the coating's delamination from the pipeline creating disbondments (loss of contact without breakage) between the coating and the pipeline, which can lead to formation of crevices. Coating disbondments can also exist on the pipe prior to its placement in the field due to poor adhesion of the coating to the pipe or resulting from the geometry of the wrapped coating at the welds (such as "tenting", which is commonly observed over the longitudinal weld crown) [7].

Loss of cohesion is related to the breakage of the coating off the pipeline surface, leaving parts of the coatings attached to the pipeline and generating larger coating holidays (breaks or gaps in the coating). Depending on the cohesive strength of the coating, it may either break off the surface in one piece (applies to coatings with great cohesion) or break within itself, leaving a part of it on the surface (applies to coatings with low cohesion). Field observations have shown that tape coatings are more ductile, creating wrinkles in the coating or longer and larger disbondment gaps, while asphalt coatings are more brittle, failing cohesively.

Coating conditions without any defects and good adhesion to the pipeline surface are expected to be full protection from external corrosion, with a standard deviation of 1 mil/year due to water and gas permeability through the coating (based on field observations). In cases of minor coating disbondments, there may be a limited exchange of gases and solutions between the disbondment gap and the soil environment, and the corrosion rate may remain low.

The main goal of this work was to obtain an understanding of the anaerobic corrosion formation under disbonded coating, and the effect of the coating condition on the extent of the corrosion (corrosion rate and corroded area). A central objective of Chapter 5 is to verify the experimental findings of Chapter 4, which showed that there is a relationship between the corrosion rate under a disbonded coating and the coating disbondment gap size. The verification of these findings was approached through field data analysis.

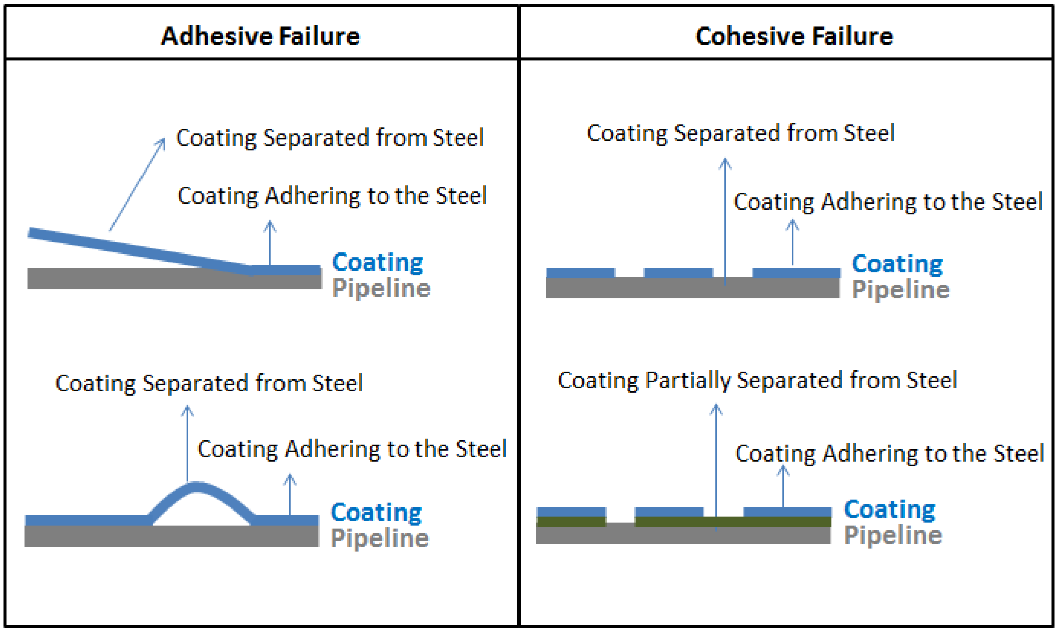

Figure 5-1: Adhesive and Cohesive Coating Failure on Pipelines

5.2 Experimental Setup

The experimental setup was comprised of a corrosion cell in which a system imitating a coating disbondment was placed; a more detailed description of the setup is presented in Chapter 4. The system contained metal coupons made out of X-65 pipeline steel, placed under a PMMA plate, imitating the disbonded coating from a pipeline (adhesion coating failure). The gap between the coupon holder and the PMMA plate varied, thus simulating a situation of various disbondment size gaps characteristic to tape coatings in the field. The gap size variation was as follows: 2 mm, 5 mm, 10 mm, and a removal of the PMMA plate signified a situation where the coating was fully disbonded from the pipeline (coating holiday). A full description of the system can be found elsewhere.

The system imitating a coating disbondment was designed to measure the electrochemical conditions inside a coating disbondment, as well as the corrosion rate of the metal coupons, based on weight loss calculations performed after an experimental duration of 30 days. In this study, the corrosion rate in three different CO_2 concentration was tested: 2% CO_2, 5% CO_2, and 20% CO_2, based on CO_2 soil gas concentrations found in the field; a study performed by Delanty and O'Beirne showed that the CO_2 concentration varied between 4% in the winter and 23% in the spring [8].

5.3 Sources of Field Data and Method of Analysis

Field data provided by a Canadian gas transportation company was used to obtain a correlation between the coating condition found during excavations and the extent of anaerobic corrosion detected on the pipeline. The presented analysis is based on data obtained for tape coatings and asphalt coatings. These coatings have different failure mechanisms: tape coatings commonly fail adhesively, delaminating from the pipeline and creating wrinkles and coating disbondment gaps between the pipeline and the coating, while asphalt coatings fail cohesively in a more brittle manner, creating disbonded patches on the pipe surface. A total of 650 anaerobic corrosion cases under tape coating in 90 distinct dig sites, and 430 anaerobic corrosion cases under asphalt coatings in 95 distinct dig sites were analyzed.

5.3.1. Assessment of Corrosion Rate in the Field

The approximate corrosion rates were assessed based on the reported corrosion depth and the pipeline operation time (calculated as the difference between the excavation year and the installation year). The calculations took into account coating incubation time (12 years), which is an approximate time required for the deterioration of the coating and the development of conditions promoting corrosion and SCC used in the industry.

5.3.2 Assessment of Coating Conditions

To characterize the coating conditions found in the field, three main coating parameters were analyzed: coating adhesion, coating disbondment, and general coating condition. These parameters were provided in the field dig reports that were associated with each corrosion defect assessment.

Coating Adhesion and Coating Disbondment

Coating adhesion and coating disbondment were ranked on a scale of 1 (very good adhesion; no coating disbondment) to 5 (poor coating adhesion; continuous disbondment), as seen in Table 5-1.

A Combined Coating Factor CCF based on both the coating adhesion and coating disbondment parameters was introduced to represent the coating condition with various degrees of adhesive coating failure at the different corrosion sites. The CCF factor was calculated based on the ranking of the coating disbondment and adhesion parameters on a scale of 6, where 6 is the worst coating condition. The correlation between the CCF values and the description of the coating condition can be found in Table 5-1.

Images from the field illustrating the coating condition for various CCF factors are shown for tape coatings and asphalt coatings in Figure 5-2 and Figure 5-3, respectfully. For CCF=1 in Figure 5-2, the purpose of the overlaid rectangle is to conceal the writing on the coating during field excavations.

From Figure 5-2 it can be seen that the tape coating was in a fairly good condition for CCF=1 and CCF=2. For CCF=3, the coating appeared to have small disbondment gaps and wrinkles, and for CCF=4 and CCF=5 the coating had large disbondment gaps. For CCF=6, large areas of the coating appeared to be detached. From Figure 5-3, it can be seen that for asphalt coatings the coating disbonded in a brittle manner, where "patches" of the coating disbonded from the pipeline. As the CCF value increased, the area of the disbonded patches appeared to increase.

The average corrosion rate for each CCF value was calculated and plotted for tape coatings and asphalt coatings

Coating Conditions

The coating condition parameter was also correlated with the sites with various CCF values to gain a better understanding of the possible coating state and its effect on the corrosion rate. It was found that where CCF=6 the coating conditions were mostly very poor, with continuous coating disbondments and big segments of bare pipe. At locations where CCF=5 the coating conditions were poor. At locations where CCF=4 the coating condition were fair to poor. For CCF=3, the coating conditions were mostly fair. For CCF =2 the coating conditions were good to fair. These findings are presented in Table 1 as well. For CCF=1 the coating condition was mostly good, with minor disbondments and good adhesion; and for CCF=0 the coating condition was excellent with no disbondments and very good adhesion.

Table 5-1: Coating Conditions Description

Industry Approach			CCF Approach		
Disbonded Area	Adhesion	Numbering	Description	CCF Value	Coating Condition
None (<1%)	Very Good	1	**No disbondment** and **very good adhesion**	0	Excellent
Minor (1-10%)	Good	2	**Minor disbondment** and **good adhesion**	1	Good
Intermittent (10-50%)	Moderate	3	**Intermitent to minor disobndment and moderate to good adhesion**	2	Good/Fair
Moderate (50-80%)	Poor	4	**Intermittent disbondment** and **moderate adhesion**	3	Fair
Continuous (>80%)	Very Poor	5	**Moderate to intermitent disbondment** and **moderate to poor adhesion**	4	Fair/Poor
			Moderate disbondment and **poor adhesion**	5	Poor
			Continuous disbondment and **very poor adhesion**	6	Very Poor

Figure 5-2: Images from the Field Showing the Tape Coating Condition for Various CCF Factors

Figure 5-3: Images from the Field Showing the Asphalt Coating Condition for Various CCF Factors

5.4 Results

5.4.1 Analysis of Field Data

The factors of coating adhesion and coating disbondment are not strictly distinct from each other; i.e. creation of large disbondment areas in the coating is a result of bad adhesion to the pipeline. The relationship between both factors for tape coatings and for asphalt coatings can be assessed based on their correlation, which is shown in Figure 5-4 and Figure 5-5, respectfully.

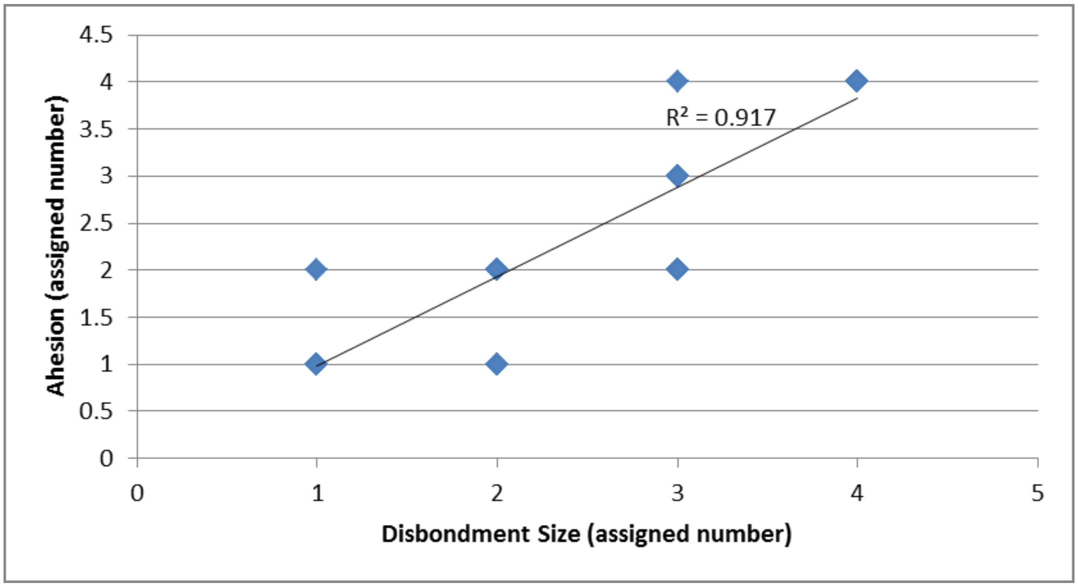

Figure 5-4: Correlation between Adhesion and Disbondment Size Parameters for Tape Coatings

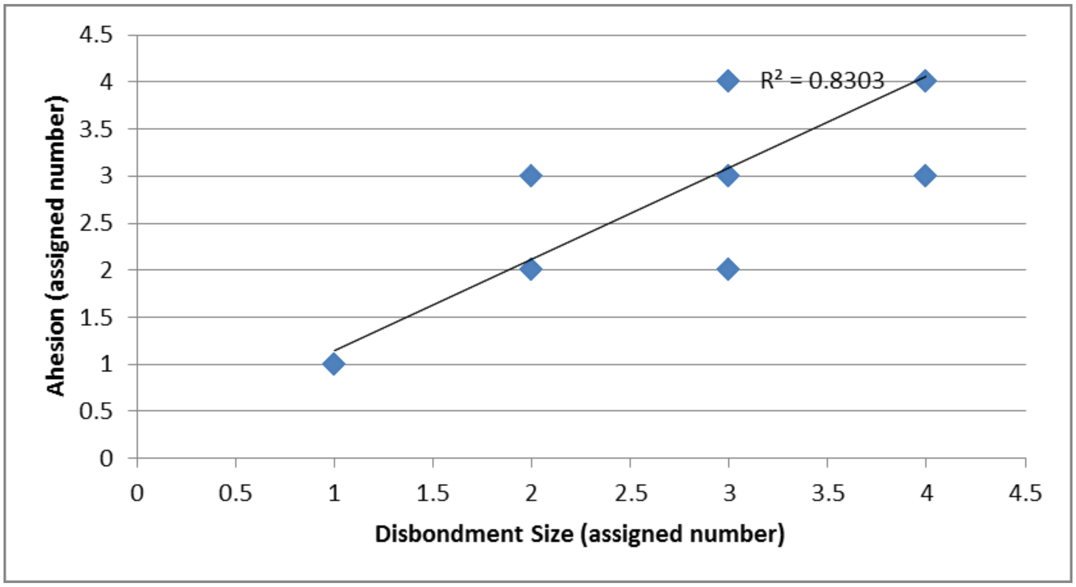

Figure 5-5: Correlation between Adhesion and Disbondment Size Parameters for Asphalt Coatings

From Figure 5-4 and Figure 5-5 it can be seen that, judging based on the R value for the linear curve, the correlation between adhesion and disbondment size is fairly strong. The correlation between both factors appears to be weaker for asphalt coatings, most likely due to the fact that asphalt coatings have a stronger tendency to fail cohesively, and create smaller coating disbondment gaps.

5.4.1.1 Corrosion Rate as a Function of CCF

The average corrosion rate for each CCF value was calculated and plotted for tape coatings and asphalt coatings, as seen in Figure 5-6. Each averaged data point consists of at least 40 cases of corrosion; the error bars represent the standard deviation in the corrosion rate. It can be seen that for certain CCF values, the data points are missing (CCF=2 for tape coatings and CCF=4 for asphalt coatings), this is due to the fact that a statistically insignificant number of corrosion cases (less than 20) was associated with the CCF value. The corrosion rate for CCF=0 (coating in a very good condition without any disbondments and good adhesion to the surface) was estimated as zero with a standard deviation of 1 mil/year, based on the field observation that even under perfectly intact coatings the corrosion rate can be as high as 1 mil/year.

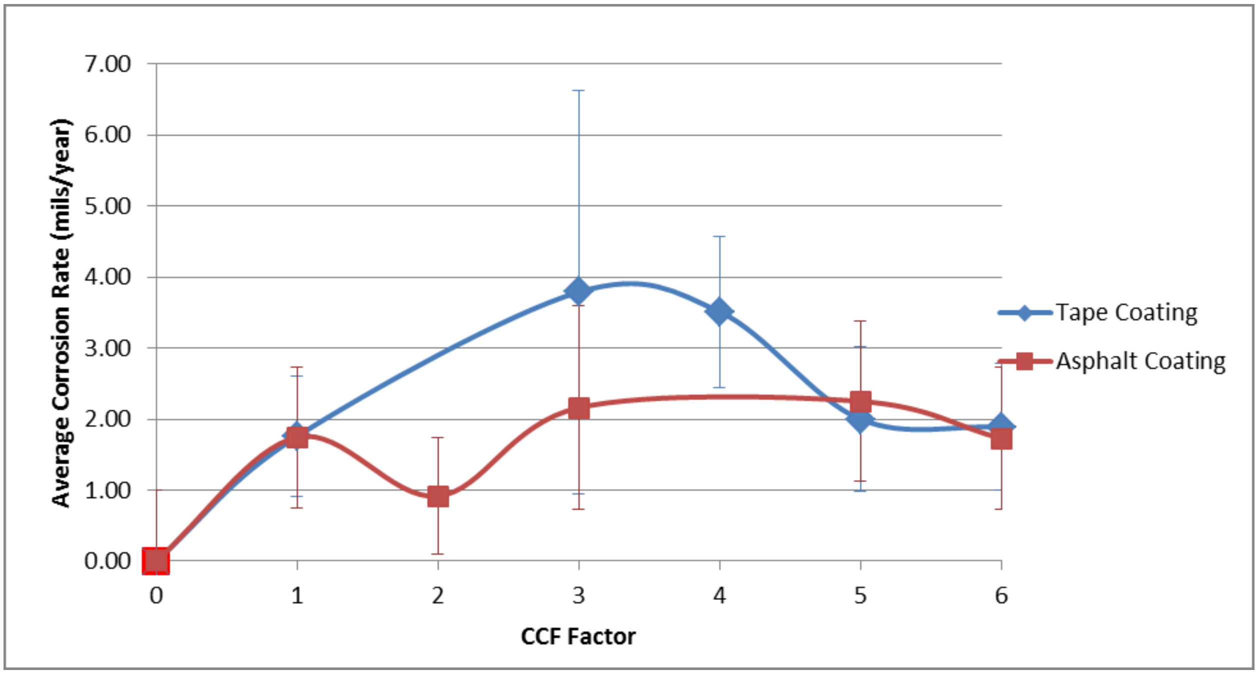

Figure 5-6: Average Corrosion Rate as a Function of the Combined Coating Factor (CCF)

To refine the data based on the estimated alkalinity of the environment under the coating, the pipeline surface under the coating was inspected through photographs provided in the dig reports. The possibility of an alkaline environment was assessed based on the presence and relative amount of white deposits ($CaCO_3$ and $FeCO_3$) that form in more alkaline conditions under disbonded coatings. Those environments can be related to the soil and ground water characteristics at the site, or can be promoted by sufficient CP penetrating towards the steel under the disbondment. The formation of an iron carbonate ($FeCO_3$) protective film inhibits further dissolution of iron and thus decreases the corrosion rate.

Environments where the amount of white deposits ($FeCO_3$ or $CaCO_3$) was relatively low and environments where no white deposits were found were classified as near-neutral pH environments. These environments suggest that insufficient CP reached the pipeline to promote the formation of a protective iron carbonate ($FeCO_3$) film to decrease the metal dissolution.

The importance of the refinement process discussed above is to isolate the cases that more likely occurred under near neutral pH conditions, where insufficient CP was reaching the pipeline and a protective iron-carbide coating did not form on the surface to inhibit the corrosion of steel. Figure 5-7 shows a corrosion site under wrinkled coating where only minor quantities of $CaCO_3$ and $FeCO_3$ can be observed; this site was characterized as a near neutral pH site. The corrosion rate as a function of CCF for the near-neutral pH environment, and potentially-high pH analysis is plotted in Figure 5-8 for tape coatings and asphalt coatings. As the main interest of this work remains with the near-neutral pH cases, the remaining potentially alkaline pH cases are not presented.

Figure 5-7: Corrosion under a Wrinkled Coating with Minor Alkaline Precipitates

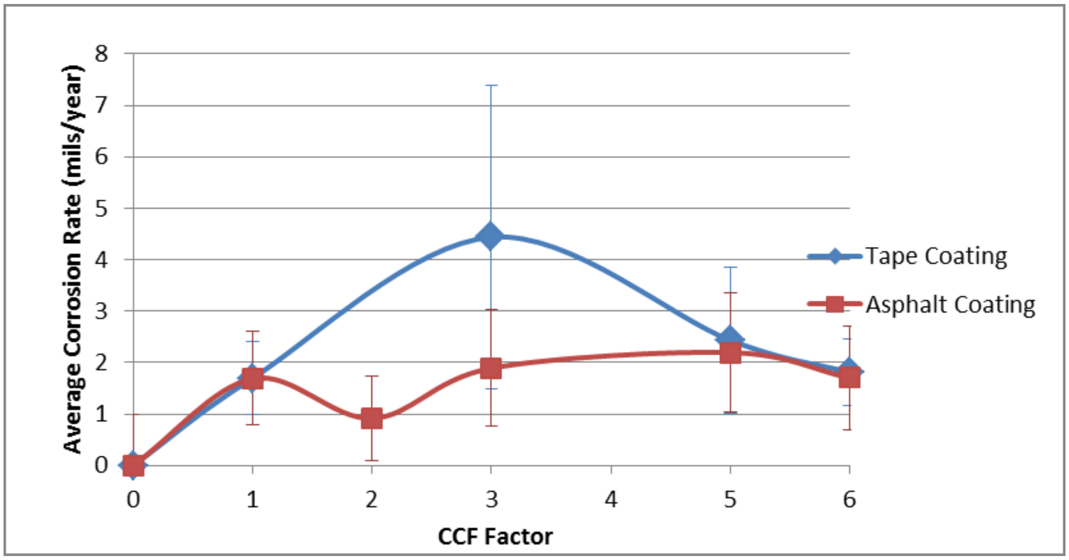

Figure 5-8: Average Corrosion Rate as a Function of the Combined Coating Factor for Refined Near-neutral pH Cases for Tape and Asphalt Coatings

5.4.1.2 Corroded Area as a Function of CCF

The corroded area for each near-neutral pH corrosion case (based on the environmental analysis above) for both tape and asphalt coatings was calculated based on the given corrosion width and corrosion length, and the average corroded area for each CCF factor was obtained, and is presented in Figure 5-9. The corroded area for CCF=0 was estimated to equal to zero in both cases, since corrosion is not expected under coatings in excellent condition. Similar to corrosion rate analysis, certain CCF values did not have a statistically-significant number of cases, and therefore were not taken into account (CCF=2 and CCF=4 for tape coatings, and CCF=4 for tape coatings). The standard deviation in the corroded area for tape and asphalt coatings is also shown in Figure 5-9.

For tape coatings, it can be seen that for CCF=1 and CCF=3 the corroded area is relatively small, and it increases almost by a factor of 5 for CCF=5, and decrease for CCF=6. For tape coatings, the corroded area remains fairly consistent for all the CCF factors, with lower values for CCF=1 and CCF=6.

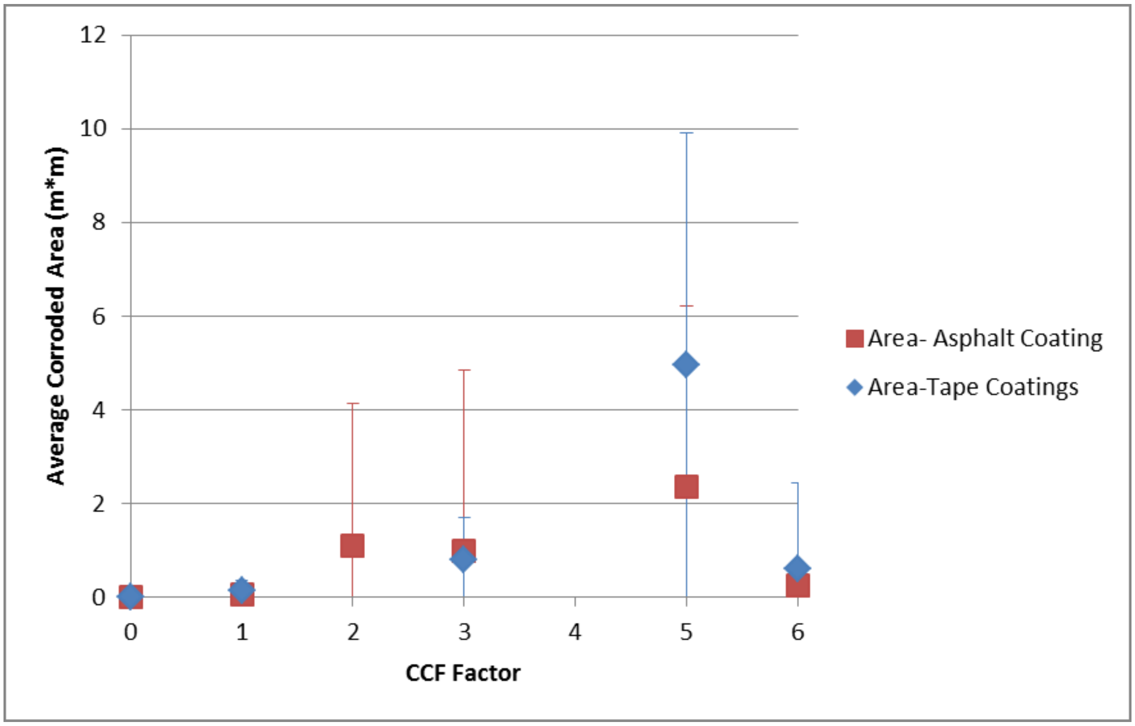

Figure 5-9: Average Corroded Area as a Function of the Combined Coating Factor for Refined Near-neutral pH Cases for Tape and Asphalt Coatings

5.4.2 Laboratory Simulations

An experimental setup designed to study the corrosion rate under disbonded coatings with various disbondment gaps (2 mm, 5 mm, 10 mm, and lack of coating) in anaerobic conditions purged with various concentrations of CO_2-nitrogen showed that the corrosion rate under disbonded coatings was affected by the size of the disbondment gap.

The overall corrosion reaction in an anaerobic environment with the presence of CO_2 is shown in Reaction 1.

$$Fe + CO_2 + H_2O \rightarrow Fe^{2+} + CO_3^{2-} + H_2 \text{ (Reaction 1)}$$

Smaller disbondment gaps (2 mm and 5 mm) yielded an enhanced corrosion rate at the positions close to the OM of the disbondment gap, The phenomena was explained by the presence of a metal-ion concentration cell inside the disbondment which was formed due to the geometrical constraint of the disbonded coating. The metal at the position adjacent to the OM was exposed to the bulk solution of the corrosion cell, where the concentration of metal ions was significantly lower than the concentration inside the disbondment, and was therefore anodic to the metal inside the disbondment that was exposed to a higher concentration of ferrous ions. This resulted in a localized enhanced corrosion at the anodic areas adjacent to the OM, and a decreased (almost null) rate of corrosion inside the disbondment at the cathodic areas.

Larger disbondment gaps (10 mm and infinite disbondment) did not form strong metal-ion concentration cells due to the ease of mass-transport of ferrous ions outside the disbondment. Therefore, the corrosion rate of the metal under the disbonded coating did not vary with distance from the OM, and was lower relative to the corrosion rate observed for smaller disbondments at the OM. As no concentration cell were formed under larger disbondments, the metal appeared corroded at all the locations underneath the disbanded coating.

Figure 5-10 shows the corrosion rate at the OM for various gap sizes obtained for 2%, 5%, and 20% CO_2 (balance nitrogen) concentrations. The corrosion rate in a situation with no coating disbondment is considered to be 0 mil/year, with a standard deviation of 1 mil/year due to a possibility of moisture and gas permeation under the coating. It can be seen that the corrosion rate at the OM decreases with disbondment size, regardless of the CO_2 concentration.

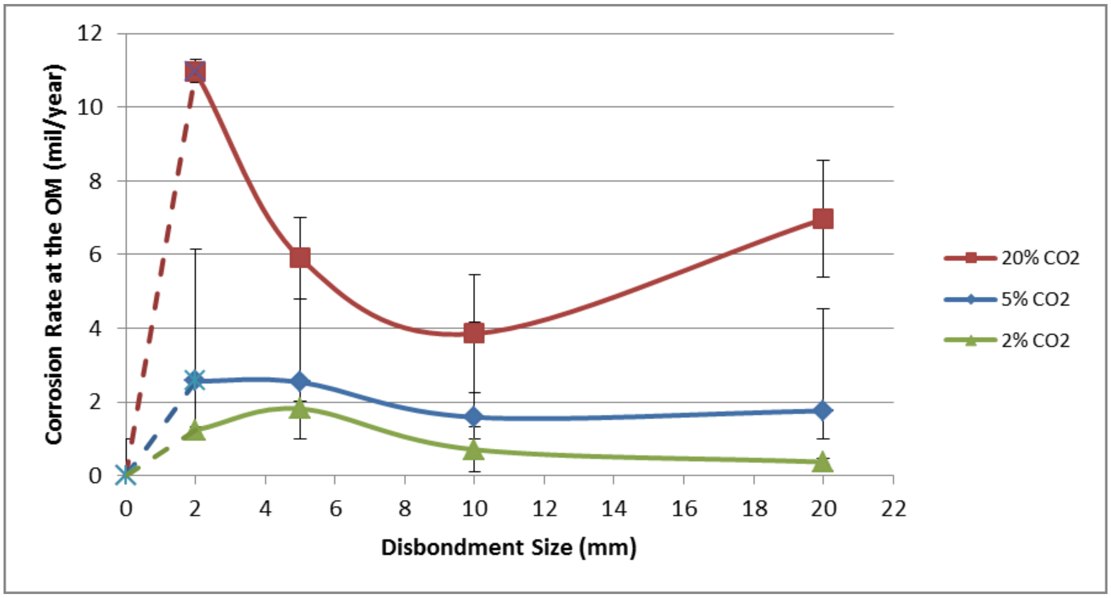

Figure 5-10: Corrosion Rate at the OM for Different Disbondment Sizes for 2%, 5% and 20% CO_2

Figure 5-11 shows the field data obtained in Figure 5-8 with superimposed corrosion rates at various CO_2 levels determined in the lab for the case of no coating shielding

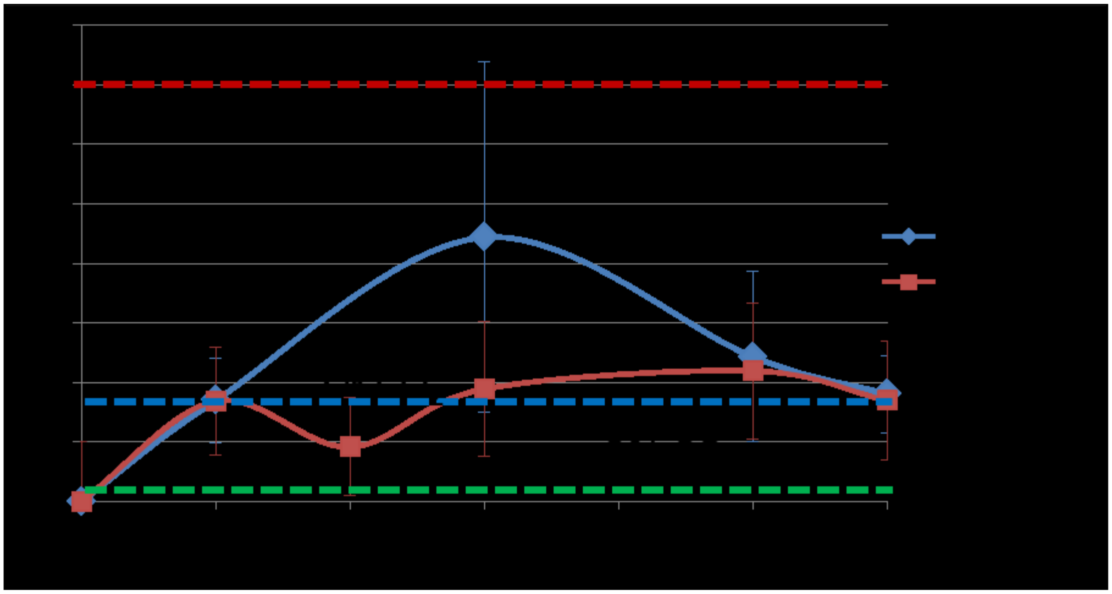

Figure 5-11: Average Corrosion Rate as a Function of the Combined Coating Factor for Refined Near-neutral pH Cases for Tape and Asphalt Coatings with Superimposed Average CO_2 Concentrations Obtained Experimentally

5.5 Analysis

5.5.1 Corrosion Behavior Characteristic of Coating Types

By analyzing Figure 5-8 it can be seen that the average corrosion rate under asphalt coatings is fairly consistent for all the CCF values, which can be explained by the fact that asphalt coatings fail cohesively in a brittle manner, often creating disbonded patches, as seen in Figure 5-3. Since asphalt coatings are known to be compatible with CP, in an event of a coating disbondment, CP can reach the pipeline and protect it from corrosion. Therefore, the corrosion rate in the case of asphalt coatings, is more dependent on the level of CP and soil characteristics (e.g. drainage, conductivity) than the coating condition. This explanation is also consistent with the average corroded area analysis, where the average corroded area remains fairly consistent for all the CCF values.

The average corrosion rate under the tape coating appears to vary based on the coating conditions, where the peak of it was observed under coatings with fair conditions with intermittent coating disbondments and moderate adhesion (CCF=3). The following discussion will explore this trend, and will attempt to provide an explanation to it.

5.5.2 Corrosion Behavior Characteristic of Coating Conditions for Tape Coatings

CCF=0 signifies locations where the coating is in a good condition, does not have any defects, and demonstrates good adhesion to the pipeline surface. In those conditions, the pipeline is expected to be fully protected from external corrosion. In certain cases, however, low corrosion rates (1 mil/year) can be observed under the coating due to ground water and gas permeation.

CCF=1 signifies locations with minor coating disbondment and very good adhesion, where the coating was found to be in good condition in all of the analyzed cases. Examining the average corrosion rate in this case it can be seen that it is fairly low, compared to the other CCF values. In this situation, minor wrinkling, small disbondments or crevices may form under the coating. However, since the coating condition was found to be good in all the cases, the access of ground water and gases into these disbondments or crevices may be limited or restricted. In this situation, there would be limited exchange of gases and solution with the environment (e.g.

through coating permeation), and the corrosion rate will remain low. This case also shows the strong effect of the environment on the corrosion rate, where coatings in good condition and minor disbondments may still experience a certain degree of corrosion due to permeation of gases (CO_2) and ground water solutions through the coating. The corrosion area analysis are consistent with the coating condition, where the average corroded area was very small, and close to 0 due to the good adhesion of the coating.

CCF=2 signifies locations with intermittent to minor disbondments and moderate to good adhesion, with good to fair coating conditions. For this case, insufficient data was available to make the results statistically significant; therefore, this category is not included in this analysis.

CCF=3 signifies locations with intermittent coating disbondments and moderate adhesion, where in most of the cases the coating was found in fair condition. In such a situation, the described coating is likely to have a certain degree of wrinkling, tenting, and sagging (as shown in Figure 3), where ground water solution can penetrate through the coating or a holiday in the coating. The average corroded area for the case where CCF=3 is relatively small.

CCF=4 signifies locations with moderate to intermittent disbondment in the coating and moderate to poor adhesion. Most of the analyzed cases in this category were excluded during the data refinement of potentially alkaline cases. Therefore, this category is not included in this analysis.

CCF=5 signifies locations with intermittent disbondment with moderate adhesion, where in most of the analyzed cases the coating condition was poor. The average corrosion rate in these locations also appears to be lower compared to CCF=3. For this case, the coating disbonds in a manner that doesn’t form wrinkles or disbondment gaps that trap ground water, but rather forms larger coating disbondments, as shown in Figure 3. As well, in these locations the poor coating condition may allow CP penetration towards the pipe, and thus protection from corrosion. Nonetheless, the average corroded area for CCF=5 is larger by a factor of 5 compared to the other cases, which is consistent with a larger metal area exposed at these coating conditions. However, the corrosion in this area is general and shallow.

CCF=6 signifies locations with continuous coating disbondment with bad coating adhesion to the pipeline surface. In these locations, the coating conditions were found to be very poor in most of the cases. The average corroded area of coatings with a CCF value of 6 also appears to be relatively low.

The analyses above discuss the apparent effect of the coating disbondment and adhesion conditions on the corrosion rate of pipelines in the field. However, other parameters such as ground water composition, ground gases, water drainage, solution resistivity, CP distribution, and seasonal changes may play an important role in the corrosion process of the pipe and can explain the standard deviation in the corrosion rate for various coating conditions.

5.5.3 Justification of the Concentration Cell Effect in Tape-coated Pipelines

In the experimental part of this research, three different CO_2 concentrations were used: 2% CO_2, 5% CO_2, and 20% CO_2; those concentrations were chosen based on winter (4% CO_2) and spring (23% CO_2) conditions. The experimental part of this research has demonstrated the significant effect of CO_2 concentration in the soil on the corrosion rate of pipeline steel. Analyzing Figure 5-11, it can be seen that the average corrosion rate in the field is very consistent with the general corrosion rate determined in the environment with 5% CO_2. This may imply that anaerobic corrosion on pipelines is predominant in the winter, when the ground CO_2 concentration is lower.

The experimental trend of the corrosion rate as a function of coating disbondment in Figure 5-10 illustrates that regardless of the CO_2 concentration in the ground, the corrosion rate reaches a local maxima at narrower coating disbondments and decreases as the disbondment size increases. The trend obtained from analysis of field data in Figure 5-8 shows that the average corrosion rate reaches a maxima peak at CCF=3, (characterized as intermittent disbondment, with a possible presence of wrinkling), and decreases for CCF=5 and CCF=6 as the coating disbondment increases. The similarity between the trends suggest that the analysis of the relation between the corrosion rate and CCF values can be based on the experimental results presented in this work. The maxima peak at CCF=3 consistent with the experimental findings, where a strong concentration cell promoted enhanced corrosion at the OM of the 2 mm gap, where a peak in the corrosion rate was observed for 5% and 20% CO_2. As seen in the experimental results, formation of wrinkles and relatively small disbondment gaps can promote the formation of a concentration cell, by retaining ground water solution inside the disbondment (or wrinkle), and gradually increasing the metal ion concentration in the trapped water solution, relative to the concentration in the surrounding soil/ground. This may cause metal sites exposed to lower concentrations of ferrous ions (closer to the OM) to experience enhanced corrosion. The concentration cell hypothesis is consistent with the corroded area analysis in Figure 5-9, where the average corroded area for the case where CCF=3 is relatively small, and is likely limited to the anodic locations in the concentration cell.

For larger coating disbondment sizes at CCF=5 and CCF=6, the average corrosion rate obtained through field data analysis in Figure 5-8 appears to decrease, The conditions in this case resemble the conditions of the coating disbondment experiment for the infinite gap disbondment, where the general corrosion rate under the coating is lower compared to coatings in good conditions with smaller disbondments. In these cases, the pipe may be cathodically protected. This hypothesis is consistent with the relatively large corroded average area for CCF=5: since no concentration cell was present under the larger coating disbondments, all the regions under the coating and at the OM have likely experienced general corrosion.

5.5.4 Implications of Current Findings on Pipeline Integrity Management

This study has shown that the coating condition of tape coatings has strong implications on the corrosion rate of the underlying pipeline, while the corrosion rate under asphalt coating is likely affected by other factors. Specifically, this study showed that tape coating with fair conditions with intermittent coating disbondments are more prone to high rates of corrosion, compared to coatings in poor conditions. This observation was also confirmed experimentally, where it was shown that a concentration cell can form under coatings that generate narrow disbondments and wrinkles.

This finding may be important for development of corrosion protection strategies of pipelines, since it suggests that assessing the coating conditions of a pipeline may provide an insight into the corrosion rate under the coating. The coating conditions of a buried pipeline can be assessed by comparison with the coating condition in adjacent dig sites or with EMAT tools. Locations with coating conditions with intermittent coating adhesion may be more prone to corrosion, and thus require special attention to the corrosion evolution underneath them.

Since near-neutral pH SCC is commonly found under tape coatings, the findings of this study can help understand the different SCC crack morphologies found under disbonded coatings, and the dissolution (corrosion) processes that may contribute to the formation of these crack morphologies.

5.6 Conclusion

This study analyzed the effect of the coating conditions in the field on the anaerobic corrosion rate of the underlying pipeline for both tape and asphalt coatings, utilizing field dig report data. Analysis of the data showed that tape coatings with fair conditions and intermittent disbondment sizes have the strongest susceptibility to anaerobic corrosion, compared to coatings in good conditions and coatings in very poor conditions. This finding was explained through experimental results that showed that narrow coating disbondment gaps (characteristic to coatings in fair conditions) form a concentration cell with enhanced corrosion at the OM of the narrow coating disbondment. Asphalt coatings fail cohesively in a brittle manner which is not expected to form a concentration cell between the pipeline and the disbonded coating. This fact was found consistent with the observation that the condition of asphalt coatings did not strongly affect the corrosion rate of the pipeline under the coating. These findings suggest that CP should be provided based on the type of coating and the coating condition at each location.

5.7 References

1. National Energy Board Data, Obtained through: Oag-bvg.gc.ca, (2015). *Chapter 1—Transportation of Dangerous Products*. [online] Available at: http://www.oagbvg.gc.ca/internet/English/parl_cesd_201112_01_e_36029.html#ex5 [Accessed 4 Jan. 2015]
2. Kiefner, J.F and Rosenfeld M.J. The Role of Pipeline Age in Pipeline Safety*, INGAA Foundation Report* No 2012.04, 2012.
3. Cheng, Y. F. *Stress Corrosion Cracking of Pipelines*. Hoboken, New Jersey: John Wiley & Sons, 2013

4. Marcus, S. Oil and gas pipeline in Canada, *J. Oil Gas* 2, 15, 2009
5. Papavinasam, S. *Corrosion control in the oil and gas industry*. Burlington: Elsevier Science, 2013.
6. Papavinasam, S., M. Attard, and W. Revie. "External Polymeric Pipeline Coating Failure Modes." *Materials Performance* (October 2006)
7. Baker, M. “Stress corrosion cracking study- final report”. Page 48. January 2005.
8. Delanty. B. and O'Beirne, J. “Major Field Study Compares Pipeline SCC with Coatings,” Oil & Gas Journal, 90 (24), pp. 39-44, 1992.

CHAPTER 6 : UNDERSTANDING SURFACE CRACK MORPHOLOGIES UNDER DISBONDED COATINGS

6.1 Introduction

Near-neutral pH Stress Corrosion Cracking (SCC) has been a concern to pipeline operators since the 1980's, when it was first identified on buried pipelines under wrinkled coating where the pH was in the range of 5.5 and 7.5. Near-neutral pH SCC, similar to high pH SCC, forms under the synergistic effect of environment, susceptible material, and stress. Near-neutral pH SCC commonly forms under disbonded tape coating where trapped water solution accumulates; in these locations, CP cannot penetrate under the coating to protect the pipeline due to its shielding by the insulating coating [11, 1].

Recoating pipelines with a coating that is not prone to SCC (e.g. Fusion Bonded Epoxy (FBE)) may provide a solution for SCC generation and development on pipelines; however, it is not economically feasible. Therefore, SCC is mitigated by the industry through the use of In Line Inspection (ILI) tools, pipeline excavations, and pipeline pressurization during hydro-tests – all aimed to detect cracks with a critical size and eliminate their threat to a leak or a rupture in service [1]. Meanwhile, cracks that are not at their critical size still remain a potential threat, due to a possibility of rapid growth. Hence, developing an understanding of the factors that affect the crack growth and morphology may assist in SCC mitigation.

As near-neutral pH SCC cracks originate and grow under disbonded tape coatings, understanding the effect of the environment under the disbonded coatings and the effect of the coating condition is of great importance. Previous studies have been performed to study the effect of the environment on crack initiation and growth. In a study performed by Eslami *et al.* in OCP near-neutral pH conditions it was found that coating disbondment and environmental parameters affect the SCC initiation mechanisms [3]. Egbewande examined the effect of a localized environment generated under an imitated coating and found that crack growth is higher at the Open Mouth (OM) of the coating compared to the bottom of the disbondment [46]. Egbewande's experiments examined the growth of pre-cracks grown from a notch; however, SCC cracks are commonly shallow surface cracks.

Experiments performed by Chen and Sutherby [5] on X-65 pipeline steel in C2 solution showed that crack growth is affected by multiple parameters :ΔK (stress intensity factor range), K_{max} (max stress intensity , and f (frequency). They showed that the threshold from crack dormancy to active growth can be represented by a combined factor containing the fore-mentioned parameters, where $\Delta K^2 * Kmax/f^{0.1} = 8500\ (MPA*m^{0.5})/f^{0.1}$.

In Chapter 4 of this thesis it was shown that narrower coating disbondment gaps (2 mm gap) promoted a formation of a metal ion concentration cell due to the narrow geometry of the coating that restricted mass-transport of species into and out of the disbondment. This effect was not found in wider coating disbondments, where mass transport (e.g. convection) of species into the disbondment was not restricted by the disbondment geometry.

This study examines the effect of the coating disbondment gap size on the morphology of shallow surface cracks at the different positions under the disbondment. The study was performed under applied cyclic tensile stress, with a combined coating factor beyond the threshold value, to avoid crack propagation. This would minimize the potential crack growth caused by mechanical driving forces but allow a better examination of the concentration cell within the crack under the disbonded coating and its effect on crack growth and the evolution of crack morphologies.

6.2 Experimental Setup

In order to simulate a pipeline under a disbonded coating subject to stress, a tensile specimen was inserted into a corrosion cell containing ground water solution with a shielding simulating a coating disbondment. A more detailed description of the corrosion cell and the tensile sample is provided below.

6.2.1 Corrosion Cell

The corrosion cell was fabricated out of transparent acrylate, and was designed to contain a shielding imitating a coating disbondment with a gap between the coating and the metal specimen. The gap between the coating and the metal specimen varied between 2 mm and 10 mm, simulating narrower and a wider coating disbondment gaps, respectfully. The cell contained C2 simulated ground water solution, previously purged for at least 48 hours with 5% CO_2-

nitrogen gas to remove dissolved oxygen from the solution and establish a pH of 6.3. The composition of the C2 solution chemistry is as follows: $MgSO_4 \cdot 7H_2O$/0.0274 g/L, $CaCl_2$/0.0255 g/L, KCl/0.0035 g/L, $NaHCO_3$/0.0195 g/L, $CaCO_3$/0.0606 g/L. The solution outside the disbondment, between the shielding and the metal specimen, imitated trapped water solution, while the solution in the cell imitated bulk ground water in the soil. The solution in the cell was purged with 5% CO_2-nitrogen to imitate field conditions. The coating disbondment did not allow solution or gas penetration from the bottom of the disbondment, so that the dissolved CO_2 in the solution and the originated CO_2-related species (carbonate and bicarbonate) could transport into the disbondment only from its OM. The design of the corrosion cell is shown in Figure 6-1.

The cell was thoroughly sealed from oxygen with silicone prior to pouring the solution inside, and the solution was poured into the cell in a manner that prevented oxygen penetration, to insure anaerobic conditions inside the cell during the experiment. The cell remained in anaerobic OCP conditions for the full duration of the test. At the end of the test, the sample was extracted from the cell, wiped with ethanol, and thoroughly dried to avoid oxidation

.

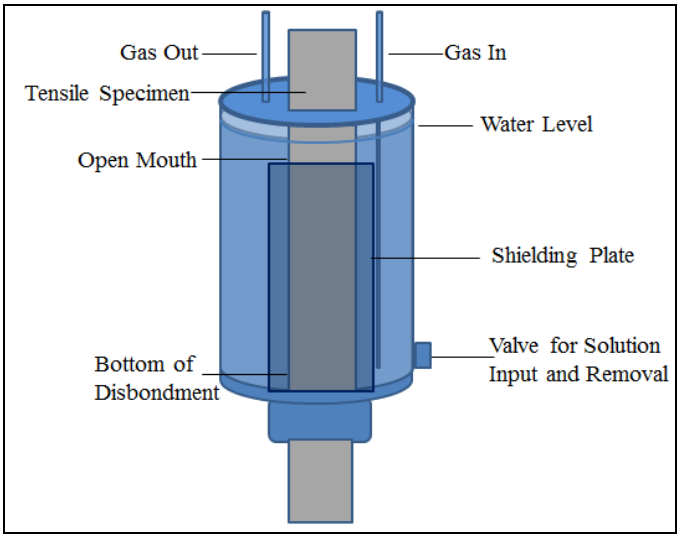

Figure 6-1: Tensile Test Corrosion Cell Components

6.2.2 Sample Preparation

The tensile specimens were machined out of X60 pipeline sections taken from the field after experiencing a service failure; the composition of the steel is shown in Table 6-1. The sections used for machining the tensile specimens did not experience any external damage, nor were they affected by SCC or corrosion; therefore, they were fit for experimental analysis. The tensile specimens had three reduced sections (gauges) with the dimensions 23*45*9.2 mm, the samples were designed to have three gauge sections to understand the crack behavior in three locations under a disbonded coating: top (OM), middle, and bottom.

Table 6-1: X-60 Composition

Element	Composition, wt%
C	0.18
Mn	1.4
P	0.0175
S	0.0131
Si	0.0364
Cu	0.0326
Ni	0.0182
Cr	0.0284
Mo	0
V	0.0061
Al	0.0493
Sn	0.0031

For pre-crack initiation, shallow electrical discharge machining (EDM) notches were made in the middle of each gauge, the notches were semi-circular with a surface length of 10 mm and a depth length of 2.5 mm. The location of the EDM notches on the tensile specimen is shown in Figure 6-2.

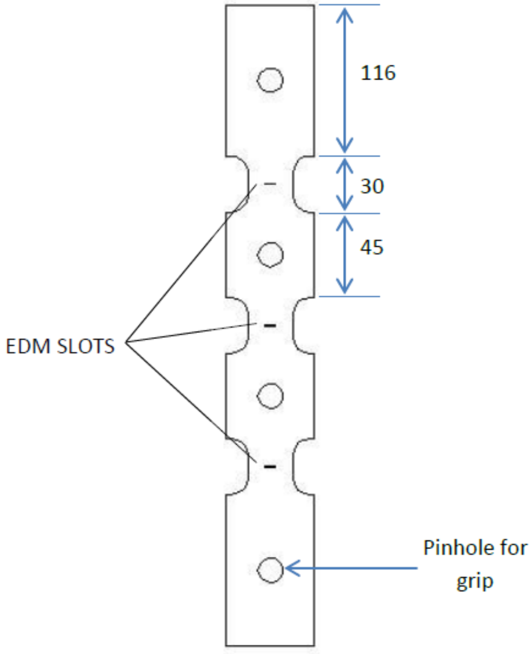

Figure 6-2: Tensile Specimen Geometry

6.2.3 Shallow Crack Production

Prior to the test, surface pre-fatigue cracks were produced on the gauge sections from the EDM notches. The combined length of the pre-fatigue cracks from both sides of the machined notch was 1.8 mm.

After the pre-fatigue cracks were produced, the front surface of the tensile specimen was ground until the machined EDM notches were completely ground off, as shown in

Figure 6-3.

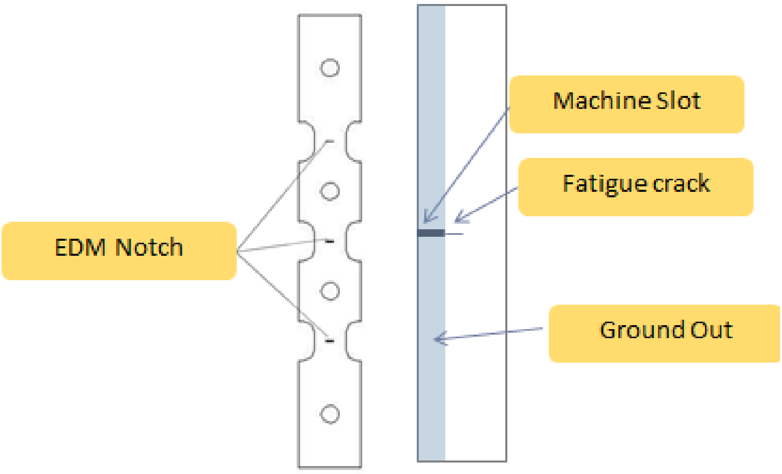

Figure 6-3: Production of Shallow Cracks

In order to simulate realistic field conditions where only one face of the pipeline was exposed to the corrosive environment, the back of the sample was coated with epoxy in order to avoid any corrosive interaction between both faces.

6.2.4 Mechanical Loading Conditions

Chen and Sutherby analyzed the corrosion-fatigue crack growth behavior of X65 pipeline steel using the compact tension specimen geometry in a near-neutral pH environment using the corrosion-fatigue model [9]. This work found that crack growth threshold conditions were below 8500 $(MPa.m^{0.5})^3/Hz^{0.1}$ in C2 solution

For this study, the loading parameters are presented in Table 6-2: Loading Parameters. The sample was loaded to 75% SMYS, which is a common loading rate of pipelines in operation. The duration of the test was 48 days for the 10 mm gap, and 45 days for the 2 mm gap. The corresponding intensity factors (ΔK and ΔK_{max}) depend on the crack length, and are presented in Table 3. From Table 3, it can be seen that the combined coating are below the threshold 8500 $(MPa.m^{0.5})^3/Hz^{0.1}$, and substantial crack growth was not expected.

Table 6-2: Loading Parameters

Material	**X60 Pipeline Steel**
75% SMYS	312.75 MPa
Area	128.8 (mm^2)
R	0.4
Mean Stress	28 (kN)
A	12 (kN)
Waveform	triangular
f	0.005 (Hz)
Test Duration	48 days (10 mm gap) 45 days (2 mm gap)

Table 6-3: Combined Factor Value before the Test

Location	**2a (m)**	**a (m)**	**ΔK ($MPa.m^{0.5}$)**	**Kmax ($MPa.m^{0.5}$)**	**Combined Factor (($(MPa.m^{0.5})^3/Hz^{0.1}$))**
2 mm					
Top	2.55E-03	1.28E-03	11.87	19.79	4738.68
Middle	2.48E-03	1.24E-03	11.71	19.52	4544.90
Bottom	2.95E-03	1.48E-03	12.77	21.28	5896.31
10 mm					
Top	3.27E-03	1.64E-03	13.45	22.41	6881.27
Middle	3.48E-03	1.74E-03	13.87	23.12	7554.67
Bottom	3.17E-03	1.59E-03	13.24	22.06	6568.04

6.2.4 Post-test Analysis

6.2.4.1 Electrochemical Conditions

To avoid interference with the test through oxygen penetration and solution mixing by insertion of micro-electrodes, the pH inside the disbondment was measured only at the end of the test. The pH inside the disbondment gap was measured at three distinct locations at the end of the test:

OM (Open Mouth), middle by using commercial combination micro-electrodes. The diameter of the microelectrodes was smaller than 1.6 mm; they were calibrated carefully in buffer solutions of pH 4 and 7 prior to each measurement.

Imaging

To illustrate the change in the crack morphology induced by the test conditions, images of the crack before the test and after the test were obtained. Due to the large sample size, SEM images of the crack could not be obtained, since the sample could not fit into the vacuum chamber. Therefore, the images of the sample prior to the test were obtained though optical microscopy after the sample was polished to 600 grit.

After the test, the tensile specimen was sectioned for scanning electron microscopy (SEM) analysis. The surface crack was examined 1) with the original corrosion products on the surface, 2) after oxide removal (with 100 ml water/4 ml Cis-2-butene-1,4-diol/3 ml HCl), 3) after polishing the surface, and 4) after etching the surface with 3% Nital.

After the SEM images of the surface crack were obtained, the sample was sectioned with EDM in the middle of its width, polished, and SEM images of the crack in the depth direction were obtained of the polished surface and after etching with 3% Nital.

Afterwards, the sample was left in liquid nitrogen for half an hour to facilitate its fracturing, in order to examine the fracture face and detect the section representing the crack growth in C2 solution during the test. The fractured surface was analyzed through SEM analysis as well.

6.3 Results

pH measurements of the solution inside and outside the disbondment for both the 2 mm gap and the 10 mm gap were within the pH range of the near-neutral pH environment.

6.3.1 Characteristics of Crack Morphology Prior to Corrosion Exposure

Images of the cracks on the tensile specimen were obtained prior to the experiment with the use of an optical microscope. Figure 6-4 shows the crack morphology and Figure 6-5 shows the crack morphology prior to exposure to the corrosive environment. From Figure 6-5 it can be seen that the crack tip is fairly sharp.

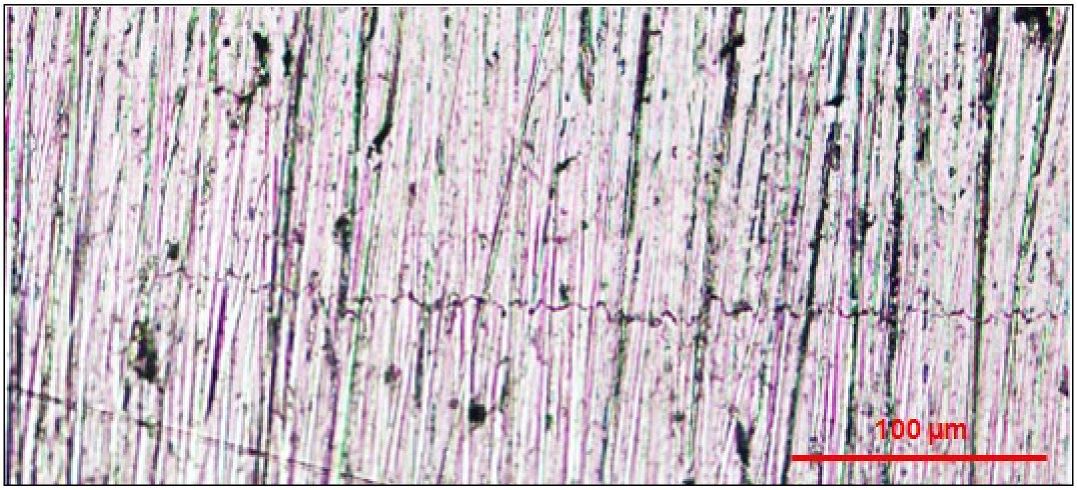

Figure 6-4: Crack Prior to Exposure to the Corrosive Environment

Figure 6-5: Crack Tip Prior to Exposure to the Corrosive Environment

6.3.2 Characteristics of Crack Morphology under Disbonded Coating with 10 mm Gap

6.3.2.1 Crack Morphology at the Surface

Figure 6-6 shows the cracks morphology under the 10 mm disbondment gap at the different positions under the disbondment (top, middle, and bottom).The cracks at all the position appear to have a uniform width, where the cracks at the middle and bottom positions appear to be wider compared to the crack at the top position. A similar trend is observed at the crack tips in Figure 6-7 where the crack tip at the top position is sharper than the crack tip at the middle and bottom positions.

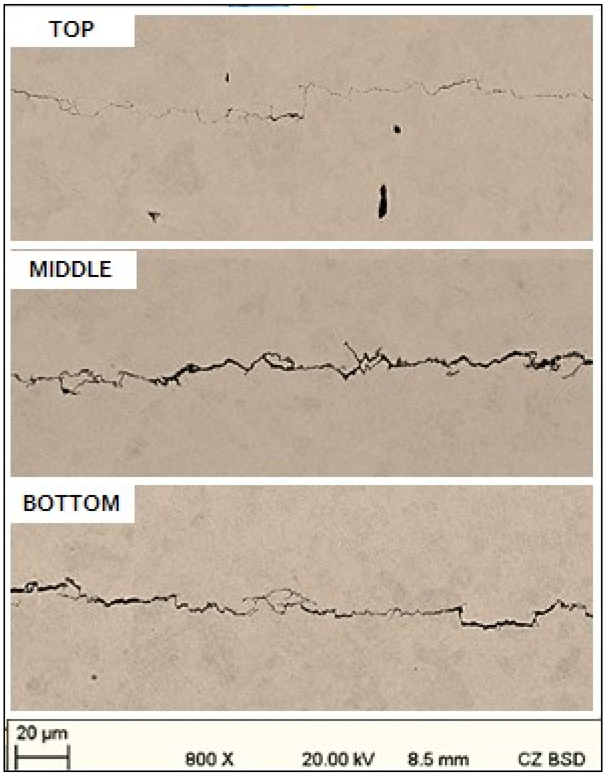

Figure 6-6: Surface Crack Morphology of the Top, Middle, and Bottom Cracks under the 10 mm Disbondment Gap

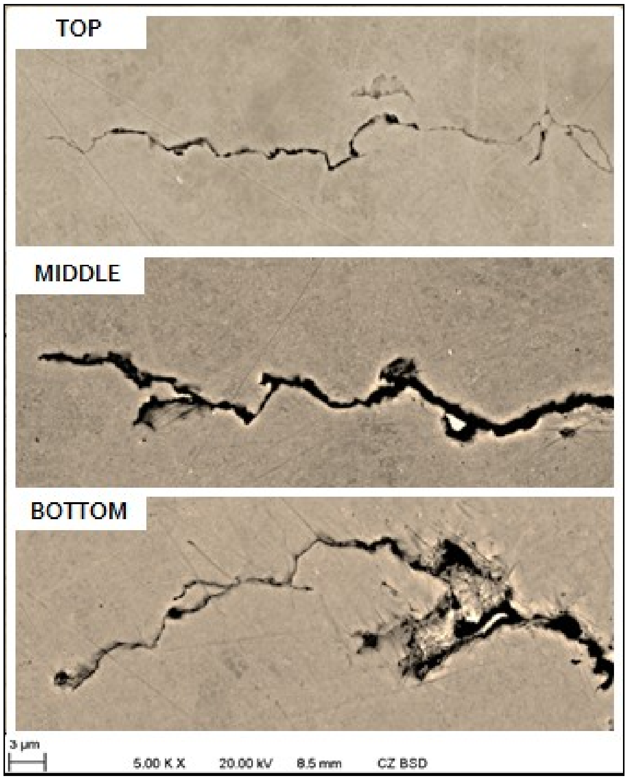

Figure 6-7: Surface Crack Tip Morphology of the Top, Middle, and Bottom Cracks under the 10 mm Disbondment Gap

Figure 6-8-a and Figure 6-8-b show the sample surface after etching at a lower and a higher magnification, respectfully. From Figure 6-8-b it can be seen that the cracking was trans-granular, which is consistent with near-neutral pH SCC.

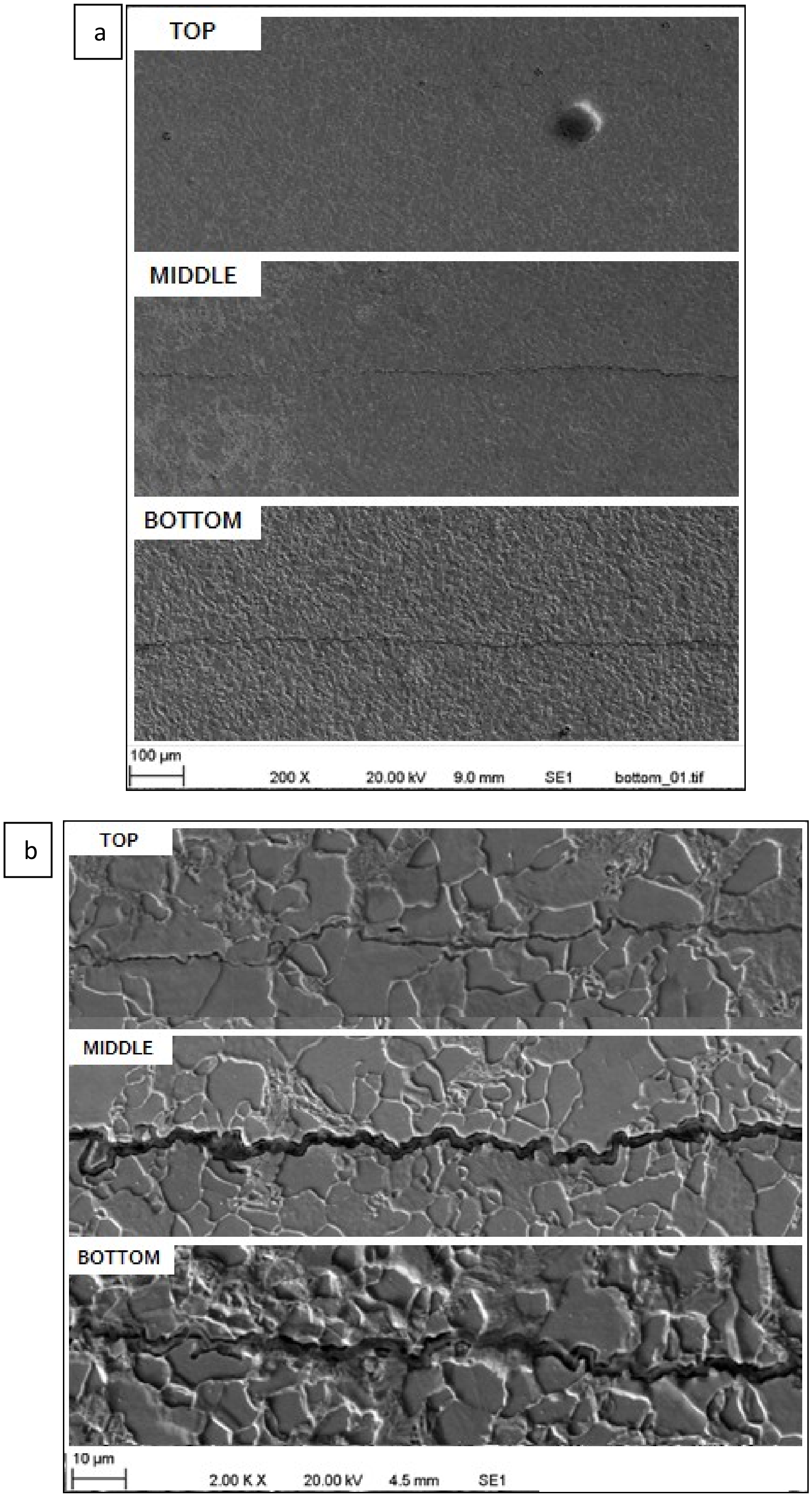

Figure 6-8: Surface Morphology after Etching by the Top, Middle, and Bottom Cracks under the 10 mm Disbondment Gap at a) Lower Magnification and b) Higher Magnification

6.3.2.2 Crack Morphology of the Cross-section

Figure 6-9 shows the crack morphology of the 10 mm disbondment gap on the cross-section of the specimen and Figure 6-10 shows the crack tip morphology under a higher magnification for the top, middle, and bottom cracks. The individual cracks appears to be none-uniform and have regions of corrosion pockets, shown in Figure 6-11. The narrowest regions of the cracks appear to be on the surface, and the crack tips of the cracks at all the positions appear to be sharp.

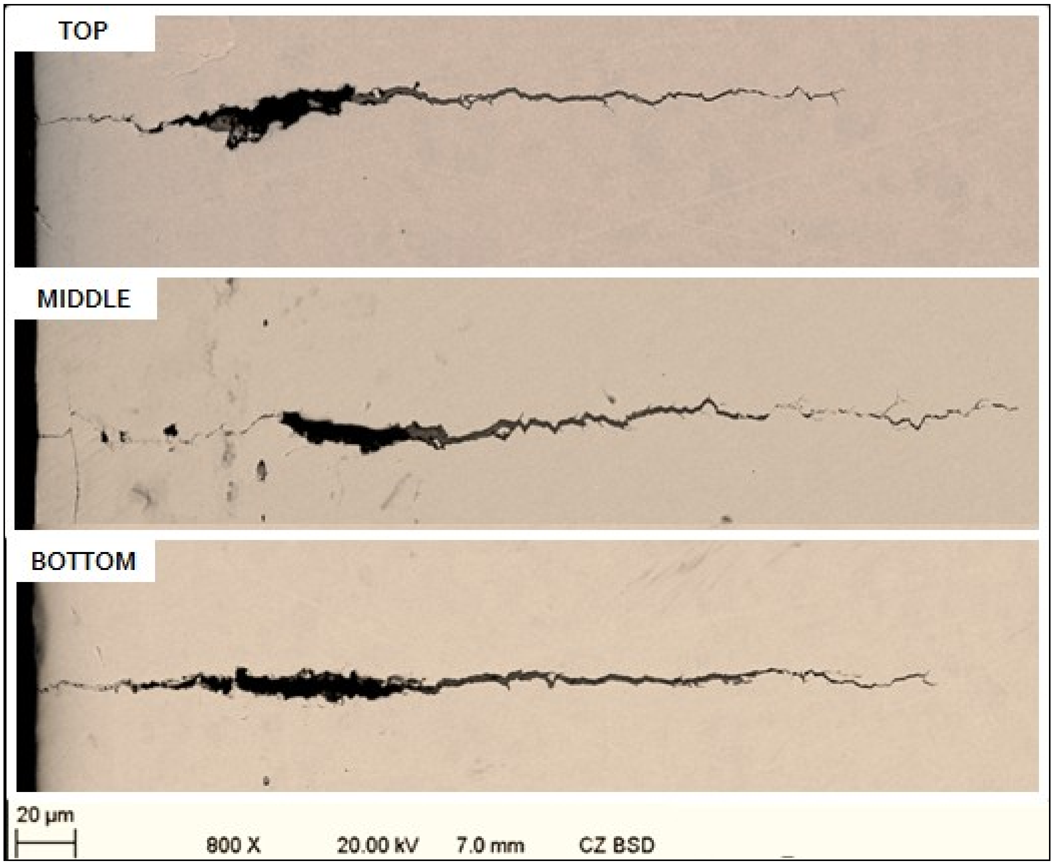

Figure 6-9: Cross-Section Crack Morphology of the Top, Middle, and Bottom Cracks under the 10 mm Disbondment Gap

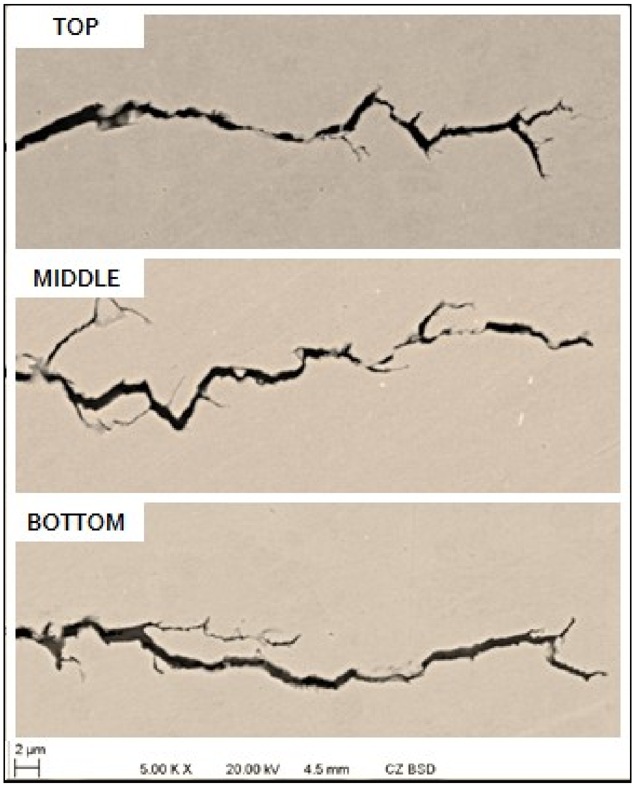

Figure 6-10: Cross-Section Crack Tip Morphology of the Top, Middle, and Bottom Cracks under the 10 mm Disbondment Gap

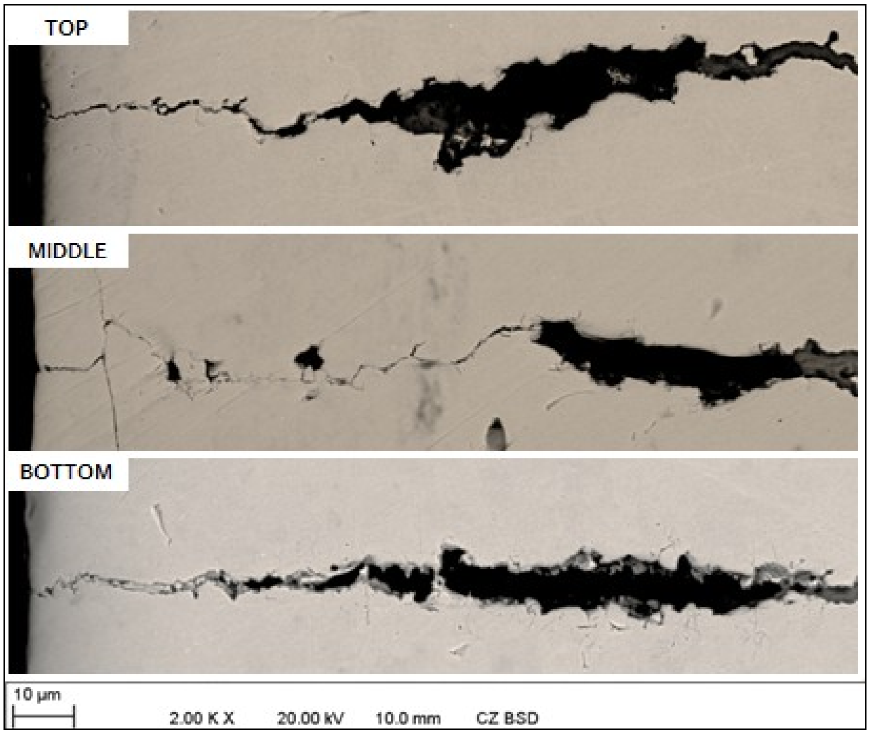

Figure 6-11: Cross-Section Corrosion Pocket Morphologies of the Top, Middle, and Bottom Cracks under the 10 mm Disbondment Gap

6.3.3 Characteristics of Crack Morphology under Disbonded Coating with 2 mm Gap

6.3.3.1 Crack Morphology at the Surface

Figure 6-12 and Figure 6-13 show the cracks' morphology of the sample under the 2 mm disbondment gap at the different positions under the disbondment (top, middle, and bottom) at a lower and a higher magnification. In Figure 6-12, it can be seen that the width of the cracks at all the positions are not consistent, and have narrower and wider sections. The wider regions of the cracks at the bottom and middle positions are wider than the wider regions of the cracks at the top position. Comparing the width at the relative positions (top, middle, and bottom) under the 2 mm and 10 the mm disbondment, it can be seen that the cracks' width of the wider sections of the cracks under the 2 mm disbondment is greater than the crack width of the 10 mm disbondment.

Figure 6-14-a and Figure 6-14-b show the cracks and the crack-tips at the top, middle, and bottom positions under the 2 mm disbondment gap at a higher magnification.

Comparing Figure 6-7 and Figure 6-14-a, it can be seen that on the crack tips of the cracks under the 2 mm disbondment gap are blunter than crack tips of the cracks under the 10 mm disbondment gap. As well, the cracks under the 2 mm disbondment gap have regions with lighter Backscattered Electron (BSE) intensity within the crack. Similar regions can be observed on the cracks away from the crack tips in Figure 6-14-a.

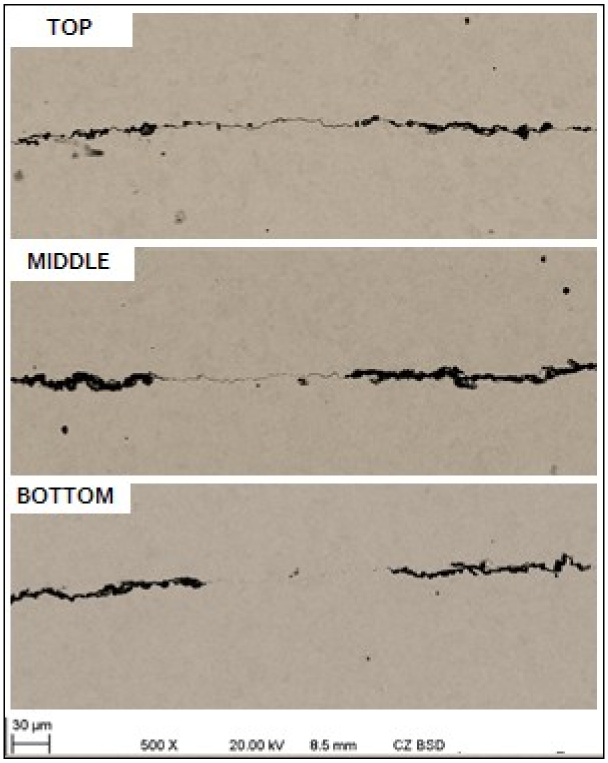

Figure 6-12: Surface Crack Morphology of the Top, Middle, and Bottom Cracks under the 2 mm Disbondment Gap

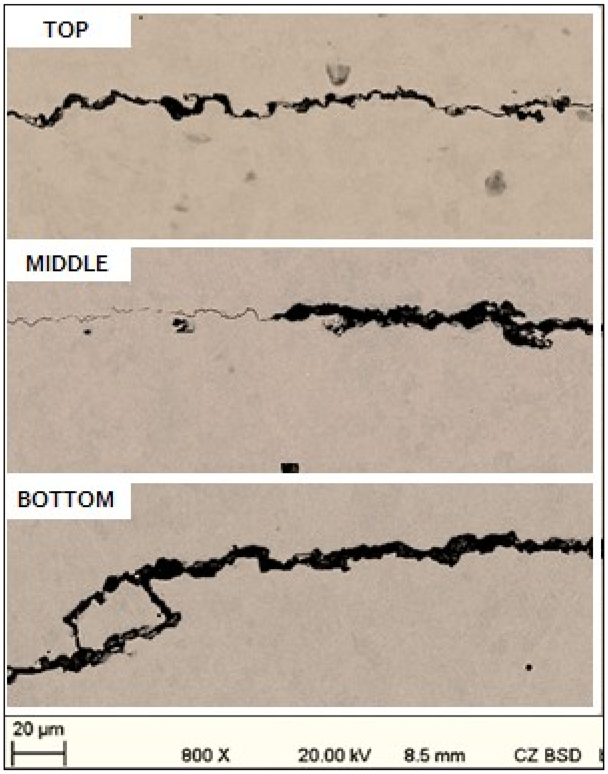

Figure 6-13: Surface Crack Morphology of the Top, Middle, and Bottom Cracks under the 2 mm Disbondment Gap at a Higher Magnification

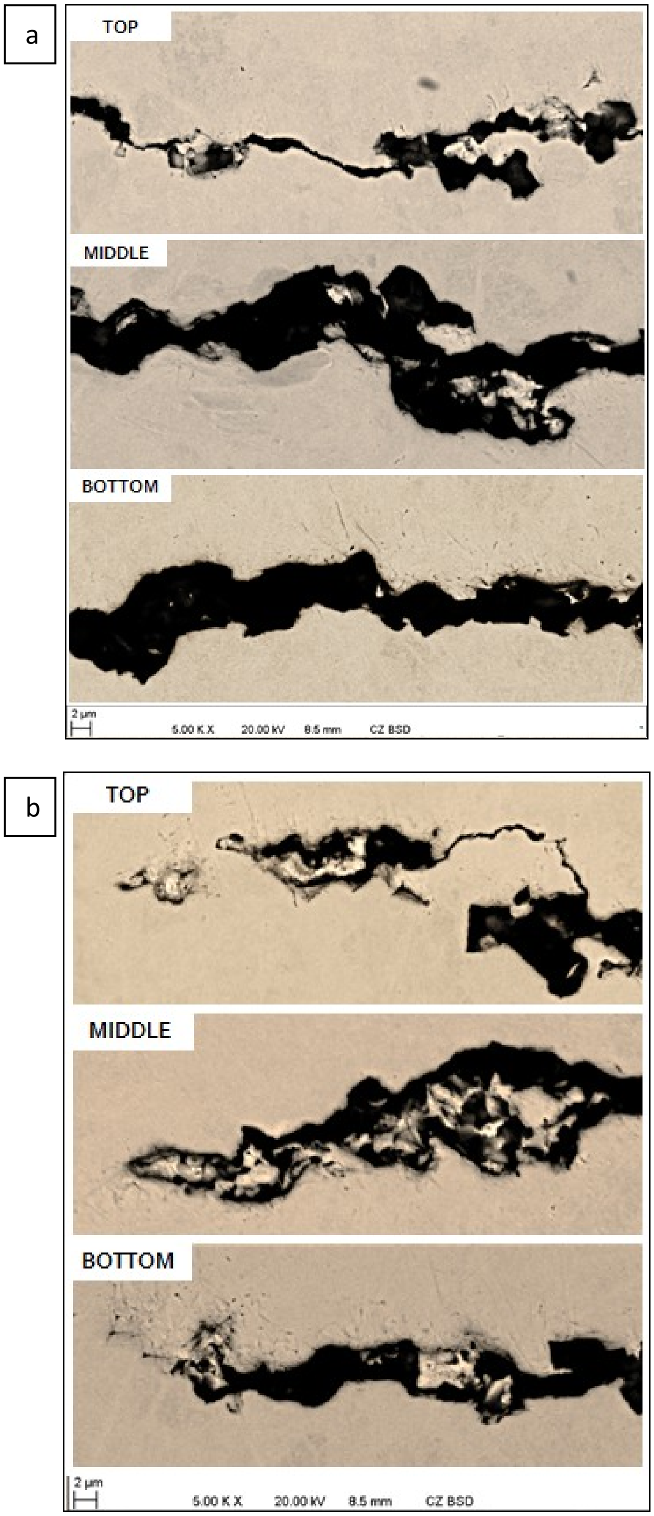

Figure 6-14: a) Surface Crack and b) Surface Crack Tip Morphology of the Top, Middle, and Bottom Cracks under the 2 mm Disbondment Gap

Figure 6-15-a and Figure 6-15-b show the sample surface after etching at a lower and a higher magnification, respectfully. Figure 6-15-a of the etched surface shows that the cracking was transgranular, which is consistent with near-neutral pH SCC.

Analyzing Figure 6-15-b of the etched cracks' surfaces of the 2 mm disbondment gap, it can be seen that the material surrounding the 2 mm crack has lighter areas at the thinner regions of the crack at the top and bottom positions. This may be indicative of the presence of a banded microstructure, where the lighter areas are areas of pearlite within a ferritic structure.

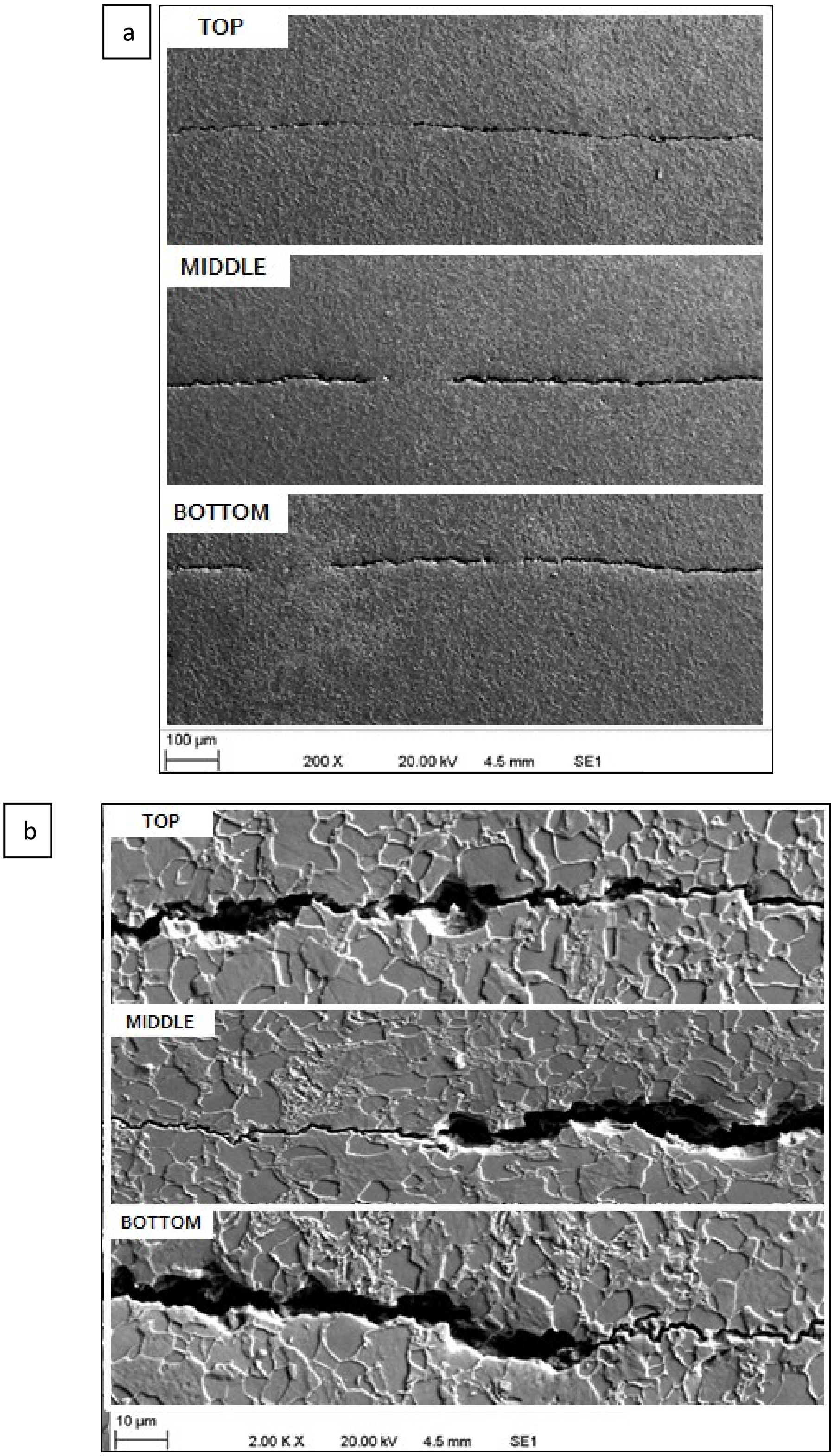

Figure 6-15: Surface Morphology after Etching by the Top, Middle, and Bottom Cracks under the 2 mm Disbondment Gap at a) Lower Magnification and b) Higher Magnification

6.3.3.2 Crack Morphology at the Cross-section

Figure 6-16 shows the crack morphology of the 2 mm disbondment gap in the depth direction and Figure 6-17 shows the crack tip under a higher magnification for the top, middle, and bottom cracks. The cracks at all the positions are wedge-shaped, with the widest crack-crevice on the surface. The crack tip of the top crack is blunter than the crack tip of the bottom crack; however, they are both sharper than the crack tip of the middle crack.

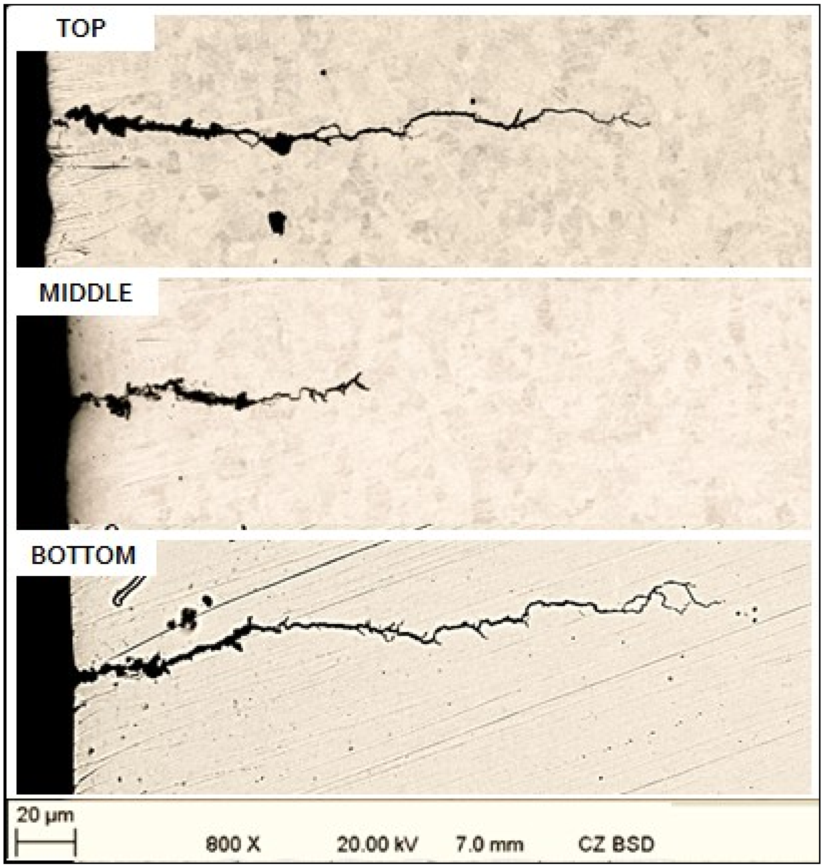

Figure 6-16: Cross-Section Crack Morphology of the Top, Middle, and Bottom Cracks under the 2 mm Disbondment Gap

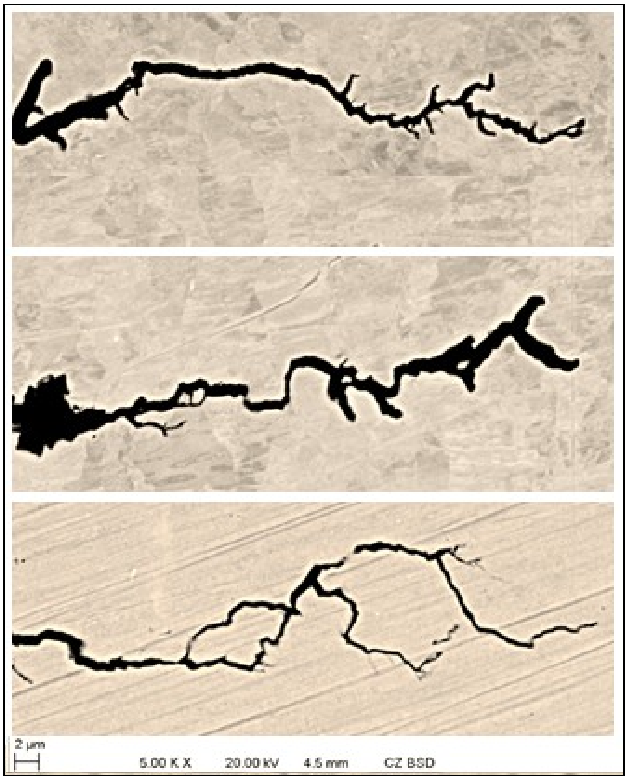

Figure 6-17: Cross-Section Crack Tip Morphology of the Top, Middle, and Bottom Cracks under the 2 mm Disbondment Gap

6.3.4 Net Crack Growth after Corrosion Exposure

Figure 6-18 and Figure 6-19 show the fractured surfaces of the cracks under the 10 mm and the 2 mm disbondment gaps at the top, middle, and bottom positions under the disbondment. It can be seen that the specimens did not experience significant crack growth, consistent with the calculation of the combined factor in Section 6.2.4.

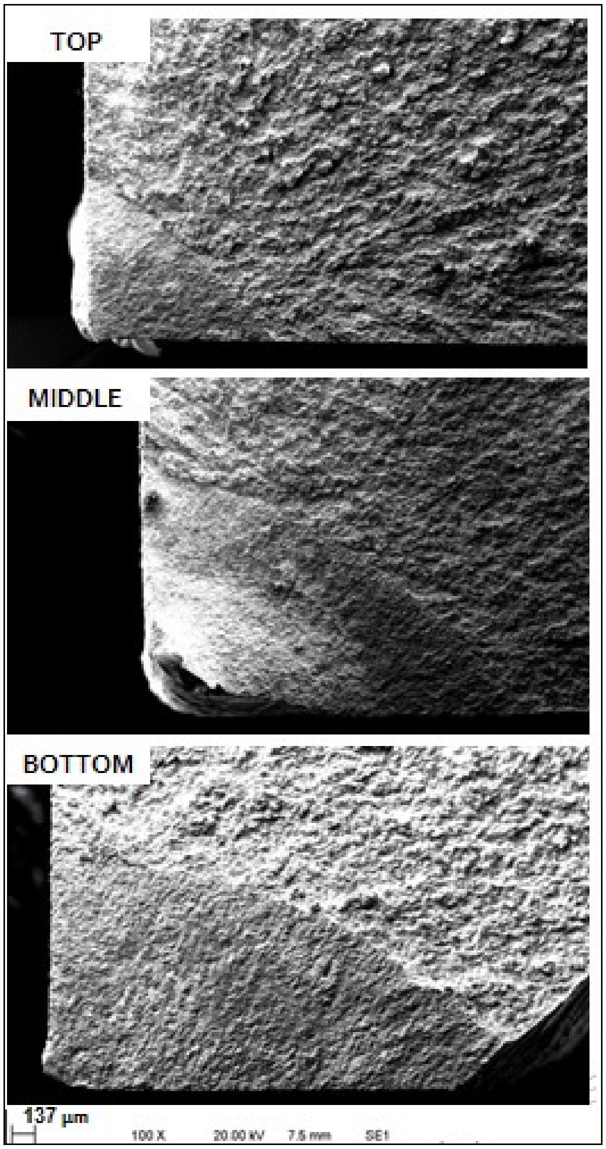

Figure 6-18: Fractured Surface Morphology of the Top, Middle, and Bottom Cracks under the 10 mm Disbondment Gap

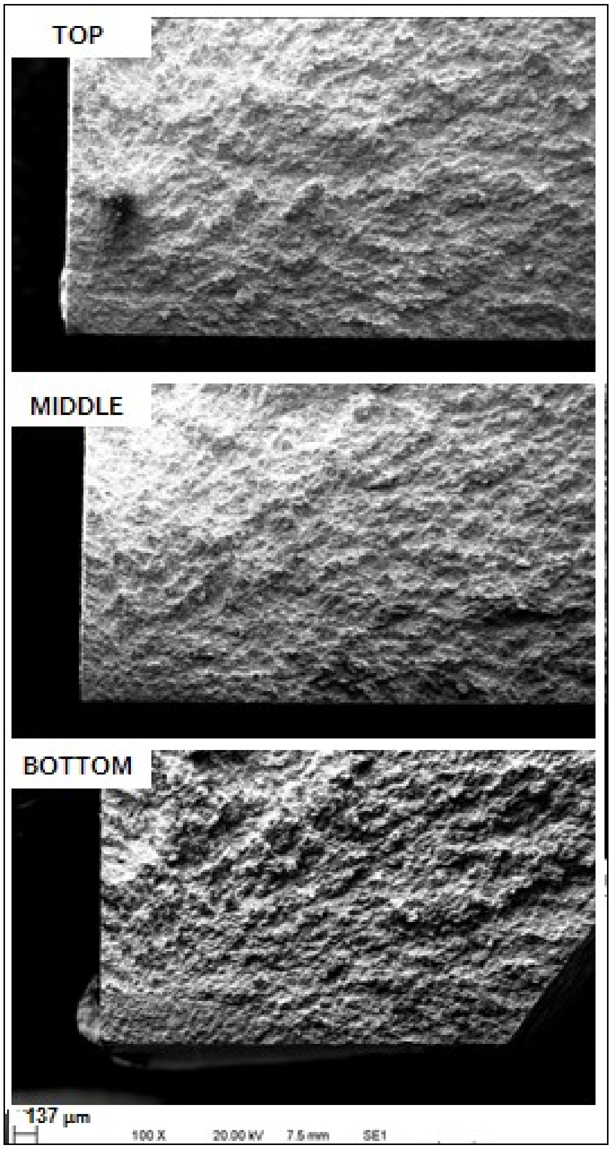

Figure 6-19: Fractured Surface Morphology of the Top, Middle, and Bottom Cracks under the 2 mm Disbondment Gap

6.3.5 Summary of the Crack Morphological Features

Table 6-4 below summarizes the surface crack morphologies of the 2 mm and 10 mm cracks.

Table 6-4: Crack Morphologies Observed on the Surface of the Specimen

General appearance			
Position	**Top**	**Middle**	**Bottom**
10 mm gap	Fine and uniform crack crevice	Wider and uniform crack crevice	Wide crack crevice and uniform
2 mm gap	Fine or wide crack crevice	Fine or wide crack crevice	Fine or wide crack crevice
Crack tip morphologies			
10 mm gap	Sharpest	Sharp	Sharp
2 mm gap	Blunt	Blunt	Blunt

Table 6-5 summarizes the cross-section crack morphologies of the 2 mm and 10 mm cracks at the top, middle, and bottom positions under the disbondment.

Table 6-5: Crack Morphologies observed on the Cross-section of the Specimens

<table>
<tr><th colspan="4">General appearance</th></tr>
<tr><th>Position</th><th>Top</th><th>Middle</th><th>Bottom</th></tr>
<tr><td>10 mm gap</td><td colspan="3">Non-uniform with internal corrosion pockets below the surface and the narrowest crevice at the surface</td></tr>
<tr><td>2 mm</td><td colspan="3">Wedge-shaped with the widest crack crevice at the surface</td></tr>
<tr><td colspan="4"></td></tr>
<tr><th colspan="4">Crack tip morphologies</th></tr>
<tr><td>10 mm gap</td><td colspan="3">It appears similar at different positions and they are all sharp</td></tr>
<tr><td>2 mm gap</td><td>Sharp</td><td>Blunter</td><td>Sharpest</td></tr>
</table>

6.4 Analysis

A previous study discussed in Chapter 4 showed that coating disbondment gap affected the corrosion rate of the underlying metal. Figure 6-20 was obtained in Chapter 4 through corrosion weight-loss experiments under various disbondment gap sizes. It exhibits the corrosion rate at the different positions from the OM for a 2 mm, 5 mm, 10 mm, and infinite disbondment gap sizes.

The main goal of this study was to understand the effect of the coating disbondment gap size on the morphology of shallow surface cracks at the different positions under the disbondment. Two different systems were analyzed: a 2 mm disbondment gap, and a 10 mm disbondment gap.

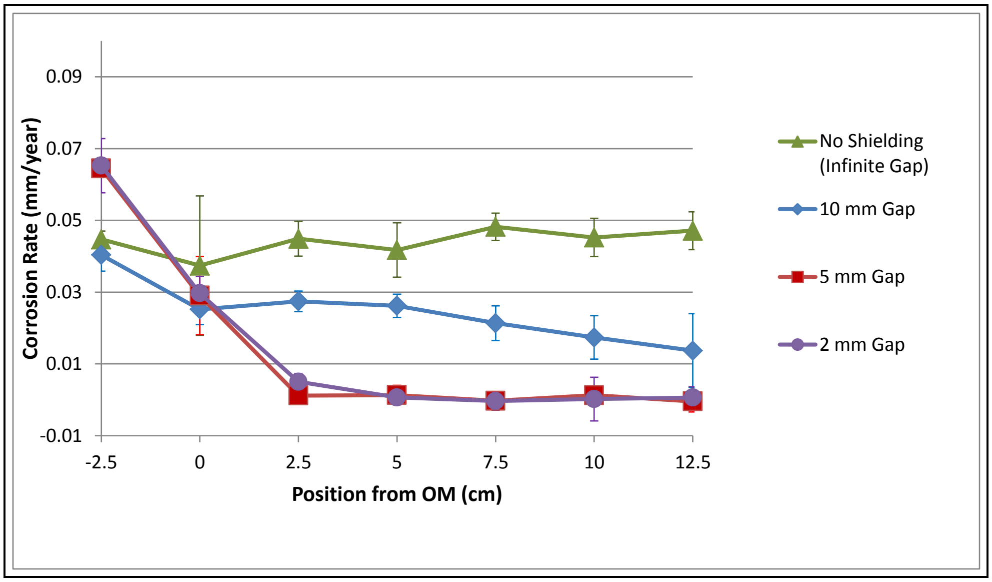

Figure 6-20: Corrosion Rate in De-aerated C2 Ground Water Solution at Various Positions From the OM for a Solution Purged with 5% CO2, Determined Based on 30-day Tests

Due to the similarity of the systems of the 2 mm disbonment gap and the 10 mm disbondment gap (in terms of solution, purging gas, and experimental duration), it is reasonable to assume that the difference in the gap size is the main contributor to the difference in the crack morphology between the samples under discussion.

According to Figure 6-20, narrower 2 mm gap disbondments promote a formation of a metal ion concentration cell with a higher rate of metal dissolution at the OM (where the ferrous ion concentration is lower) and a decreased rate of metal dissolution (almost null) at the middle and the bottom of the disbondment (where the metal ion concentration was higher). The higher metal ion concentrations assumed inside narrower disbondment gaps was attributed to the difficulty of mass-transport of the metal ions out of the disbondment.

Wider 10 mm gap disbondment gaps don't allow the formation of a metal ion concentration cell due to the ease of mass-transport of metal ions in and out of the disbondment. Therefore, under a 10 mm disbondment gap there weren't observed strictly anodic and strictly cathodic sites, but rather a gradual decrease in the corrosion rate towards the bottom of the disbondment.

As well, the geometry of the 2 mm disbondment gap restricts mass transport of CO_2 and CO_2-related species (carbonate and bicarbonate) into the disbondment. Therefore, the concentration of these species would be expected to be significantly lower inside the 2 mm disbondment gap compared to the 10 mm disbondment gap.

6.4.1 General Dependence of the Coating Disbondment Gap Size on the Cracks' Morphological Features

In order to understand the effect of the corrosive environment on the crack morphology, a comparison of the crack images obtained prior to the experiment and the images obtained after the experiment is required. The pre-corrosion surface crack morphology was obtained with an optical microscope, as the available SEM chamber could not contain the tensile specimen. After the experiment, the tensile specimen was sectioned, and SEM analysis was performed on the cracks to obtain a more-precise morphology. Due to the use of different microscopy techniques for crack-morphology imaging prior to the experiment and after the experiment, an exact comparison of the cracks was not possible; therefore, only a qualitative comparison was performed.

Comparing the pre-corrosion surface crack morphology in Figure 6-4 with the 10 mm disbondment gap cracks' (top, middle, and bottom) morphologies in Figure 6-6, it can be seen that the crack morphology at the top position was not greatly affected by the corrosive environment. The middle and the bottom cracks appear to have a small degree of widening in the corrosive environment. As well, the corrosive environment affected the crack tip (Figure 6-7) at the middle and bottom positions by slightly blunting them, while the top position crack appears to remain unchanged.

Comparing the pre-corrosion surface crack morphology in Figure 6-4 with the 2 mm disbondment gap cracks' (top, middle, and bottom) morphologies in Figure 6-13, it can be seen that the crack under the 2 mm disbondment gap has widened at certain regions. The narrow regions on the crack appear almost unchanged, compared to the initial pre-corrosion crack width. As well, the corrosive environment promoted crack-tip blunting (Figure 6-14) of the cracks at all the positions under the 2 mm disbondment gap.

6.4.2 Effect of Coating Disbondment Gap Size on the Morphology of the Cracks at the Surface

It was observed in Figure 6-12 that the cracks under the 2 mm disbondment gap have narrower and wider regions. These phenomena can be explained by the presence of a banded microstructure on the tested specimen, where pearlite regions are cathodic to ferrite regions, and can promote galvanic corrosion between the different regions on the crack.

Analyzing Figure 6-14, areas with lighter BSE intensity were observed at the crack tip and away from the crack tip on the cracks under the 2 mm disbondment at all the positions. These areas may be an indication of pearlitic structures that formed a galvanic cell with the surrounding ferrite, creating a wider crack crevice through dissolution of the ferrite phase. The degree of crack widening and crack tip blunting is likely to be dependent on the relative size and location of the ferrite regions at the crack locations.

6.4.3 Effect of Coating Disbondment Gap Size on the Morphology of the Cracks' Cross-section

6.4.3.1 Corrosion-Pocket Formation under the 10 mm Disbondment Gap

According to Figure 6-20 the 10 mm disbondment gap does not promote a strong concentration cell; therefore, the morphology of the cracks under the 10 mm disbondment gap is likely to be affected more by a factor different from the ferrous-ion concentration.

Corrosion-Pocket Initiation

A factor that may be considered to contribute to corrosion and dissolution processes inside the cracks is the concentration of dissolved carbon dioxide, carbonate and bi-carbonate. Carbonate and bi-carbonate are present inside the cell due to the dissociation reaction of the bubbled carbon dioxide-nitrogen gas mixture, where carbon dioxide dissociates into carbonate and bi-carbonate. The cell in both of the experiments was continuously purged with gas with a content of 5% CO_2-nitrogen; however, the concentration of the gas inside the disbondment gap is different due to the geometric constraint of the disbondment. Since the concentration of CO_2 and CO_2-related species is convection-related, its concentration inside the narrower 2 mm disbondment gap is lower compared to its concentration inside the 10 mm disbondment gap.

As the cracks experience cyclic loading, the opening and closure of the cracks may promote a pumping action, where CO_2-related species may penetrate inside the crack. The distance of the CO_2 penetration into the crack may be limited, thus promoting a CO_2 concentration where regions exposed to a higher CO_2 concentration (the section between the crack face and the corrosion pocket) would be more cathodic compared to regions inside the crack. This difference in the CO_2 concentration may be responsible for the initiation of the corrosion pockets, observed in Figure 6-11, through Reaction 1.

$$Fe + CO_2 + H_2O \rightarrow Fe^{2+} + CO_3^{2-} + H_2 \text{ (Reaction 1)}$$

Corrosion Pocket Growth

As anodic dissolution inside the cracks initiates due to a CO_2 concentration cell, the concentration of ferrous Fe^{+2} inside the disbondment increases. However, since the crack experiences opening and closure promoted by the cyclic loading, the ferrous ions initiating at the anodic locations transport into other locations inside the crack. Thus, accumulation of metal ions at a single location on the crack and creation of a ferrous-ion concentration cell is prevented.

Therefore, the anodic locations of the CO_2-concentration cell continue to dissolve, creating the observed corrosion-pockets. The increase in the volume of the corrosion-pockets on the crack as a result of the anodic dissolution may also decrease the concentration of species (ferrous ions and CO_2) inside the pockets, compared to the narrower locations on the crack, thus promoting the concentration cell effect of both CO_2 and ferrous ions between the crack regions closer to the front face and the corrosion pocket region.

The crack regions closer to the crack tip would not experience the same pumping effect as the ones closer to the specimen front, and the CO_2 reaching the crack region of the corrosion-pockets is likely to be entirely consumed by the corrosion reaction. Therefore, the crack regions between the corrosion-pockets and the crack tip appear unaffected by the CO_2 concentration cell.

As the CO_2 concentration would be consistent at all the positions inside the disbondment (top, middle, and bottom), the pumping of CO_2 and the concentration cell effect inside the crack would be expected to be similar at all the positions. This would promote a similar dissolution rate inside the cracks at all the positions, resulting in corrosion pockets of similar sizes, which is fairly consistent with the experimental observations, as seen in Figure 6-11.

6.4.3.2 Wedge-shape Crack Formation under the 2 mm Disbondment Gap

a. Middle and Bottom Cracks

For the 2 mm disbondment gap, the solution inside the disbondment would have a lower CO_2 concentration and a higher ferrous ion concentration. Therefore, the initiation of corrosion pockets (promoted by a CO_2 concentration cell) would not be expected for the cracks under the 2 mm disbondment gap. As ferrous ions may be pumped into the crack during the cyclic opening and closure of the crack, the ferrous ion concentration may differ inside the crack. Regions away from the crack face may have a higher ferrous ion concentration due to the geometrical constrain of the crack which decreases the ease of ferrous ion convection out of these areas during cyclic crack opening and closure (compared to the areas closer to the face of the crack). This may promote a ferrous ion concentration cell inside the crack, where regions closer to the crack face are anodic to the regions away from the crack face. The metal ion concentration cell inside the crack may result in a higher dissolution of areas closer to the crack face, giving the crack a wedge shape.

b. Top Crack

Based on Figure 6-20, the crack at the top (OM) of the 2 mm disbondment is likely to be exposed to a lower concentrations of ferrous ions, and a higher concentration of CO_2. However, as the metal at this position undergoes dissolution, the concentration of ferrous ions immediately adjacent to the crack may be high. The dissolved ferrous ions and CO_2 may penetrate into the crack through pumping during the cyclic opening and closure of the crack.

Based on the discussion above for the 10 mm disbondment, pumping of CO_2 may result in a CO_2 concentration cell between regions inside the crack closer to the front surface with a higher CO_2 concentration and regions away from the front surface with a lower CO_2 concentration. This concentration cell was noted to result in formation of corrosion pockets, as seen in Figure 6-11 for the cracks under the 10 mm disbondment gap. However, based on Figure 6-20, this is not the case for the crack at the OM of the 2 mm disbondment gap.

This phenomena may be explained through a formation of a ferrous ion concentration cell inside the crack at the OM similar to the one described for the middle and bottom cracks, resulting in the same crack shape. This concentration cell formation may be thermodynamically more favorable compared to the CO_2 concentration cell formation.

The top crack may also be affected by the CO_2 concentration at the OM, which is higher than the CO_2 concentration inside the disbondment.

c. <u>Contribution of a Banded Microstructures</u>

In addition to the ferrous ion concentration cell, another mechanism may contribute to the formation of a wedge-shaped morphology of surface cracks. Section 6.4.2 discussed the effect of banded microstructures on the morphology of surface cracks, where surface crack dissolution occurs through galvanic corrosion between the ferrite and pearlite structures on the steel. This shows that the surface of the specimen under the 2 mm disbondment gap has pearlite areas, which may cause the enhanced dissolution of cracks at all the positions under the disbondment at locations close to the surface. Regions away from the specimen surface closer to the crack tips may be more ferritic, resulting in a lower dissolution at these locations.

6.4.4 General Consideration of Crack Morphologies of the Cracks under Disbonded Coatings in Near-neutral pH Environments

One of the general features commonly observed with respect to near-neutral pH SCC is the widening of the crack crevice. This investigation proposed several mechanisms for crack widening, generating different crack morphologies. Two main mechanisms for crack dissolution (causing widening) discussed in this study are the effect if CO_2 and CO_2-concentration cell and galvanic corrosion of banded microstructures.

6.4.4.1 Surface Crack Morphologies

Effect of CO_2

With the presence of CO_2 inside wider coating disbondment gaps, general dissolution of the steel surface promotes a uniform corrosion of the crack face, resulting in cracks with uniform widths.

The metal dissolution at the locations with lower CO_2 concentrations would be fairly uniform, as Shown in Figure 6-21.

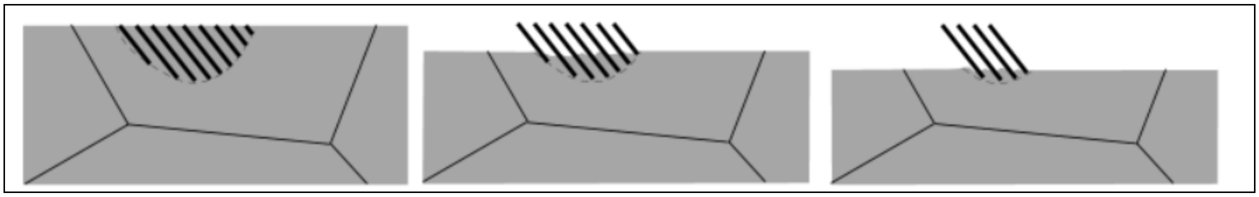

Figure 6-21: Schematic of Metal Dissolution Promoted by the Presence of CO_2

Effect of Banded Microstructure

In lower CO_2 concentrations characteristic to narrower disbondment gaps, in a situation where the surface of the specimen does not experience a high degree of dissolution, galvanic corrosion of banded microstructure may be enabled. In this case, the dissolution of the cracks can be attributed to galvanic corrosion between ferrite and pearlite phases of the banded microstructure. This situation is illustrated in Figure 6-22.

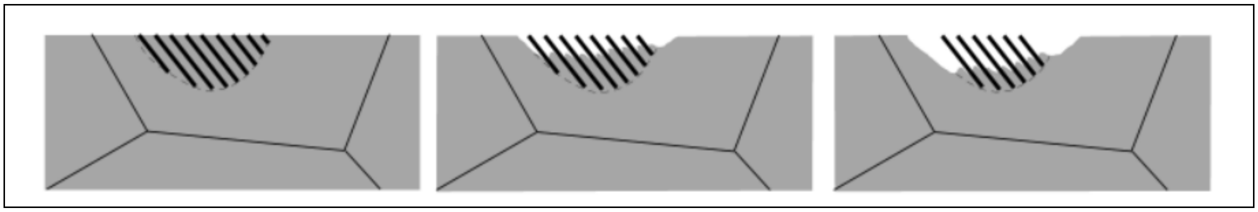

Figure 6-22: Schematic of Metal Dissolution Promoted by a Galvanic Effect of the Banded Microstructure

6.4.4.2 Cross-sectional Crack Morphologies

Effect of a CO_2 Concentration Cell

The formation of corrosion pockets on cross-sectional cracks was proposed to occur due to the presence of a CO_2 concentration cell between the regions closer to the crack surface and regions away from the crack surfaces due to differences in concentration of CO_2 and CO_2-related species pumped into the crack. This situation is possible when a sufficient concentration of CO_2 is present adjacent to the crack, as in the case of larger disbondment gaps.

In this situation, the potential difference created by the concentration difference of the CO_2 species drives the metal dissolution, and may be predominant over the potential difference between pearlite and cementite.

This may also explain why the cracks under the 10 mm disbondment gaps did not show any widening closer to the front face of the specimen, as was observed for the 2 mm disbondment gap. First, these crack regions were at the cathodic regions of the CO_2 concentration cell formed inside the crack. Second, the presence of CO_2 hinders the galvanic dissolution of banded microstructures, which may have contributed to the dissolution of the cross-sectional crack at areas adjacent to the specimen front face.

Effect of Banded Microstructures

When the CO_2 concentration inside the disbondment is low, galvanic corrosion between the banded microstructures may be prevalent and contribute to the crack widening at the regions adjacent to the specimen surface. The galvanic effect of the banded microstructures, coupled with a ferrous-ion concentration cell inside the crack, may promote the formation of a wedged morphology, as observed for a narrower disbondment gap.

6.5 Conclusion

This study discussed the crack morphologies formed on X-60 steel under smaller and larger assemblies imitating tape coating disbondment gaps on pipelines (2 mm and 10 mm) in anaerobic conditions inside a simulated ground water solution, continuously bubbled with 5%

CO_2-nitrogen under cyclic loading. It was shown that under larger coating disbondment gaps (10 mm), the surface cracks at all the positions under the coating were relatively narrow and formed corrosion pockets on the cracks' cross-sections. These crack morphologies were attributed to a formation of a CO_2 concentration cell between the locations away from the crack surface that were exposed to lower CO_2 concentrations, and locations closer to the crack surface, where the CO_2 concentration was higher. For narrower coating disbondments (2 mm), the surface cracks at all the positions under the disbondment appeared to have narrower and wider regions, and the cracks' cross-sections appeared to be wedge-shaped. The formation of narrower and wider regions on the crack were attributed to the presence of banded microstructure, where a galvanic cell formed between the ferrite and pearlite microstructures. The same effect was assumed to be responsible for the wedge shape of the cross-section crack, in conjunction with a ferrous-ion concentration cell between the cracks' surfaces and regions away from the crack surfaces.

6.6 References

1. Baker, M. *Stress Corrosion Cracking Study- Final Report*. Rep, 2005.
2. Cheng, Y. F. *Stress Corrosion Cracking of Pipelines*. Hoboken, New Jersey: John Wiley & Sons, 2013.
3. Eslami, A., Kania, R., Worthingham, B., Van Boven, G., Eadie, R., and Chen, W. "Effect of CO_2 and R-ratio on Near-neutral pH Stress Corrosion Cracking Initiation under a Disbonded Coating of Pipeline Steel." *Corros. Sci*. 53, 2318–2327, 2011.
4. Egbewande, A. Growth Behavior of Surface Cracks in Pipeline Steels Exposed to Near-neutral pH Environments. Thesis. University of Alberta, 2013.
5. W. Chen and R. Sutherby. "Crack Growth Behavior of Pipeline Steel in Near-neutral pH Soil Environments". *Metallurgical and Materials Transections A,* Volume 38A, 2007.

CHAPTER 7: THESIS SUMMARY AND FUTURE WORK

The objective of this thesis was to enhance the understanding of the effect of pipeline coating conditions on anaerobic corrosion and Stress Corrosion Cracking (SCC) of pipeline steel. Specifically, it was of interest to understand the effect of the coating disbondment gap size on the location and extent of corrosion of the underlying steel, and the effect of those processes on crack morphologies at the different positions under the disbondment. The main goal of the studies presented in the thesis was to understand the conditions forming under tape coatings when Cathodic Protection (CP) is shielded by the coating and the metal remains in Open Circuit Potential (OCP) conditions.

7.1 Understanding Anaerobic Corrosion under Disbonded Coatings

Chapter 4 discusses the study on corrosion affected by the coating disbondment gap size and ground water CO_2 concentration. The experiments of this study were performed inside a corrosion cell containing a simulated ground water solution in anaerobic conditions, with various CO_2 concentrations (characteristic to field conditions) ranging from 2% CO_2 to 20% CO_2. In these experiments, the coating disbondment gap was simulated with the use of an assembly containing metal coupons under a shielding made out of Poly Methyl Methacrylate (PMMA). The distance between the shielding and the coupons varied from narrow disbondment gaps to wide disbondment gaps, and infinite disbondment gaps (where the shielding was removed). The metal coupons simulated the pipeline under the coating. The corrosion rate of these coupons was assessed through weight loss measurements before and after 30 days of exposure to the corrosive environment. The main findings of these tests were as follows:

1) A metal ion concentration cell generated under narrowed disbondments and formed anodic sites with enhanced metal dissolution at the OM and cathodic sites protected from metal dissolution at the bottom of the disbondment.

2) Larger coating disbondments did not form metal ion concentration cells and exhibited a uniform corrosion rate at all the locations under the coating disbondment.

3) The ferrous ion concentration cell effect has not been previously documented for coating crevices and disbondment gaps, and may play an important role in corrosion processes under disbonded coatings in the field.

7.2 Analyzing Anaerobic Corrosion under Disbonded Coatings Through Field Data

Chapter 5 discusses a study performed on field data obtained from a Canadian pipeline company to understand the effect of the extent of the coating disbondment and coating conditions on the anaerobic corrosion of the pipeline. The study compared the effect of the coating condition on tape coatings (that are known to fail adhesively) and asphalt coatings (that fail cohesively). In order to understand the effect of the coating conditions, a Combined Coating Factor (CCF) parameter was developed for each case based on the coating disbondment and adhesion parameters.

The results showed the following:

1) The coating condition had no effect on the average corrosion rate under asphalt coatings, but greatly affected the average corrosion rate under tape coatings.

2) For tape coatings, the highest corrosion rate was found under coatings in a fair condition with intermittent disbondments and moderate adhesion. The results obtained in Chapter 4 representing the dependence of the corrosion rate on the coating disbondment gap size showed a good correlation with the trends obtained in this study showing the effect of the CCF factor on the average corrosion rate. This finding suggested that pipeline in the field may be affected by the presence of a metal ion concentration cell formation under narrower coating disbondments and wrinkles.

3) Locations with good coating conditions may still be prone to higher rates of corrosion due to a formation of a metal ion concentration cell or a different type of a concentration cell between the environment inside the coating and the OM.

4) CP should be provided based on the type of coating and the coating condition at each location.

7.3 Understanding Surface Crack Morphologies under Disbonded Coatings

Chapter 6 discusses a study performed to understand the effect of the coating disbondment gap size on crack morphology at the different locations under the disbondment. In this study, a tensile specimen was inserted into a corrosion cell containing ground water solution in an anaerobic environment bubbled with gap with a composition of 5% CO_2-nitrogen. The corrosion cell contained different shielding sizes for each experiment generating 2 mm and 10 mm disbondment gap sizes between the tensile specimen and the shielding. The loaded specimen had three shallow surface cracks at different positions under the shielding: top (OM), middle, and bottom. The cyclic loading applied on the specimen was not expected to generate crack growth, as the goal of the experiment was to understand the effect of the corrosion processes under the coating on the crack morphology. The results of this study showed the following:

1) The crack morphology under disbonded coatings in the generated environment was affected by either a CO_2-concentration cell corrosion or galvanic corrosion between the pearlite and ferrite phases on the banded microstructure of the metal.

2) The CO_2-concentration cell corrosion was assumed to initiate under a wider (10 mm) disbondment gap, between the crack surface and locations inside of the crack with a lower CO_2 concentrations. It results in a uniform localized corrosion inside the crack, generating corrosion pockets on the crack cross-section and narrower crack morphologies on the surface.

3) In the absence of a CO_2 concentration cell, which is likely in narrower disbondment gaps (2 mm) that constrain the entry of CO_2 and CO_2-related species (carbonate and bi-carbonate) into the disbondment, a galvanic effect between the constituents of a banded microstructure may be prevailant. In that case, locations on the crack containing ferrite are anodic to locations on the crack containing pearlite, which results in dissolution of certain sections of the crack, and possibly crack tip blunting. This galvanic cell may also be responsible for a wedged morphology of the cross-sectional cracks, which may depend on the location and distribution of the banded microstructure.

4) While both the CO_2 concentration cell and the galvanic effect of a banded microstructure are responsible for crack tip widening, they generate different crack morphologies.

7.4 Recommendations for Future Work

1) This research showed the presence of a concentration cell under a particular disbondment geometry used in the experiments. In order to obtain a more profound understanding of the concentration cell effect, corrosion tests conducted under various disbondment geometries may be required. As the coating geometry on pipelines may be tapered with, it may be of interest to understand the concentration cell effect under a shielding with a gradual decrease in width. Additional geometries may include holidays with varying sizes on long wrinkles and disbondments with two openings.

2) The research in this work was performed in OCP conditions assuming that the CP is fully shielded. In order to understand the effect of the concentration cell on pipelines where CP is only partially shielded, it may be important to conduct corrosion experiments to understand the corrosion behavior under a simulated coating disbondment with application of different CP potentials.

3) In this work, the investigation of the effect of the coating disbondment on the corrosion behavior and crack morphology was performed with a simulated coating disbondment. Corrosion and tensile test experiments similar to the ones described in this work performed with real coatings may further confirm the validity of the obtained results.

4) The hypothesis proposed in Chapter 6 regarding the formation of corrosion pockets due to a CO_2 concentration cell between the specimen surface and the crack region with lower CO_2 concentration require confirmation through similar experiments with varying levels of CO_2.

BIBLIOGRAPHY

1. Cheng, Y. F. *Stress Corrosion Cracking of Pipelines*. Hoboken, New Jersey: John Wiley & Sons, 2013.
2. Canadian Energy Pipeline Association, n.d. Web. http://www.cepa.com/about-pipelines/why-pipelines
3. Marcus, S. Oil and gas pipeline in Canada, *J. Oil Gas* 2, 15, 2009.
4. *Stress Corrosion Cracking on Canadian Oil and Gas Pipelines,* Report of the Inquiry, National Energy Board (NEB), 1996.
5. Kiefner, J.F and Rosenfeld M.J. The Role of Pipeline Age in Pipeline Safety*, INGAA Foundation Report* No 2012.04, 2012.
6. *Stress Corrosion Cracking Recommended Practices*. Rep. 2nd ed. Canadian Energy Pipeline Association (CEPA). 2007.
7. Beavers, J. A. "Integrity Management of Natural Gas and Petroleum Pipelines Subject To Stress Corrosion Cracking." *Corrosion* 70.1 (2014)
8. Leeds, J. M., and S. S. Leeds. "Coating Properties and Test Procedures." *Pipeline and Gas* 237.3. 2010.
9. Papavinasam, S. *Corrosion Control in the Oil and Gas Industry*. Burlington: Elsevier Science, 2013.
10. *Dissecting Coating Disbondments*. Rep. no. 101131, Det Norse Veritas (DNV). 2009.
11. Baker, M. *Stress Corrosion Cracking Study- Final Report*. Rep, 2005.
12. Varughese, K. "Coatings and Cathodic Protection for Underground Pipelines - What a Corrosion Engineer Should Know." Review. DuPont Coatings. Web.
13. Callister, W. D., and Rethwisch D. G. *Fundamentals of Materials Science and Engineering: An Integrated Approach*. Hoboken, NJ: Wiley, 2012.
14. Beavers, J. A. and Thompson, N. “External Corrosion of Oil and Natural Gas Pipelines” *ASM Handbook*, Volume 13C, Corrosion: Environments and Industries (#05145)
15. Focus on Safety and Environment: A Comparative Analysis of Pipeline Performance 2000-2009. National Energy Board (NEB), 2009.

16. Sherar, B. W. A. *The Effect of the Environment on the Corrosion Products and Corrosion Rates on Gas Transmission Pipelines*. PhD Thesis. London, Ontario, 2011.

17. Rozenfeld I. L. *Corrosion Inhibitors*. McGraw Hill, New York, p. 161. 1981.

18. Zhang, L., Li, X.G., Du, C.W., and Cheng, Y.F. "Corrosion and Stress Corrosion Cracking Behaviour of X70 Pipeline Steel in a CO_2-Containing Solution." *Journal of Materials Engineering and Performance* 18.3 (2009): 319-23.

19. Yan, M., Wang, J., Han, E., and Ke, W. "Local Environment under Simulated Disbonded Coating on Steel Pipelines in Soil Solution." *Corrosion Science* 50.5 (2008): 1331-339.

20. Nesic, S. "Carbon Dioxide Corrosion of Mild Steel", *Uhlig's Corrosion Handbook, Third Edition*, Edited by R. Winston Revie, 2011.

21. Niu, L., and Cheng, Y.F. "Corrosion Behaviour of X-70 Pipe Steel in Near-Neutral pH Solution." *Applied Surface Science* 253 (2007) 8626–8631.

22. Fajardo, V., Brown, B., Young, D.S. "Study of the Solubility of Iron Carbonate in the Presence of Acetic Acid Using an EQCM". *NACE International 2013*, 2452.

23. Nordsveen, M., S. Nešić, R. Nyborg, and A. Stangeland. "A Mechanistic Model for Carbon Dioxide Corrosion of Mild Steel in the Presence of Protective Iron Carbonate Films—Part 1: Theory and Verification." *Corrosion* 59.5 (2003): 443.

24. Jones, D. A. *Principles and Prevention of Corrosion*. Upper Saddle River, NJ: Prentice Hall, 1996. Print.

25. Jenney, C. L. O'Brien, A. *Welding Handbook, Volume 1 - Welding Science and Technology* (9th Edition). American Welding Society (AWS). Online version available at: p. 150. 2001.

26. Ahmad, Z. *Principles of Corrosion Engineering and Corrosion Control*. Boston, MA: Elsevier/BH, 2006.

27. Parkins, R.N. "A Review of Stress Corrosion Cracking of High Pressure Gas Pipelines."*Corrosion 2000*, Paper 363, NACE, Houston, TX, 2000.

28. Asher, S. L., Leis, B., Colwell, J., Singh, P. M. "Investigating a Mechanism for Transgranular Stress Corrosion Cracking on Buried Pipelines in Near-neutral pH Environments". *Corrosion* 63, 932–939. 2007.

29. Parkins, R.N. “Factors Influencing Stress Corrosion Crack Growth Kinetics.” *Corrosion*. Vol. 43. pp. 130-138. 1987.
30. Been, J., King, F., Yang, L., Song, F., Sridhar, N. “The Role of Coatings in the Generation of High- and Near-neutral pH Environments that Promote Environmentally Assisted Cracking.” *Corrosion 2005*, Paper 05167, NACE, Houston, TX, 2005.
31. Van Boven, G., Chen, W., Rogge, R. “The Role of Residual Stress in Neutral pH Stress Corrosion Cracking of Pipeline Steels: I. Pitting and Cracking Occurrence.” *Acta Mater*. 55, 29–42, 2007.
32. Van Boven, G., Chen, W., Rogge, R. “The Role of Residual Stress in Neutral pH Stress Corrosion Cracking of Pipeline Steels: Part II. Crack Dormancy.” *Acta Mater*. 55, 43–53, 2007.
33. Sutherby, R., Jack, T., Van Boven, G., and Wilmott, M. “CEPA Study on Characterization of Pipeline Pressure Fluctuations in Terms Relevant to Stress Corrosion Cracking.” *Proc. IPC/2000*, Calgary, Canada, 2000.
34. Eslami, A., Kania, R., Worthingham, B., Van Boven, G., Eadie, R., and Chen, W. “Effect of CO_2 and R-ratio on Near-neutral pH Stress Corrosion Cracking Initiation under a Disbonded Coating of Pipeline Steel.” *Corros. Sci*. 53, 2318–2327, 2011.
35. Fang, B., Eadie, R., Chen, W., and Elboujdaini, M. “Pit to Crack Transition in X-52 Pipeline Steel in Near-neutral pH Environment: 1. Formation of Blunt Cracks from Pits under cyclic loading, *Corros. Eng. Sci. Technol*. 45, 302–312, 2010.
36. Parkins, R.N. , Blanchard, W. K., Delanty, B. S. “Transgranular Stress Corrosion Cracking of High Pressure Pipelines in Contact with Solutions of Near-neutral pH.” *Corrosion 50, 394–408*, 1994.
37. Jack, T.R., B. Erno, K. Krist, and R.R. Fessler. “Generation of Near Neutral pH and High pH SCC Environments on Buried Pipelines”. *NACE International Corrosion 2000*. Paper No. 00362.
38. Delanty, B. and O'Beirne, J. “Major Field Study Compares Pipeline SCC with Coatings,” *Oil & Gas Journal*, 90 (24), pp. 39-44. 1992

39. Cheng, Y.F. "Fundamentals of Hydrogen Evolution Reaction and Its Implications on Near-neutral PH Stress Corrosion Cracking of Pipelines." *Electrochimica Acta* 52.7: 2661-667. 2007.
40. Delanty, B.S., and Marr, J.E. " Stress Corrosion Cracking Severity Rating Model". *Proc. International Conference on Pipeline Reliability*, CANMET, Ottawa, Ontario, Canada, 1992.
41. Capelle, J., Dmytrakh, I., and Pluvinage, G. "Comparative Assessment of Electrochemical Hydrogen Absorption by Pipeline Steels with Different Strength." *Corros. Sci. 52*, 1554–1559, 2010.
42. Chu, R., Chen, W., Wang, S. H., King, F., Jack, T. R., and Fessler R.R. "Microstructure Dependence of Stress Corrosion Cracking Initiation in X-65 Pipeline Steel Exposed to a Near-neutral pH Soil Environment." *Corrosion* 60, 275–283, 2004.
43. Liu, Z. Y., Li, X.G., Cheng, Y.F. " In-situ Characterization of the Electrochemistry of Grain and Grain Boundary of an X70 Steel in a Near-neutral pH Solution." *Electrochem. Commun.*12, 936–938, 2010.
44. Elboujdaini, M., Wang, Y. Z., Revie, R.W., Parkins, R.N., and Shehata, M.T. "Stress Corrosion Crack Initiation Processes: Pitting and Microcrack Coalescence". *Corrosion 2000*, Paper 00379, NACE, Houston, TX, 2000.
45. Jin, T.Y., Cheng, Y.F. "In-situ Characterization by Localized Electrochemical Impedance Spectroscopy of the Electrochemical Activity of Microscopic Inclusions in an X100 Steel." *Corros. Sci.* 53, 850–853, 2011.
46. Kushida, T., Nose, K., Asahi, H., Kimura, M., Yamane, Y., Endo, S., and Kawano, H. "Effects of Metallurgical Factors and Test Conditions on Near-neutral pH SCC of Pipeline Steels." *Corrosion 2001*, Paper 01213, NACE, Houston, TX, 2001.
47. Qin, Z., Demko, B., Noel, J., Shoesmith, D., King, F.,Worthingham, R., and Keith, K. "Localized Dissolution of Mill Scale-covered Pipeline Steel Surfaces." *Corrosion 60*, 906–914, 2004.
48. Chen, W., Kania, R., Worthingham, R. and Van Boven, G. "Transgranular Crack Growth in the Pipeline Steels Exposed to Near-neutral pH Soil Aqueous Solutions: The Role of Hydrogen." *Acta Materialia* 57: 6200-6214, 2009.

49. King, F., Jack, T., Chen, W., Wilmott, M., and Fessler, R. “Mechanistic Studies of Initiation and Early Stage Crack Growth for Near-neutral pH SCC on Pipelines.” *Corrosion 2000*, Paper No. 00361, 2000.
50. W. Chen, F. King, E. Vokes, Characteristics of near-neutral-pH stress corrosion cracks in an X-65 pipeline, Corrosion 58 (2002) 267–275.
51. Asher, S., Singh, P.M. “Hydrogen Production and Permeation of X-65 Pipeline Steel in Near-neutral pH Environments.” *Corrosion 2008*, NACE International, Houston, Paper No. 08411, 2008.
52. Lu, B.T., Luo, J.L., Norton, P.R., and Ma, H.Y.” Effect of Dissolved Hydrogen and Elastic and Plastic Deformation on Active Dissolution of Pipeline Steel in Anaerobic Groundwater of Near-neutral pH.” *Acta Mater*. 57: 41–49, 2009.
53. Lu, B.T., Luo, J.L., and Norton, P.R. “Environmentally Assisted Cracking Mechanism of Pipeline Steel in Near-neutral pH Groundwater.” *Corros. Sci.* 52: 1787– 1795, 2010.
54. Wang, R., “Effects of Hydrogen on the Fracture Toughness of a X70 Pipeline Steel.” *Corros. Sci.* 51: 2803–2810, 2009.
55. Lu, B.T.,Qiao, L.J., Luo, J.L., Gao,K.W., *Philosophical Magazine, 91(2)(2011)208–228*
56. Gangloff, R.P. “Hydrogen-assisted Cracking”, in: Milne, I., Ritchie, R.O., Karihaloo, B., (Eds.), *Comprehensive Structure Integrity, volume 6: Environmentally-Assisted Fracture*, Elsevier, Oxford, pp. 31–34, 2003.
57. Gu, B., Luo, J., and Mao, X. “Hydrogen-Facilitated Anodic Dissolution-Type Stress Corrosion Cracking of Pipeline Steels in Near-Neutral pH Solution.” *Corrosion*: January 1999, Vol. 55, No. 1, pp. 96-106, 1999.
58. Zhang, X.Y. , Lambert, S.B., Sutherby, R., and Plumtree, A. “Transgranular Stress Corrosion Cracking of X-60 Pipeline Steel in Simulated Ground Water”, *Corrosion*. Vol. 55. pp. 297-305, 1999.
59. Chen, W., and R. L. Sutherby. "Crack Growth Behavior of Pipeline Steel in Near-Neutral pH Soil Environments." *Metallurgical and Materials Transactions A* 38.6: 1260-268, 2007.

60. Johnson, J. T., Beavers, J. A., Durr, C. L., and Delanty, B. S. “Effects of O_2 and CO_2 on Near-Neutral-pH and Stress Corrosion Crack Propagation”. *NACE International*, 2000.

61. Parkins, R.N. “Transgranular Stress Corrosion Cracking of High-Pressure Pipelines in Contact with Near Neutral pH Solutions,” *8th Symp. Line Pipe Research*, Catalog no. L51680 (Washington, DC: American Gas Association, 1993), p. 16-1.

62. Egbewande, A., Eslami, A., Chen, W., Worthingham, R., Kania, R., VanBoven, G. “Growth of Surface Cracks in Near-neutral pH Environments under Disbonded Coatings”, *Proceedings of IPC 2010*, Calgary, 2010.

63. Chen, X., Du, C., Li, X., and Huang, Y. “Effects of Cathodic Potential on the Local Electrochemical Environment under a Disbonded Coating.” *J Appl Electrochem* 39: 697-704, 2009.

64. Yan, M., Wang, J., Han, E., and Ke, W.”Local Environment under Simulated Disbonded Coating on Steel Pipelines in Soil Solution”. *Corrosion Science*, 50 (5), pp. 1331—1339, 2008.

65. Yan, M.C., Wang, J. Q., Han, E. H., and Ke, W. “Electrochemical Measurements Using Combination Micro-Electrodes in Crevice Simulating Disbonded of Pipeline Coatings under Cathodic Protection”, *Corrosion Engineering Science and Technology*, 42-1, 42-49, 2007.

66. Song, F.M., and N. Sridhar. "Modeling Pipeline Crevice Corrosion under a Disbonded Coating with or without Cathodic Protection under Transient and Steady State Conditions." *Corrosion Science* 50.1: 70-83, 2

67. Perdomo, J. J., Chabica, M. E., and Song, I. “Chemical and electrochemical conditions on steel under disbonded coatings: the effect of previously corroded surfaces and wet and dry cycles,” *Corrosion Science* 43 (2001) 515-532.

68. Eslami, A., Fang, B., Kania, R., Worthingham, R., Been, J., Eadie, R. and Chen. W. “Stress corrosion cracking initiation under the disbonded coating of pipeline steel in near-neutral pH environment,” Corrosion Science 52 (2010) 3750-3756.

69. Egbewande, A., Chen, W., Eadie, R., Kania, R., Van Boven, G., Worthingham, R and Been, J. Unpublished work. “Transgranular crack growth in the pipeline steels exposed to

near-neutral pH soil aqueous solutions: Discontinuous crack growth mechanism.” Currently revised for Corrosion Science.

70. Eslami, A. *Near-neutral PH Stress Corrosion Crack Initiation under Simulated Coating Disbondment.* Thesis. University of Alberta, 2012. N.p.: n.p., n.d.
71. Papavinasam, S., M. Attard, and W. Revie. "External Polymeric Pipeline Coating Failure Modes." *Materials Performance* (October 2006)
72. Egbewande, A. Growth Behavior of Surface Cracks in Pipeline Steels Exposed to Near-neutral pH Environments. Thesis. University of Alberta, 2013.

APPENDIX A- ADDITIONAL IMAGES FROM CHAPTER 4

In Chapter 4, images of the coupon surfaces after corrosion exposure at the different positions under the coating disbondment gap were introduced for 5% CO_2. A comparison of the coupons at the position above the OM, the middle of the disbondment, and the bottom of the disbondment is shown in Figure A-1, Figure A-2, Figure A-3, and Figure A-4 for 2% CO_2, 2 mm, 5 mm, 10 mm disbondment gap, and infinite disbondment gap, respectively. As well, A comparison of the coupons at the position above the OM, the middle of the disbondment, and the bottom of the disbondment is shown in Figure A-5, Figure A-6, Figure A-7, and Figure A-8 for 20% CO_2, 2 mm, 5 mm, 10 mm disbondment gap, and infinite disbondment gap, respectively.

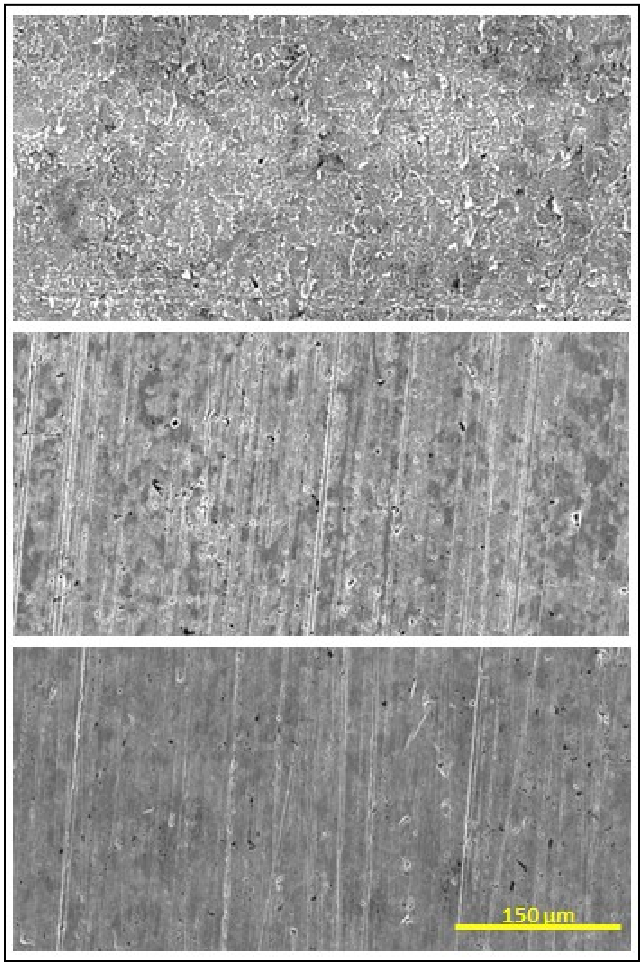

Figure A-1: Sample Surface at the Top, Middle, and Bottom for 2% CO_2, 2 mm Gap

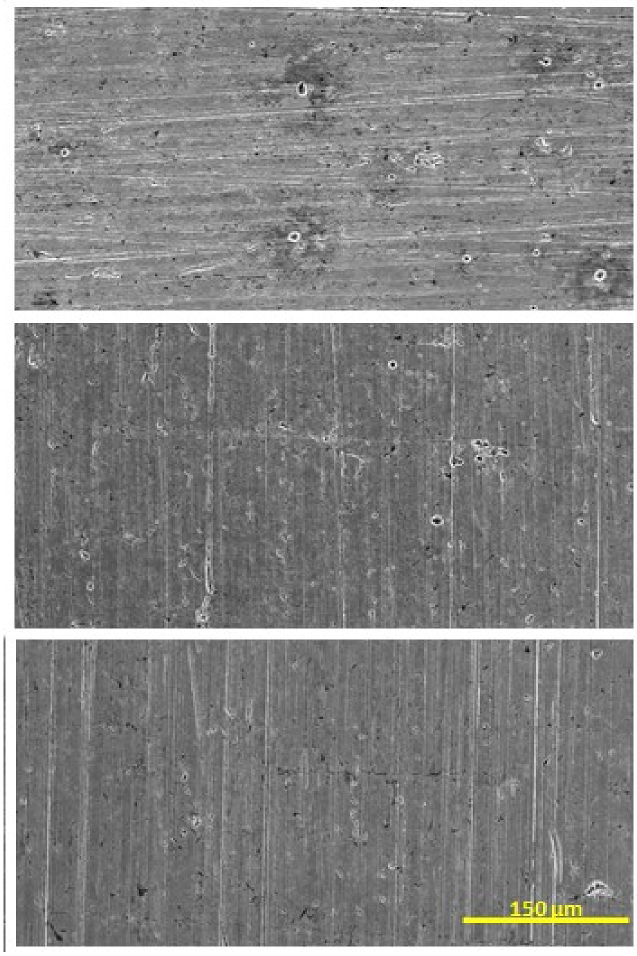

Figure A-2: Sample Surface at the Top, Middle, and Bottom for 5% CO_2, 5 mm Gap

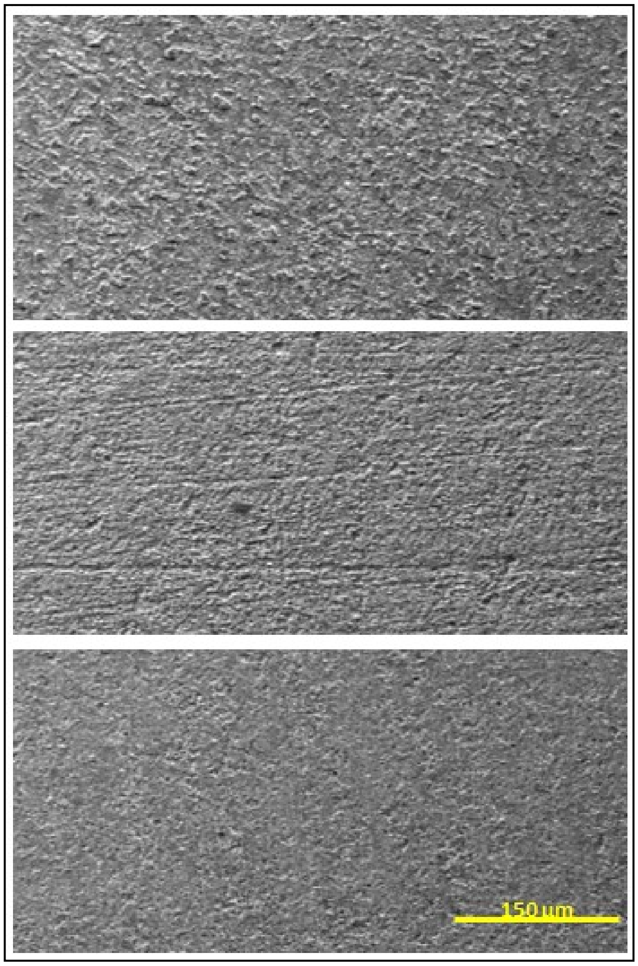

Figure A-3: Sample Surface at the Top, Middle, and Bottom for 2% CO_2, 10 mm Gap

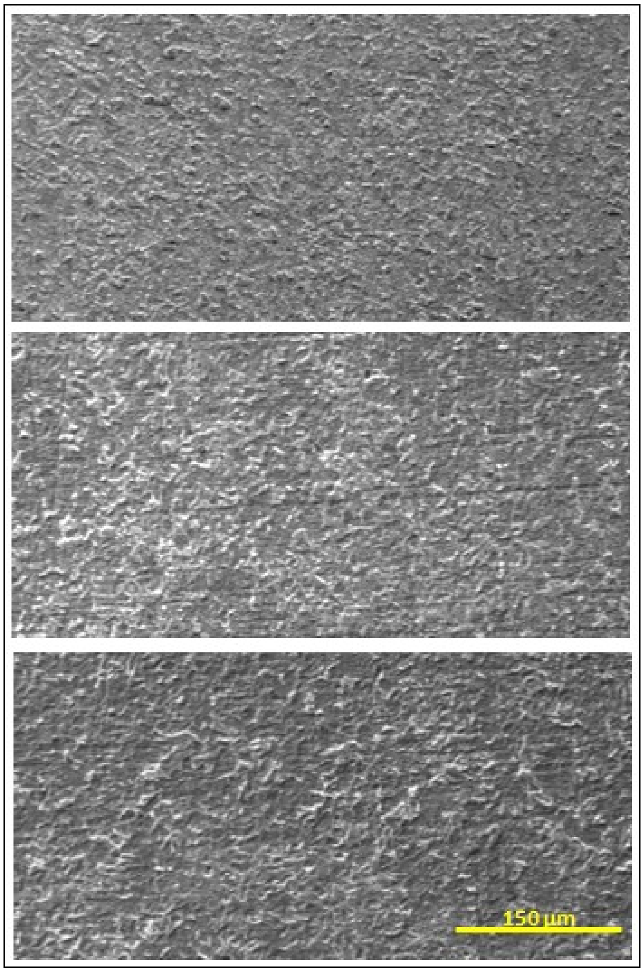

Figure A-4: Sample Surface at the Top, Middle, and Bottom for 2% CO_2, Infinite Disbondment Gap

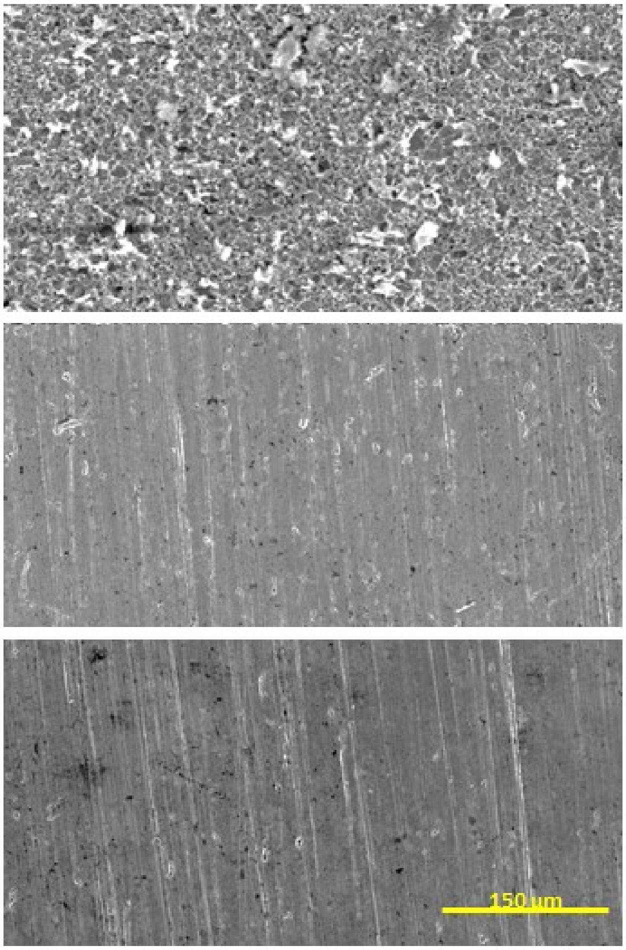

Figure A-5: Sample Surface at the Top, Middle, and Bottom for 20% CO_2, 2 mm Gap

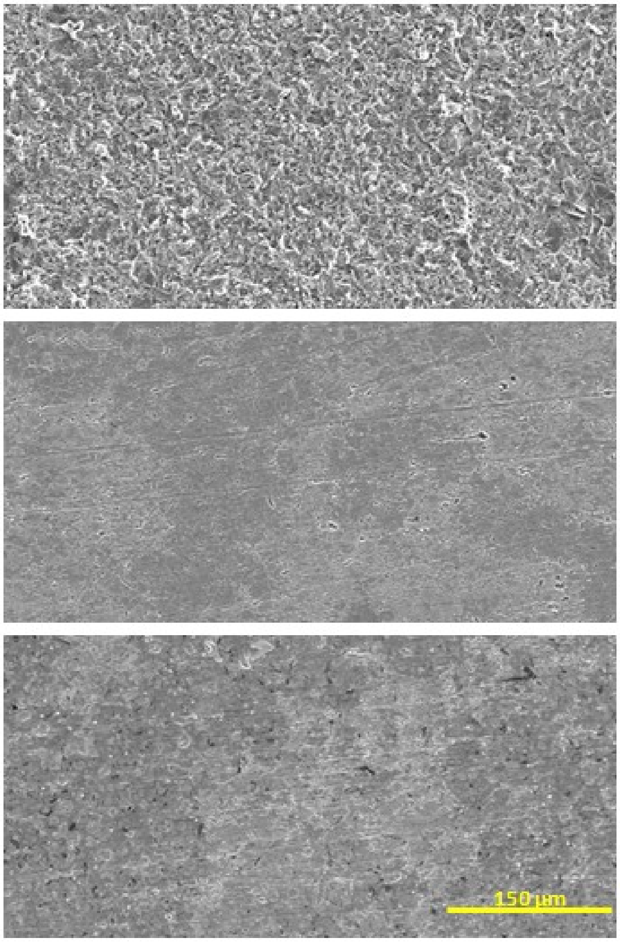

Figure A-6: Sample Surface at the Top, Middle, and Bottom for 20% CO_2, 5 mm Gap

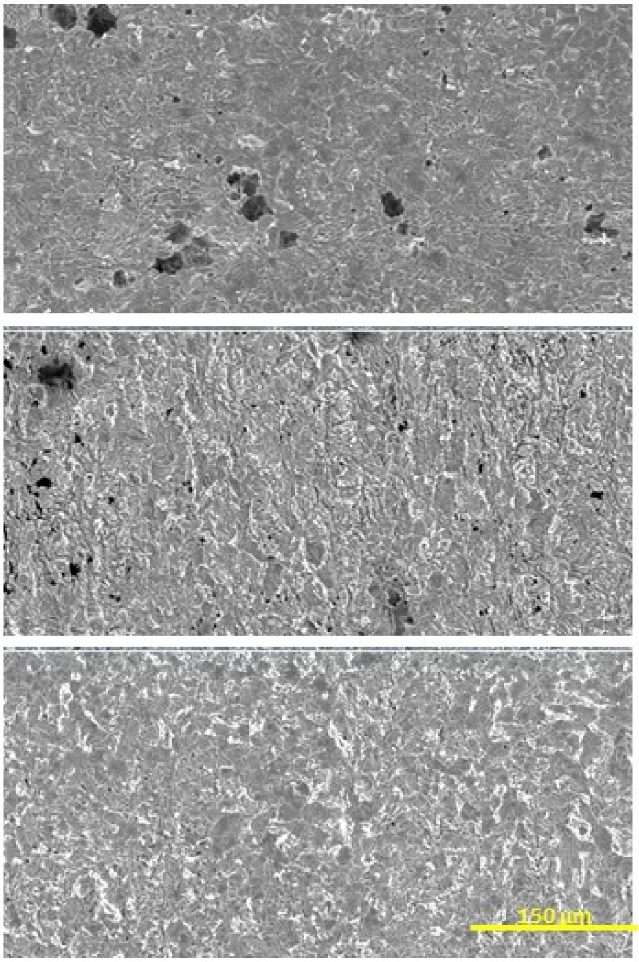

Figure A-7: Sample Surface at the Top, Middle, and Bottom for 20% CO_2, 10 mm Gap

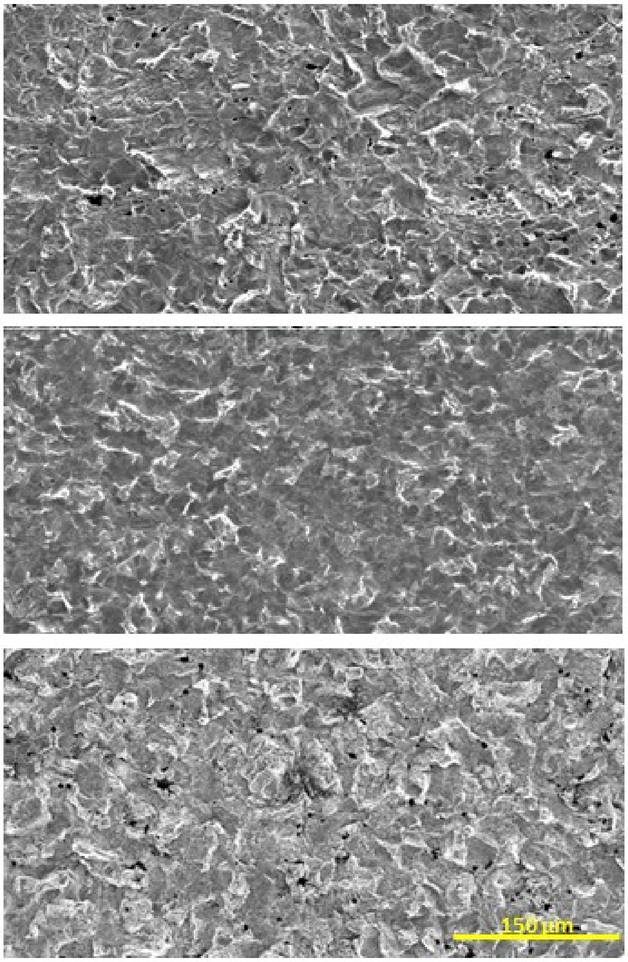

Figure A-8: Sample Surface at the Top, Middle, and Bottom for 20% CO_2, Infinite Disbondment Gap

APPENDIX B-ADDITIONAL IMAGES FROM CHAPTER 6

In Chapter 6, images of the surface crack morphologies were obtained at all the positions (top, middle, and bottom) under the 2 mm and the 10 mm disbondment gaps. Figure B-1 and Figure B-2 present the images obtained under the 10 mm disbondment gap in secondary electron SEM mode, and backscatter SEM mode respectfully. Figure B-3 and Figure B-4 present the images obtained under the 2 mm disbondment gap in secondary electron SEM mode, and backscatter SEM mode respectfully.

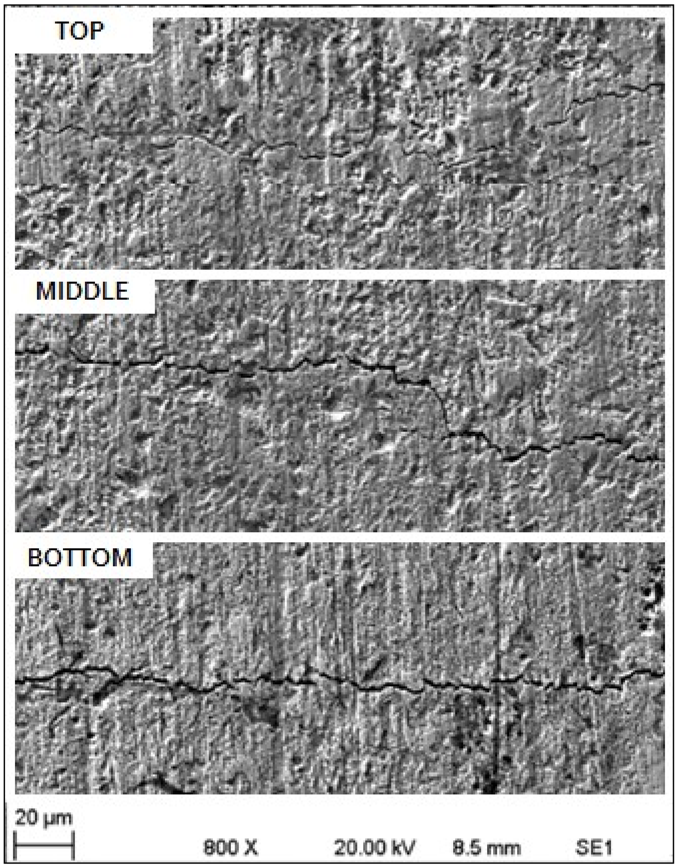

Figure B-1: Surface Crack Morphology of the Top, Middle, and Bottom Cracks under the 10 mm Disbondment Gap after Oxide Removal and Prior to Polishing (Secondary Electron SEM Imaging)

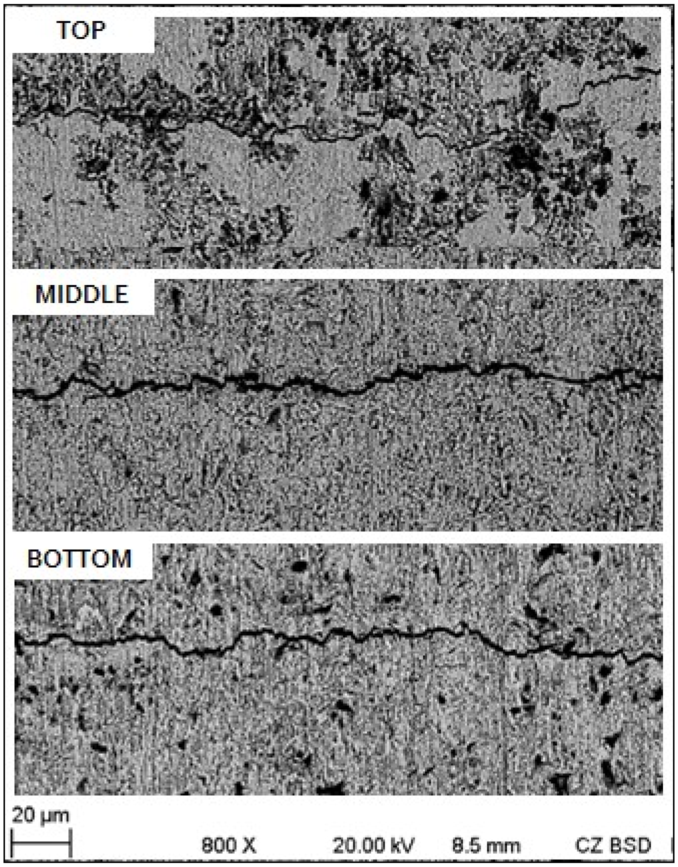

Figure B-2: Surface Crack Morphology of the Top, Middle, and Bottom Cracks under the 10 mm Disbondment Gap after Oxide Removal and Prior to Polishing (Backscatter SEM Imaging)

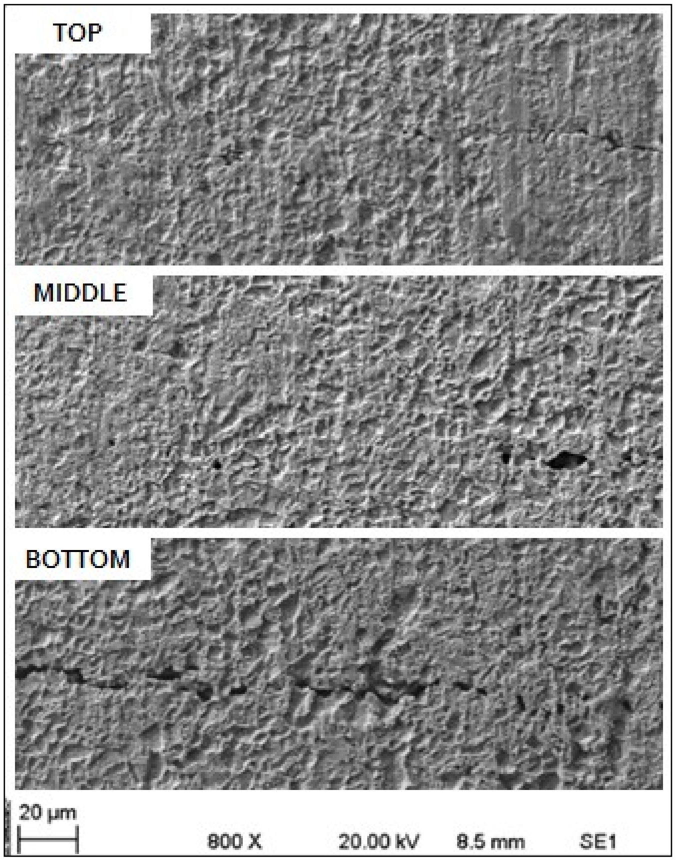

Figure B-3: Surface Crack Morphology of the Top, Middle, and Bottom Cracks under the 2 mm Disbondment Gap after Oxide Removal and Prior to Polishing (Secondary Electron SEM Imaging)

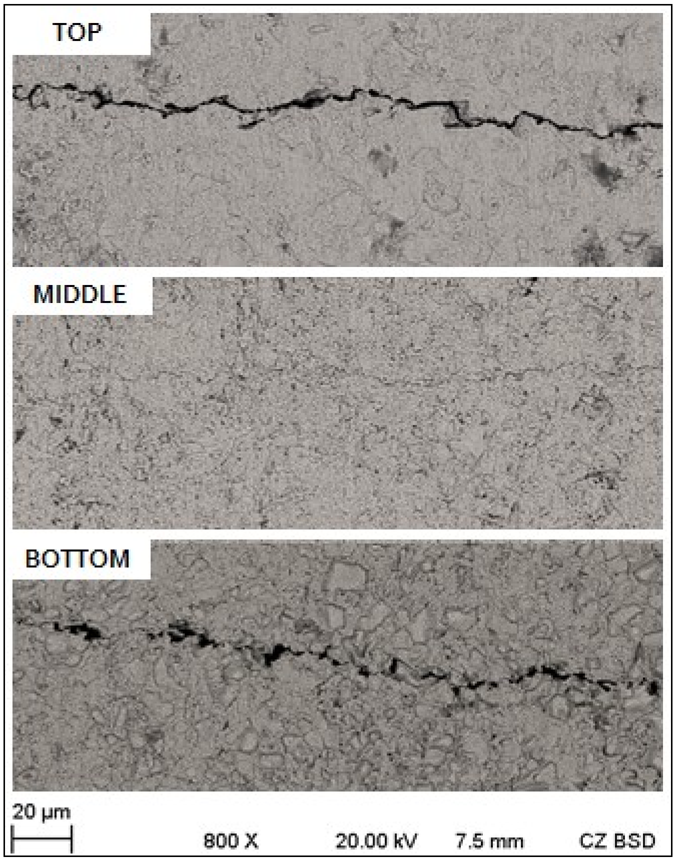

Figure B-4: Surface Crack Morphology of the Top, Middle, and Bottom Cracks under the 2 mm Disbondment Gap after Oxide Removal and Prior to Polishing (Backscatter SEM Imaging)